



NAVAL POSTGRADUATE SCHOOL

MONTEREY, CALIFORNIA

THESIS

**A VERIFICATION OF THE COAMPS-TC MODEL
PREDICTIONS OF TYPHOON NURI (2008)**

by

Jennifer M. Hensley

March 2009

Thesis Advisor:
Second Reader:

Patrick A. Harr
Russell L. Elsberry

Approved for public release; distribution is unlimited

THIS PAGE INTENTIONALLY LEFT BLANK

REPORT DOCUMENTATION PAGE			<i>Form Approved OHPA No. 0704-0188</i>	
Public reporting burden for this collection of information is estimated to average 1 hour per response, including the time for reviewing instruction, searching existing data sources, gathering and maintaining the data needed, and completing and reviewing the collection of information. Send comments regarding this burden estimate or any other aspect of this collection of information, including suggestions for reducing this burden, to Washington headquarters Services, Directorate for Information Operations and Reports, 1215 Jefferson Davis Highway, Suite 1204, Arlington, VA 22202-4302, and to the Office of Management and Budget, Paperwork Reduction Project (0704-0188) Washington DC 20503.				
1. AGENCY USE ONLY (Leave blank)		2. REPORT DATE March 2009	3. REPORT TYPE AND DATES COVERED Master's Thesis	
4. TITLE AND SUBTITLE A Verification of the COAMPS-TC Model Predictions of Typhoon Nuri (2008)			5. FUNDING NUMBERS	
6. AUTHOR(S) Jennifer M. Hensley				
7. PERFORMING ORGANIZATION NAME(S) AND ADDRESS(ES) Naval Postgraduate School Monterey, CA 93943-5000			8. PERFORMING ORGANIZATION REPORT NUMBER	
9. SPONSORING /MONITORING AGENCY NAME(S) AND ADDRESS(ES) N/A			10. SPONSORING/MONITORING AGENCY REPORT NUMBER	
11. SUPPLEMENTARY NOTES The views expressed in this thesis are those of the author and do not reflect the official policy or position of the Department of Defense or the U.S. Government.				
12a. DISTRIBUTION / AVAILABILITY STATEMENT Approved for public release; distribution is unlimited			12b. DISTRIBUTION CODE	
13. ABSTRACT (maximum 200 words) The objective of this thesis is to examine the predictions of the COAMPS-TC model for Typhoon Nuri during the THORPEX Pacific Asian Regional Campaign (T-PARC) and the Tropical Cyclone Structure 2008 (TCS-08) experiment that occurred in August through October 2008 in the western North Pacific. This case study on Typhoon Nuri examines the dynamic and thermodynamic structure changes of this tropical cyclone, including the intensity, track, radar reflectivity, and azimuthally-averaged plots of tangential winds, radial winds, vertical velocity, and cloud water. The life cycle of Typhoon Nuri was broken down into the formation, intensification, and decay stages and one model run from each stage was evaluated. The minimum sea-level pressure and maximum winds were found for each of the three grids of the COAMPS-TC model and the high-resolution (T799) ECMWF model and compared to the Joint Typhoon Warning Center best-track values. The forecast tracks from both models were examined and compared to the best-track values. Overall, the models did the best during the intensification stage. Lastly, the aircraft data were compared to the initial conditions for the model, and it is concluded that this aspect is the major source of forecast error.				
14. SUBJECT TERMS Typhoon Nuri, COAMPS-TC model, THORPEX Asian Pacific Regional Campaign, Tropical Cyclone Structure (TCS) 2008, Western North Pacific Typhoons, ECMWF			15. NUMBER OF PAGES 98	
			16. PRICE CODE	
17. SECURITY CLASSIFICATION OF REPORT Unclassified	18. SECURITY CLASSIFICATION OF THIS PAGE Unclassified	19. SECURITY CLASSIFICATION OF ABSTRACT Unclassified	20. LIMITATION OF ABSTRACT UU	

THIS PAGE INTENTIONALLY LEFT BLANK

Approved for public release; distribution is unlimited

**A VERIFICATION OF THE COAMPS-TC MODEL PREDICTIONS OF
TYPHOON NURI (2008)**

Jennifer M. Hensley
Captain, United States Air Force
B.S., Valparaiso University, 2003

Submitted in partial fulfillment of the
requirements for the degree of

MASTER OF SCIENCE IN METEOROLOGY

from the

**NAVAL POSTGRADUATE SCHOOL
March 2009**

Author: Jennifer M. Hensley

Approved by: Patrick A. Harr
Thesis Advisor

Russell L. Elsberry
Second Reader

Philip A. Durkee
Chairman, Department of Meteorology

THIS PAGE INTENTIONALLY LEFT BLANK

ABSTRACT

The objective of this thesis is to examine the predictions of the COAMPS-TC model for Typhoon Nuri during the THORPEX Pacific Asian Regional Campaign (T-PARC) and the Tropical Cyclone Structure 2008 (TCS-08) experiment that occurred in August through October 2008 in the western North Pacific. This case study on Typhoon Nuri examines the dynamic and thermodynamic structure changes of this tropical cyclone, including the intensity, track, radar reflectivity, and azimuthally-averaged plots of tangential winds, radial winds, vertical velocity, and cloud water. The life cycle of Typhoon Nuri was broken down into the formation, intensification, and decay stages and one model run from each stage was evaluated. The minimum sea-level pressure and maximum winds were found for each of the three grids of the COAMPS-TC model and the high-resolution (T799) ECMWF model and compared to the Joint Typhoon Warning Center best-track values. The forecast tracks from both models were examined and compared to the best-track values. Overall, the models did the best during the intensification stage. Lastly, the aircraft data were compared to the initial conditions for the model, and it is concluded that this aspect is the major source of forecast error.

THIS PAGE INTENTIONALLY LEFT BLANK

TABLE OF CONTENTS

I.	INTRODUCTION	1
A.	MOTIVATION.....	1
B.	TROPICAL CYCLONE FORMATION.....	2
C.	HISTORY OF TYPHOON NURI	3
II.	DATA AND METHODOLOGY	9
A.	NUMERICAL MODELS.....	9
1.	COAMPS-TC Model	9
2.	European Centre for Medium-range Weather Forecasts (ECMWF)	11
B.	TIME PERIODS	12
C.	SPECIAL TCS-08 OBSERVATIONS.....	13
D.	SATELLITE DATA.....	13
III.	ANALYSIS AND DISCUSSION.....	15
A.	INTENSITY	15
1.	Formation Stage.....	15
2.	Intensification Stage	24
3.	Decay Stage.....	26
4.	Intensity Error	28
B.	TRACK.....	29
C.	STRUCTURE FORECAST CHARACTERISTICS.....	33
1.	Formation Stage.....	34
2.	Intensification Stage	38
a.	<i>Simulated Radar Reflectivity</i>	<i>38</i>
b.	<i>Vertical Wind Shear</i>	<i>42</i>
c.	<i>Azimuthally-averaged Structure.....</i>	<i>44</i>
3.	Decay Stage	51
a.	<i>Simulated Radar Reflectivity</i>	<i>51</i>
b.	<i>Vertical Wind Shear</i>	<i>55</i>
c.	<i>Azimuthally-Averaged Structure</i>	<i>57</i>
D.	AIRCRAFT OBSERVATIONS.....	61
1.	0000 UTC 18 August Flight.....	62
2.	0000 UTC 19 August Flight.....	66
IV.	SUMMARY AND RECOMMENDATIONS	71
A.	SUMMARY	71
B.	RECOMMENDATIONS FOR FUTURE WORK.....	74
	LIST OF REFERENCES.....	75
	INITIAL DISTRIBUTION LIST	77

THIS PAGE INTENTIONALLY LEFT BLANK

LIST OF FIGURES

Figure 1.	JTWC best track of Typhoon Nuri with 6-h positions indicated by circles. The the labels indicate the 0000 UTC positions on days 16-22 August 2008.....	4
Figure 2.	Infrared satellite image during the beginning stages of Typhoon Nuri starting from (a) TCS-015 at 0000 UTC 16 August, (b) TD 13W at 1800 UTC 16 August, (c) TS Nuri on 1200 UTC 17 August, and (d) Typhoon Nuri on 1200 UTC 18 August. Images courtesy of NRL Monterey Tropical Cyclone homepage http://www.nrlmry.navy.mil/tc-bin/tc_home2.cgi	5
Figure 3.	Sea-surface temperatures (SST°C) on 16 August 2008. Image courtesy of http://catalog.eol.ucar.edu/cgi-bin/tparc_2008/imagewrap.nonav?file_url=/tparc_2008/ops/aoml_analyses/20080816/ops.AOML_Analyses.200808160000.SST_analysis.png	7
Figure 4.	Flow chart indicating the steps in the TC initialization in COAMPS-TC model. Image courtesy of http://www.nrlmry.navy.mil/coamps-web/web/research?spg=3&no=2	10
Figure 5.	Five aircraft observing periods (AOPs) along the track of Nuri from Figure 1.....	12
Figure 6.	ECMWF forecasts of MSLP (hPa) from various initial times (DDHHs, see insert) compared to the JTWC best-track MSLP values for Nuri.....	17
Figure 7.	COAMPS-TC grid 1 forecasts of MSLP (hPa) from various initial times (DDHHs, see insert) compared to the JTWC best-track MSLP values for Nuri.....	17
Figure 8.	COAMPS-TC grid 2 forecasts of MSLP (hPa) from various initial times (DDHHs, see insert) compared to the JTWC best-track MSLP values for Nuri.....	18
Figure 9.	COAMPS-TC grid 3 forecasts of MSLP (hPa) from various initial times (DDHHs, see insert) compared to the JTWC best-track MSLP values for Nuri. Grid 3 forecasts only began with the 1200 UTC 17 August integration when JTWC had declared Nuri was a tropical storm.	18
Figure 10.	ECMWF forecasts of maximum winds (kt) at 950 hPa from various initial times (DDHHs, see insert) compared with the JTWC best-track maximum wind values for Nuri.....	19
Figure 11.	COAMPS-TC grid 1 forecasts of maximum winds (kt) at 950 hPa from various initial times (DDHHs, see insert) compared with the JTWC best-track maximum wind values for Nuri.....	20
Figure 12.	COAMPS-TC grid 1 forecasts of 10-m maximum winds (kt) from various initial times (DDHHs, see insert) that may be more directly compared with the JTWC best-track maximum wind values for Nuri.	20
Figure 13.	COAMPS-TC grid 2 forecasts of maximum winds (kt) at 950 hPa from various initial times (DDHHs, see insert) compared with the JTWC best track maximum wind values for Nuri.....	21

Figure 14.	COAMPS-TC grid 2 forecasts of 10-m maximum winds (kt) from various initial times (DDHHs, see insert) that may be more directly compared with the JTWC best-track maximum wind values for Nuri.	22
Figure 15.	COAMPS-TC grid 3 forecasts of maximum winds (kt) at 950 hPa from various initial times (DDHHs, see insert) compared with the JTWC best-track maximum wind values for Nuri. Grid 3 forecasts only began with the 1200 UTC 17 August integration when JTWC had declared Nuri was a tropical storm.	23
Figure 16.	COAMPS-TC grid 3 forecasts of 10-m maximum winds (kt) from various initial times (DDHHs, see insert) that may be more directly compared with the JTWC best-track maximum wind values for Nuri. Grid 3 forecasts only began with the 1200 UTC 17 August integration when JTWC had declared Nuri was a tropical storm.	23
Figure 17.	COAMPS-TC grid 3 intensity errors (kt) for forecasts of Nuri each 12 h from initial conditions between 1200 UTC 17 August and 0000 UTC 21 August. Error bars represent a 10% variation in mean values.	28
Figure 18.	Track errors (km) for the ECMWF and COAMPS-TC models. Error bars represent a 10% variation in mean values.	30
Figure 19.	Track errors (km) for TC 08W-18W during TCS-08 for various models (see insert). Image courtesy of Mr. Buck Sampson, NRL-Monterey.	31
Figure 20.	Comparison of ECMWF track forecasts and JTWC best-track as in Figure 1.	32
Figure 21.	Comparison of COAMPS-TC grid 3 track forecasts with the JTWC best-track as in Figure 1.	33
Figure 22.	Simulated radar reflectivity from the 1200 UTC 16 August COAMPS-TC model run that verifies at (a) 0000 UTC 17 August, and (c) 1200 UTC 17 August. Microwave imagery at 91 Ghz at (b) 2253 UTC 16 August, and (d) 1005 UTC 17 August. Satellite imagery from http://www.nrlmry.navy.mil/sat_products.html	35
Figure 23.	Simulated radar reflectivity from the 1200 UTC 16 August COAMPS-TC model run that verifies at (a) 0000 UTC 18 August, and (c) 1200 UTC 18 August. Microwave imagery at 91 Ghz and 89 Ghz respectively at (b) 2240 UTC 17 August, and (d) 1220 UTC 18 August. Satellite imagery from http://www.nrlmry.navy.mil/sat_products.html	36
Figure 24.	Simulated radar reflectivity from the 1200 UTC 16 August COAMPS-TC model run that verifies at (a) 0000 UTC 19 August, and (c) 1200 UTC 19 August. Microwave imagery at 89 Ghz and 91 Ghz respectively at (b) 0100 UTC 19 August, and (d) 1121 UTC 19 August. Satellite imagery from http://www.nrlmry.navy.mil/sat_products.html	38
Figure 25.	Simulated radar reflectivity from the 1200 UTC 18 August COAMPS-TC model run that verifies at (a) 0000 UTC 19 August, and (c) 1200 UTC 19 August. Microwave imagery at 89 Ghz and 91 Ghz respectively at (b) 0100 UTC 19 August, and (d) 1121 UTC 19 August. Satellite imagery from http://www.nrlmry.navy.mil/sat_products.html	39

Figure 26.	Simulated radar reflectivity from the 1200 UTC 18 August COAMPS-TC model run that verifies at (a) 0000 UTC 20 August, and (c) 1200 UTC 20 August. Microwave imagery at 91 Ghz at (b) 2356 UTC 19 August, and (d) 1110 UTC 20 August. Satellite imagery from http://www.nrlmry.navy.mil/sat_products.html	40
Figure 27.	Simulated radar reflectivity from the 1200 UTC 18 August COAMPS-TC model run that verifies at (a) 0000 UTC 21 August, and (c) 1200 UTC 21 August. Microwave imagery at 91 Ghz and 89 Ghz respectively at (b) 2343 UTC 20 August, and (d) 1300 UTC 21 August. Satellite imagery from http://www.nrlmry.navy.mil/sat_products.html	42
Figure 28.	Vertical wind shear (kt) between 200-850 hPa for the COAMPS-TC grid 2 from 1200 UTC 18 August – 0000 UTC 21 August (see insert).....	43
Figure 29.	COAMPS-TC grid 2 200-850 hPa wind shear (kt) for the 1200 UTC 18 August model run for (a) 12-h forecast, (b) 24-h forecast, (c) 36-h forecast, and (d) 48-h forecast. The inner dotted (outer solid circle) represents a 20 (40) kt vertical shear. The black (red) arrow is the analysis (forecast) vertical shear.	44
Figure 30.	Azimuthally-averaged radial winds (kt) (contoured) and vertical velocity (kt) (shaded, see scale in middle) at (a) 15-h forecast from the 1200 UTC 18 August model run, (b) 3-h forecast from the 0000 UTC 19 August model run, (c) 27-h forecast from the 1200 UTC 18 August model run, and (d) 3-h forecast from the 1200 UTC 19 August model run.....	45
Figure 31.	Azimuthally-averaged radial winds (kt) (contoured) and vertical velocity (kt) (shaded, see scale in middle) at (a) 39-h forecast from the 1200 UTC 18 August model run, (b) 3-h forecast from the 0000 UTC 20 August model run, (c) 51-h forecast from the 1200 UTC 18 August model run, and (d) 3-h forecast from the 1200 UTC 20 August model run.....	47
Figure 32.	Azimuthally-averaged radial winds (kt) (contoured) and vertical velocity (kt) (shaded, see scale in middle) at (a) 63-h forecast from the 1200 UTC 18 August model run, and (b) 3-h forecast from the 0000 UTC 21 August model run.	48
Figure 33.	Azimuthally-averaged tangential winds (kt) (contoured) and cloud water (g/kg) (shaded, see scale in middle) at (a) 15-h forecast from the 1200 UTC 18 August model run, (b) 3-h forecast from the 0000 UTC 19 August model run, (c) 27-h forecast from the 1200 UTC 18 August model run, and (d) 3-h forecast from the 1200 UTC 19 August model run.....	49
Figure 34.	Azimuthally-averaged tangential winds (kt) (contoured) and cloud water (g/kg) (shaded, see scale in middle) at (a) 39-h forecast from the 1200 UTC 18 August model run, (b) 3-h forecast from the 0000 UTC 20 August model run, (c) 51-h forecast from the 1200 UTC 18 August model run, and (d) 3-h forecast from the 1200 UTC 20 August model run.....	50
Figure 35.	Azimuthally-averaged tangential winds (kt) (contoured) and cloud water (g/kg) (shaded) at (a) 63-h forecast from the 1200 UTC 18 August model run and (b) 3-h forecast from the 0000 UTC 21 August model run.	51

Figure 36.	Simulated radar reflectivity from the 1200 UTC 19 August COAMPS-TC model run that verifies at (a) 0000 UTC 20 August, and (c) 1200 UTC 20 August. Microwave imagery at 91 Ghz at (b) 2356 UTC 19 August, and (d) 1110 UTC 20 August. Satellite imagery from http://www.nrlmry.navy.mil/sat_products.html	52
Figure 37.	Simulated radar reflectivity from the 1200 UTC 19 August COAMPS-TC model run that verifies at (a) 0000 UTC 21 August, and (c) 1200 UTC 21 August. Microwave imagery at 91 Ghz and 89 Ghz respectively at (b) 2343 UTC 20 August, and (d) 1300 UTC 21 August. Satellite imagery from http://www.nrlmry.navy.mil/sat_products.html	53
Figure 38.	Simulated radar reflectivity from the 1200 UTC 19 August COAMPS-TC model run that verifies at (a) 0000 UTC 22 August, and (c) 1200 UTC 22 August. Microwave imagery at 89 Ghz and 91 Ghz respectively at (b) 2153 UTC 21 August, and (d) 1226 UTC 22 August. Satellite imagery from http://www.nrlmry.navy.mil/sat_products.html	54
Figure 39.	Vertical wind shear (kt) between 200-850 hPa for the COAMPS-TC grid 2 from 1200 UTC 19 August – 0000 UTC 21 August (see insert).	56
Figure 40.	COAMPS-TC grid 2 200-850 hPa wind shear (kt) for the 1200 UTC 19 August model run for (a) 12-h forecast, (b) 24-h forecast, (c) 36-h forecast, and (d) 42-h forecast. The inner dotted (outer solid circle) represents a 20 (40) kt vertical shear in the 12- and 24-h forecast while the inner dotted (outer solid circle) represents a 25 (50) kt vertical shear in the 36- and 42-h forecast. The black (red) arrow is the analysis (forecast) vertical shear.	57
Figure 41.	Azimuthally-averaged radial winds (kt) (contoured) and vertical velocity (kt) (shaded) at (a) 15-h forecast from the 1200 UTC 19 August model run, (b) 3-h forecast from the 0000 UTC 20 August model run, (c) 27-h forecast from the 1200 UTC 19 August model run, and (d) 3-h forecast from the 1200 UTC 20 August model run.	58
Figure 42.	Azimuthally-averaged radial winds (kt) (contoured) and vertical velocity (kt) (shaded) at (a) 39-h forecast from the 1200 UTC 19 August model run and (b) 3-h forecast from the 0000 UTC 21 August model run.	59
Figure 43.	Azimuthally-averaged tangential winds (kt) (contoured) and cloud water (g/kg) (shaded) at (a) 15-h forecast from the 1200 UTC 19 August model run, (b) 3-h forecast from the 0000 UTC 20 August model run, (c) 27-h forecast from the 1200 UTC 19 August model run, and (d) 3-h forecast from the 1200 UTC 20 August model run.	60
Figure 44.	Azimuthally-averaged tangential winds (kt) (contoured) and cloud water (g/kg) (shaded) at (a) 39-h forecast from the 1200 UTC 19 August model run and (b) 3-h forecast from the 0000 UTC 21 August model run.	61
Figure 45.	Flight information for 0000 UTC 18 August (a) WC-130J flight path (pink) and (b) 10-m wind (kt) analysis for the 0000 UTC 18 August model run with flight path overlay (Pass 1-black, Pass 2-pink). Satellite image is from 0930 UTC 17 August 2008.	62

Figure 46.	Flight-level winds (kt) at 0000 UTC 18 August from pass 1 (diamonds) and COAMPS-TC 0000 UTC 18 August 700 hPa winds (kt) (triangles).	63
Figure 47.	Surface winds (kt) from pass 1 (squares) and COAMPS-TC 0000 UTC 18 August 10-m winds (kt) (circles).	64
Figure 48.	Flight-level winds (kt) at 0000 UTC 18 August from pass 2 (diamonds) and COAMPS-TC 0000 UTC 18 August 700 hPa winds (kt) (triangles).	65
Figure 49.	Surface winds (kt) from pass 2 (squares) and COAMPS-TC 0000 UTC 18 August 10-m winds (kt) (circles).	65
Figure 50.	Flight information for 0000 UTC 19 August (a) WC-130J flight path and (b) 10-m winds (kt) analysis from the 0000 UTC 19 August model run with flight path overlay (Pass 1-black, Pass 2-pink). Satellite image is from 1230 UTC 19 August 2008.	66
Figure 51.	Flight-level winds (kt) at 0000 UTC 19 August from pass 1 (diamonds) and COAMPS-TC 0000 UTC 19 August 700 hPa winds (kt) (triangles).	67
Figure 52.	Surface winds (kt) at 0000 UTC 19 August from pass 1 (squares) and COAMPS-TC 0000 UTC 19 August 10-m winds (kt) (circles).	68
Figure 53.	Flight-level winds (kt) at 0000 UTC 19 August from pass 2 (diamonds) and COAMPS-TC 0000 UTC 19 August 700 hPa winds (kt) (triangles).	69
Figure 54.	Surface winds (kt) at 0000 UTC 19 August from pass 2 (squares) and COAMPS-TC 0000 UTC 19 August 10-m winds (kt) (circles).	69

THIS PAGE INTENTIONALLY LEFT BLANK

LIST OF TABLES

Table 1.	Beginning and ending times for the three stages in the life cycle of Nuri.	15
Table 2.	Sample sizes for intensity forecast errors in Figure 17.	29
Table 3.	Sample sizes for COAMPS-TC and ECMWF track errors.	29

THIS PAGE INTENTIONALLY LEFT BLANK

ACKNOWLEDGMENTS

First, I would like to thank my thesis advisor Professor Patrick Harr for all his help with the computer programs and answering my millions of questions while I was working on my thesis. I would also like to thank my second reader Professor Russell Elsberry, who helped me in the editing process.

Without my classmates, I would have never made it through the classes here at NPS, so I would like to extend my deepest thanks to them. I would also like to thank Professor Michael Montgomery and the advanced tropical class for the long nights this summer learning all about tropical meteorology. My thanks also to the COAMPS team at the Naval Research Laboratory, Bob Creasey, Mary Jordan, Beth Sanabia, and Stephanie Zick for helping me succeed while here at NPS.

Finally, thanks to my husband for his patience and support throughout the years and spending time alone while I was working long nights up at school trying to finish my thesis. Thank you.

THIS PAGE INTENTIONALLY LEFT BLANK

I. INTRODUCTION

A. MOTIVATION

Accurately forecasting a tropical cyclone (TC) in the western North Pacific (WNP) is important for the protection of many Department of Defense (DoD) assets. One of the most important tools available for prediction of the TC track, intensity, and structure is the numerical computer models. To improve the track and intensity prediction, it is necessary to accurately model the structure of the TC. While operational global models have routinely been used to forecast the track and intensity of a TC, higher resolution regional and mesoscale models have become more common in operational forecasting. The Navy Research Laboratory (NRL) developed the Coupled Ocean/Atmosphere Mesoscale Prediction System (COAMPS) model to serve as a high-resolution mesoscale model that could be applied over regions of interest to the military. Following the development of COAMPS, NRL started developing a TC version of COAMPS, which will be labeled hereafter as COAMPS-TC.

Because of the importance of TC activity over the WNP, several field programs were conducted during August through October 2008. Many of the programs were organized under the THORPEX Pacific Asian Regional Campaign (T-PARC). The primary objectives of T-PARC were adaptive sampling for targeted observations to improve TC track forecasts, extratropical transition of tropical cyclones, and downstream impacts of tropical cyclones. A second major program defined as the Tropical Cyclone Structure — 2008 (TCS-08) was conducted to address TC formation, structure, and intensification. Overall, there were nine participating nations in the experiments: Canada, China, England, France, Germany, Japan, South Korea, Taiwan, and the United States. The aircraft that participated in the experiments included the WC-130J from the U.S. Air Force 53rd Weather Reconnaissance Squadron, the Naval Research Laboratory (NRL) P-3, the Dropwindsonde Observations for Typhoon Surveillance near the Taiwan Region (DOTSTAR) aircraft from Taiwan, and the German Aerospace Research Establishment (DLR) Falcon. Another observing platform was the zero-pressure balloon called

Driftsonde that was launched from Hawaii. The Driftsonde carried dropsondes across the Pacific Ocean that were released at intervals between three and six hours.

In this thesis, products generated by the COAMPS-TC model during Typhoon (TY) Nuri (13W) in the TCS-08 period of August 2008 are examined and compared to best track and *in situ* observations gathered from aircraft operated during the field programs. The WC-130J and P-3 were the primary aircraft used for formation and structure changes. Tropical cyclone characteristics to be investigated include the distribution of deep convection, thermodynamic structure, wind distribution, and track. Particular emphasis is placed on the representation of the formation of TY Nuri and the structural changes associated with the intensification from a wave disturbance to typhoon.

B. TROPICAL CYCLONE FORMATION

Over the WNP, tropical cyclones can form from a variety of precursor circulations, which include easterly waves, monsoon troughs, monsoon depression, mesoscale convective systems, cells in the tropical upper-tropospheric trough (TUTT), and subtropical cyclones. Gray (1968, 1979) identified a set of thermodynamic and dynamic conditions that are necessary but not sufficient for a tropical cyclone to form. The conditions include sea-surface temperature (SST) $> 26^{\circ}\text{C}$, conditional instability, low-level vorticity, moist mid-tropospheric levels, and low vertical wind shear.

The release of latent heat in the rising plumes of a tropical cyclone drives the generation of a warm core and low surface pressure. The passage of low-level air over the warm ocean that flows into the tropical cyclone allows for the transfer of moisture and heat from the sea to the air surface. Therefore, the ocean needs to be very warm to provide the necessary environment to sustain the release of latent heat in the mid-levels of the troposphere. Conditional instability means that a moist parcel needs to remain unstable compared to the environment so that it continues to rise and release latent heat high in the atmosphere. In addition, the mid-levels of the troposphere must become more moist to suppress saturated downdrafts that will penetrate into the boundary layer and counteract the import of moisture and heat from the ocean. Tropical cyclone formation is

more likely when there is some background cyclonic rotation or when an initial disturbance exists in a region of background cyclonic vorticity. Surface friction causes air flowing around a low-level circulation to tend toward the center of the circulation, which will draw air into the developing storm. This provides a favorable environment for import of energy from the ocean and updrafts near the circulation center. Vertical wind shear is defined as the change in direction and/or speed of the wind with height. The region of latent heat being released aloft needs to stay above the surface low-pressure center so that the pressure drop being driven by the heating aloft can work in conjunction with the surface low pressure.

C. HISTORY OF TYPHOON NURI

The focus of this thesis will be on the structure changes of Typhoon Nuri as it went from a tropical circulation system (TCS) to a typhoon. The pre-Nuri disturbance was the subject of several aircraft missions, as it was suspected to intensify into a TC. According to the Joint Typhoon Warning Center (JTWC), Typhoon Nuri was the eighth typhoon of the season. Nuri made landfall in the northern province of the Philippines Islands on August 20, as a category 3 typhoon. On 22 August, TY Nuri made a second landfall in Hong Kong as a strong tropical storm. The JTWC best track indicates that Nuri moved at an average speed of 11.2 kt to the west/northwest (Figure 1).

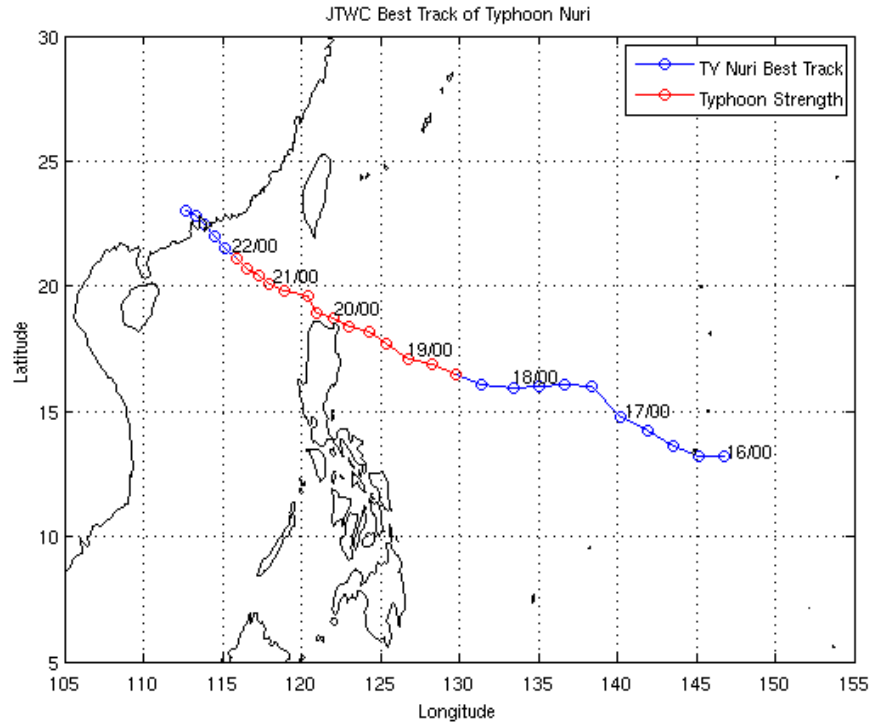


Figure 1. JTWC best track of Typhoon Nuri with 6-h positions indicated by circles. The the labels indicate the 0000 UTC positions on days 16-22 August 2008.

Typhoon Nuri was the first typhoon to occur during TCS-08. The WC-130J, P-3, and DOTSTAR aircraft participated in missions during TY Nuri. The pre-Nuri disturbance was labeled TCS-015 on 10 August north of the Marshall Islands as a tropical easterly wave. As the TCS-015 disturbance approached Guam on 16 August, most of the convection was located on the west side of the wave axis with stratiform and suppressed conditions east of the axis (Figure 2a). The steering flow of TCS-015 was easterly, with an anticyclone located to the northwest of the wave. Only 5-10 kt of vertical wind shear was present at this time.

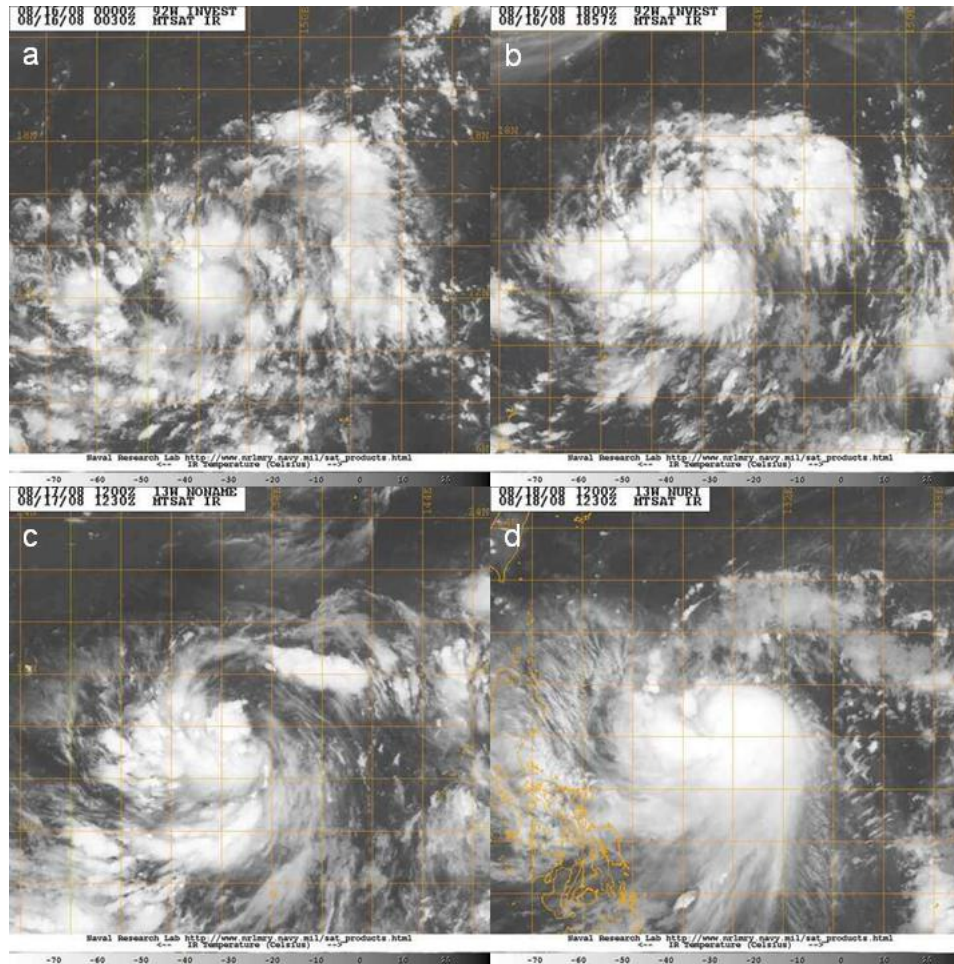


Figure 2. Infrared satellite image during the beginning stages of Typhoon Nuri starting from (a) TCS-015 at 0000 UTC 16 August, (b) TD 13W at 1800 UTC 16 August, (c) TS Nuri on 1200 UTC 17 August, and (d) Typhoon Nuri on 1200 UTC 18 August. Images courtesy of NRL Monterey Tropical Cyclone homepage http://www.nrlmry.navy.mil/tc-bin/tc_home2.cgi.

By 1800 UTC 16 August (Figure 2b), TCS-015 became better organized and was declared TD 13W by JTWC. At the time that TD 13W formed, it was over very warm water with a maximum SST of 30°C (Figure 3). At this time, TD 13W had a broad surface and mid-level circulations that were mapped by the WC-130J. Examination of dropwindsondes suggests that the circulation was tilted in the vertical during this early stage of development. The ocean thermal mixed layer was the deepest on the south side of the storm with a depth ranging between 40 to 80 meters.

On 17 August, the vertical wind shear progressively increased to 10-20 kt. However, the storm continued to strengthen into a tropical storm at 1200 UTC 17 August (Figure 2c). Late on 17 August, a partial eyewall was defined by the aircraft, but a well-defined center was not identified due to an unorganized cloud distribution and a vertical tilt from the surface to the 700-hPa center. The eyewall was closed on the southern side but there was no eyewall evident on the northern side. A secondary band was also starting to form to the west of the western eyewall. The ocean-mixed layer in this region was about 40 to 50 meters in depth. The circulation of Nuri was definitely starting to take on TS characteristics with a persistent rainband wrapping around the system on the east and north sides that extended to the core on the north side with a dry slot inside the band. Another inner rainband was also wrapping around and starting to form the proto-eyewall. During this time, the vertical wind shear was from the northeast at 20 kt. Although such a large shear is often unfavorable for development, it did not seem to impact Nuri in a significant manner.

At 1200 UTC 18 August (Figure 2d), TS Nuri was upgraded to typhoon strength. During the aircraft mission late on 18 August, a minimum mean sea-level pressure (MSLP) of 976.3 and a maximum surface wind of 79 kt from a dropwindsonde was observed during a penetration to the eye. The ocean-mixed layer was quite shallow on the northwest side with a depth of only 20 m, but larger depths existed to the east of the storm. The eyewall was now closed, which indicates the development from the previous day when it was open on the north side. The eyewall diameter was estimated at 32 n mi. Nuri continued to intensify despite having 15-20 kt of northeasterly shear over the circulation. Nuri continued to be steered by an anticyclone to the north, which led a west/northwestward track. With upper-level divergence above the storm, Nuri continued to have good outflow that contributed to its intensification. Based on JTWC advisories, the maximum winds in TY Nuri were 100 kt at 0000 UTC 20 August and the minimum MSLP was 948 hPa on the same day (JTWC 2009). TY Nuri was declared to have dissipated on 0000 UTC 23 August (Figure 1).

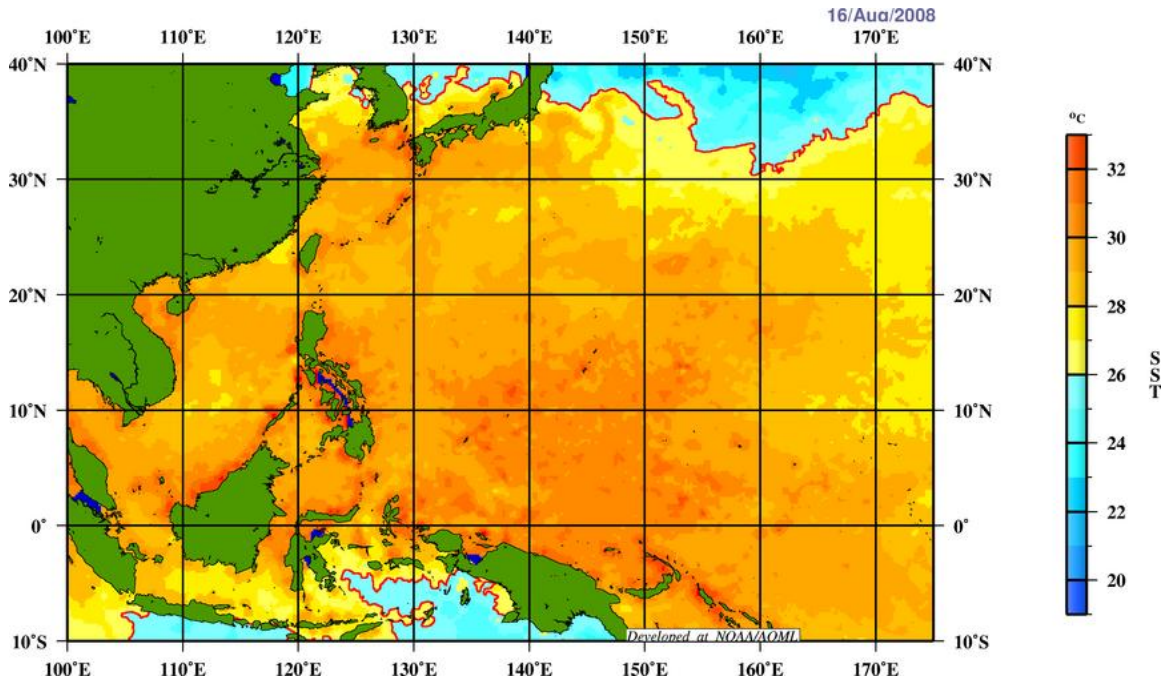


Figure 3. Sea-surface temperatures (SST°C) on 16 August 2008. Image courtesy of http://catalog.eol.ucar.edu/cgi-bin/tparc_2008/imagewrap.nonav?file_url=/tparc_2008/ops/aoml_analyses/20080816/ops.AOML_Analyses.200808160000.SST_analysis.png.

There were five TCS-08 aircraft observing periods (AOPs) during Nuri's lifetime. The first AOP (AOP-1), which was centered at 0000 UTC 16 August, was a survey mission to determine a closed circulation in TCS-015 (Figure 2a). The next period (AOP-2), which was centered at 0000 UTC 17 August (6 h after Figure 2b), found a closed circulation in TCS-015. At this time, the system was upgraded to TD 13W. The third AOP (AOP-3), which was centered at 0000 UTC 18 August (between Figures 2c and 2d), examined the structure during the TS stage. The fourth AOP (AOP-4), which was centered at 0000 UTC 19 August, focused on the structure and satellite validation of TY Nuri. The last AOP (AOP-5) was centered on 1200 UTC 20 August and studied the structure of TY Nuri.

These aircraft observations provided several snapshots of the evolution of Nuri from a pre-TC disturbance to a typhoon. During the life cycle of Nuri, the COAMPS-TC model was run operationally to provide guidance for the design of the aircraft missions

and predict the track and intensity as the system matured. In the following sections, the depiction of TY Nuri in the COAMPS-TC model is analyzed in comparison with best-track data and satellite data. The use of aircraft data is limited at the time of completion of this thesis due to post-processing procedures that are yet to be completed. The forecasts of Nuri by the COAMPS-TC are also compared to the forecasts from the operational global model from the European Centre for Medium-range Weather Forecasts (ECMWF).

The forecasts of Nuri are examined in three stages, which include initial formation, intensification, and decay. Representative forecast sequences are examined in detail to diagnose model traits with respect to the TC evolution.

II. DATA AND METHODOLOGY

A. NUMERICAL MODELS

Although a suite of other model forecast products were available during TCS-08, this case study examines a variety of derived products from the COAMPS-TC mesoscale model and the ECMWF global model.

1. COAMPS-TC Model

The 2008 WNP TC season is the first tropical season that the COAMPS-TC model was run operationally. The COAMPS-TC model has three grids with horizontal resolutions of 45, 15, and 5 km. The 45 km grid is geographically fixed while the inner two grids move with the storm. A two-way interaction between the grids is predicted, which means a feedback occurs from the inner grid 3 to the medium grid 2 and then to the outer grid 1. Once JTWC posts a TC warning message, the COAMPS-TC model will automatically run. The TC initialization process of the COAMPS-TC model inserts a TC structure that is a modified Rankine vortex based on the JTWC TC warning message (Figure 4) (COAMPS 2009). These TC synthetic observations are comprised of one profile at the center of the TC, four profiles at 1/2-deg. (55 km) radius, and then profiles at each 1/2-deg. (55 km) radius for a total 41 profiles. The TC synthetic observations are used in the analysis of each of the three grids. The Navy Atmospheric Variational Data Assimilation System (NAVDAS) for COAMPS then combines the TC structure model and the Navy Operational Global Atmospheric Prediction System (NOGAPS) truncated analysis fields to provide the initial conditions. The NAVDAS also incorporates conventional observations, satellite-derived cloud-drift winds, satellite-derived soundings, SSM/I total column precipitable water and surface wind speeds, and high-density multispectral wind observations. The COAMPS-TC initialization may also use the most recent COAMPS forecast as a first-guess field instead of the NOGAPS model.

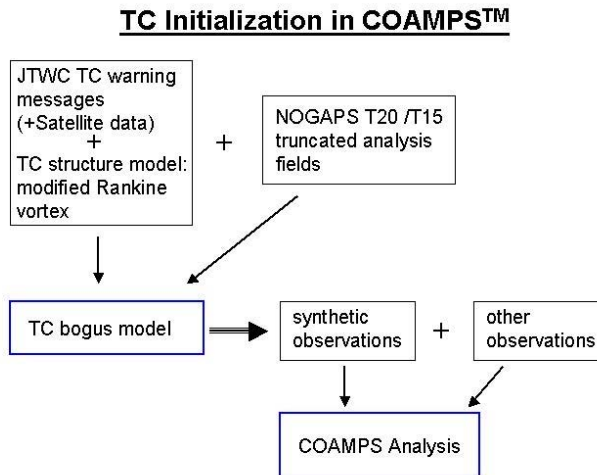


Figure 4. Flow chart indicating the steps in the TC initialization in COAMPS-TC model. Image courtesy of <http://www.nrlmry.navy.mil/coamps-web/web/research?spg=3&no=2>.

The tropical cyclone center in the COAMPS-TC forecast is defined from the locations of minimum sea-level pressure L , maximum vorticity ζ , circulation center (vortex center) x , and the “mass center” M (COAMPS, 2009). The model is run to 72 hour at 0000 UTC and 1200 UTC each day. Some of the model features of COAMPS-TC are: non-hydrostatic, compressible equations, sigma- z vertical coordinates, Louis (1979) scheme for surface layer parameterization, subgrid scale mixing, and time-dependent boundary conditions (NRL, 2003). The boundary conditions are also provided by the NOGAPS model and are interpolated to the COAMPS vertical resolution. The model output is available every three hours on 19 pressure levels starting at 1000 hPa and extending to 100 hPa in 50-hPa increments.

The numerical solution in COAMPS-TC is on an Arakawa C-grid, which has vertically and horizontally staggered grid boxes. A split-explicit time integration scheme is used. The topography is from the 1 km terrain database developed from the Defense Mapping Agency Digital Terrain Elevation Data (DMA DTED) level 1 data set. Fourth-order diffusion is applied to all prognostic variables except the Exner perturbation (π). The moisture physics include the Kain-Fritsch (1990, 1993) convective parameterization for the grid with a horizontal resolution > 10 km, shallow cumulus mixing (Tiedtke), and

grid-point precipitation. On grid 3, the precipitation is calculated explicitly. Harshvardhan solar and longwave radiation are computed every hour. The microphysics package is a single-moment microphysics class 5 scheme that includes cloud droplets, cloud ice, snow, rain, and graupel. The planetary boundary layer parameterization is a 1.5 order closure, level-2.5 scheme that solves both the prognostic equation for turbulence kinetic energy (TKE) and diagnostic equations for second-moment quantities such as fluxes of heat, moisture, and momentum (NRL, 2003). The land surface is a single layer/bucket model.

COAMPS uses the Navy Coupled Ocean Data Assimilation (NCODA) for its ocean analysis. The ocean analysis is similar to the atmospheric analysis in the way that its analysis background or first-guess fields may be generated from short-term ocean model forecast or from a previous analysis (NRL, 2003). Similar to the atmospheric analysis, NCODA uses all the conventional ocean observations and satellite-derived SST and sea-surface height (SSH). A NCODA analysis includes temperature, salinity, geopotential (dynamic height), and current velocity components.

2. European Centre for Medium-range Weather Forecasts (ECMWF)

The output from European Centre for Medium-range Weather Forecasts (ECMWF) is provided on a $\frac{1}{4}$ -degree resolution grid at 0000, 0600, 1200, and 1800 UTC. The ECMWF computational model uses a triangular truncation (T799) numerical scheme and a semi-Lagrangian, two-time-level, semi-implicit formulation. This version of the ECMWF was introduced in February 2006 and has 91 levels between the surface and 80 km. The grid is a Gaussian grid with the average distance between grid points being close to 25 km. At each grid point, the variables are wind, temperature, humidity, cloud fraction and water/ice content, pressure at surface grid points only, and ozone. Some of the parameters that are included in the model are orography, four surface and sub-surface levels, stratiform and convective precipitation, carbon dioxide, aerosol, ozone, ground and sea-surface temperature, ground humidity, snowfall, snowcover and snow melt, radiation, sub-grid-scale orographic drag, gravity waves and blocking effects, evaporation, and sensible and latent heat flux (ECMWF, 2006).

The data assimilation scheme includes a global analysis of wind, temperature, surface pressure, humidity, and ozone using a four-dimensional multivariate variational assimilation on 12-hour periods on all model levels (ECMWF, 2006). The observations used include in-situ conventional observations and satellite data, which includes radiances, surface winds, ozone, and altimetry data.

B. TIME PERIODS

The TPARC 2008 field experiment was conducted in the western North Pacific from August through October 2008. The U.S. Air Force 53rd Weather Reconnaissance Squadron WC-130J aircraft and the Naval Research Laboratory (NRL) P-3 with the NSF/National Center for Atmospheric Research ELDORA radar and a Doppler wind lidar were the primary aircraft for the tropical measurements (Elsberry & Harr, 2008). The five AOPs of interest in this experiment were conducted from 2252 UTC 15 August to 0426 UTC 16 August 2008 (AOP-1), 1945 UTC 16 August to 0415 17 August 2008 (AOP-2), 1647 UTC 17 August to 0525 UTC 18 August 2008 (AOP-3), 1804 UTC 18 August to 0325 UTC 19 August 2008 (AOP-4), and 0843 UTC to 1325 UTC 20 August 2008 (AOP-5) (Figure 5).

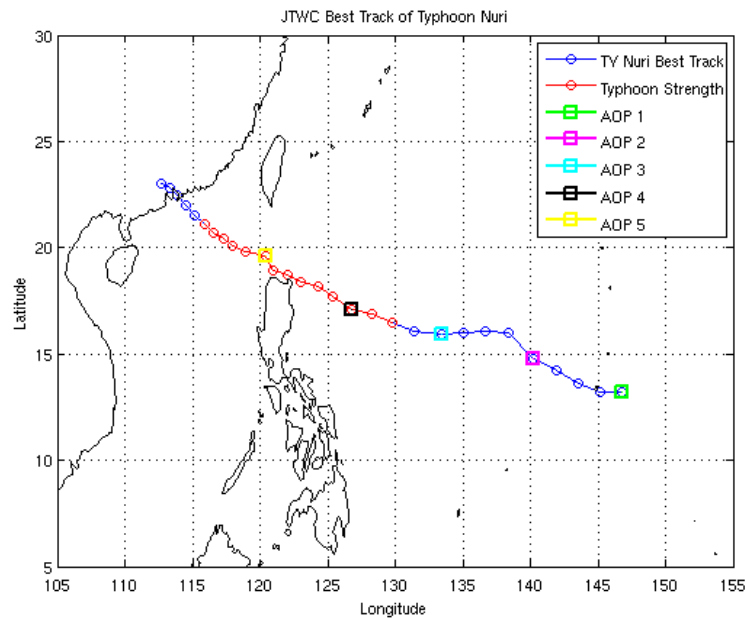


Figure 5. Five aircraft observing periods (AOPs) along the track of Nuri from Figure 1.

C. SPECIAL TCS-08 OBSERVATIONS

Approximately 140 National Center for Atmospheric Research (NCAR) global positioning system dropwindsondes were released into the inner and outer core of Nuri during the five flights. These dropwindsondes from the P-3 and C-130 usually had an average spacing of 100 km. The post-processing of the GPS dropwindsondes is in accordance with Hock and Franklin (1999). This instrument provides pressure, temperature, and relative humidity (PTH), and horizontal wind vectors at 2-Hz temporal resolution along a Lagrangian trajectory falling between 12 and 15 m/s in the lower troposphere (Bell & Montgomery, 2008). Pressure, temperature, humidity, and wind speed and direction were computed every 0.5 s. Thus, the vertical resolution is approximately 5 m, with typical PTH errors less than 1.0 hPa, 0.2 °C, and 5% respectively, and wind errors less than 2.0 m/s (Hock and Franklin 1999).

Dropwindsondes were dropped from a variety of flight levels. The P-3 mostly flew at 12,000 feet to sample the convection with the Electra Doppler Radar (ELDORA), but also ascended to 24,000 feet on a couple of the flights to obtain deeper profiles from the dropwindsondes. Although the C-130 would fly at 10,000 feet for eyewall penetration and fixes of the center in a mature typhoon, the transits to and from the storm were at 30,000 feet to sample the rest of the storm. The DOTSTAR aircraft flies at an altitude of 35000 feet and the spacing between sondes is on average 100 km. Each dropwindsonde observation is quality checked on the aircraft to remove noise and check for other instrument errors before they are transmitted to the operational modeling centers. However, detailed post-processing of the dropwindsonde for research-quality data sets is still in progress at the time of completion of this thesis.

D. SATELLITE DATA

On polar-orbiting satellites, the 85 GHz microwave channel is a useful tool for examining the distribution of deep convection in the tropics. This channel measures radiation scattered by ice crystals that are present at high altitudes in deep convective clouds. Therefore, the ice cloud-free TC eye is clearly represented with this product.

Most of the microwave satellites have an 85, 89, or 91 GHz channel. All three frequencies provide equivalent information and are one aid used for estimating the low-level circulation center position of a TC. The wavelength for the 85 GHz channel is 3.5 mm. The resolution ranges from 5 km to 16 km and the swath widths range from 780 km to 1400 km. Convective rainbands in a TC tend to have very low black-body temperatures because of all the scattering by large precipitation particles, especially ice crystals. Thus, the 85 GHz channel can be used similar to radar to depict where the strong rainbands are and the convective parts of the storm.

III. ANALYSIS AND DISCUSSION

The forecasts of Typhoon Nuri were evaluated using the traditional metrics of hurricane position error and intensity error. Intensity is assessed using the maximum sustained wind at 10-meter elevation (Davis et al., 2008). The COAMPS-TC 5 km grid is the only model output that was used for calculating the intensity error, and the maximum wind at any grid-point is an instantaneous output unlike the 1-min average upon which the best track is based. Intensity and position errors from the COAMPS-TC and ECMWF were verified against the best-track data from JTWC.

In this analysis, the model forecasts are evaluated in three stages of the evolution of Nuri (Table 1). The first group of forecasts are during the formation stage of Nuri. The second group of forecasts focuses on the intensification stage of Nuri. The final group of forecasts are during the decay stage of Nuri.

Table 1. Beginning and ending times for the three stages in the life cycle of Nuri.

Stage	Beginning	End
Formation	0000 UTC 16 August	1200 UTC 17 August
Intensification	0000 UTC 18 August	0000 UTC 19 August
Decay	1200 UTC 19 August	0000 UTC 21 August

A. INTENSITY

Initially, the minimum MSLP and maximum wind will be used to examine the forecasts from COAMPS-TC and the ECMWF. Because the ECMWF output was available on pressure surfaces at 50-hPa intervals, the maximum wind will be measured at 950 hPa for both models and then at 10 meters for the COAMPS-TC model.

1. Formation Stage

The evaluation of the COAMPS-TC during the formation stage were for forecast initial conditions prior to the time Nuri was declared by JTWC to be a tropical storm (Table 1). During this stage, Nuri was still a tropical disturbance and tropical depression,

so no TC synthetic observations were created in the COAMPS-TC model. Also, only the outer two grids were used in COAMPS-TC until Nuri was declared a tropical storm on 1200 UTC 17 August. At that time grid 3 was initialized and grid 2 and 3 became moving nests within grid 1.

During the formation stage, ECMWF model only slowly deepened Nuri (Figure 6), which may be due to Nuri being a small storm and the ECMWF does not use any synthetic observations or TC bogus vortex for the structure. A similar lack of deepening was predicted on the COAMPS-TC model grid 1 (Figure 7), as the forecast MSLPs were steady around 1010 hPa prior to the 1200 UTC 17 August forecast when the bogus vortex was introduced in the model. Although the formation stage of Nuri was better predicted in grid 2 (Figure 8) as a deepening trend was clearly indicated, the pressures were still too high. By 1200 UTC 17 August, the grid 2 forecast had attained the lowest pressure during this stage. The 1200 UTC 17 August model run is the first run with grid 3 included that begins at the end of the formation stage. The forecast MSLP was only off by 10 hPa (Figure 9), but peak intensity was reached 12 hours too early. Therefore, the ECMWF and COAMPS-TC models made poor predictions during the formation stage of Nuri. However, the forecasts in the inner grids of the COAMPS-TC model were improved relative to grid 1.

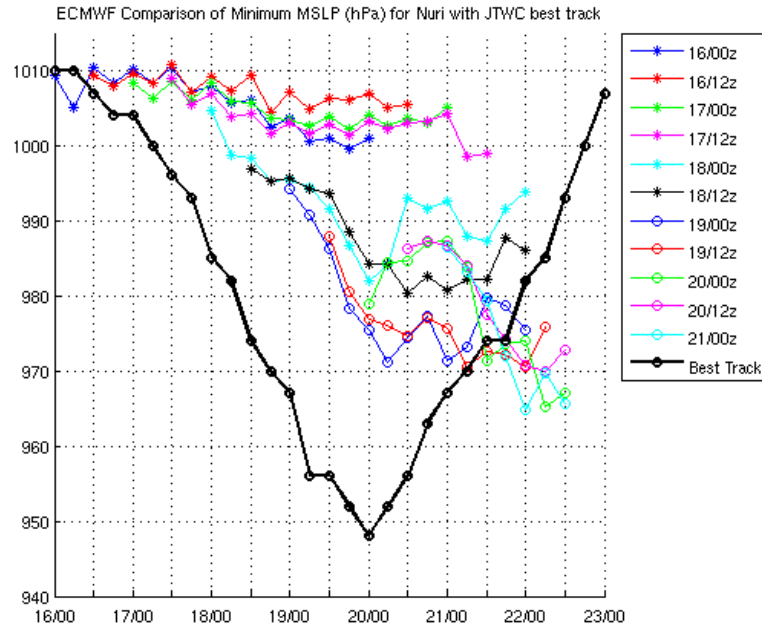


Figure 6. ECMWF forecasts of MSLP (hPa) from various initial times (DDHHs, see insert) compared to the JTWC best-track MSLP values for Nuri.

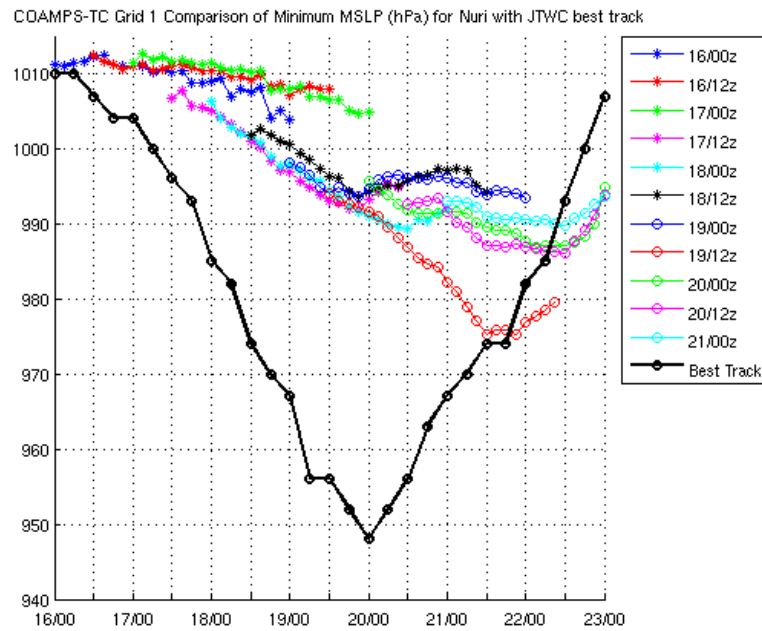


Figure 7. COAMPS-TC grid 1 forecasts of MSLP (hPa) from various initial times (DDHHs, see insert) compared to the JTWC best-track MSLP values for Nuri.

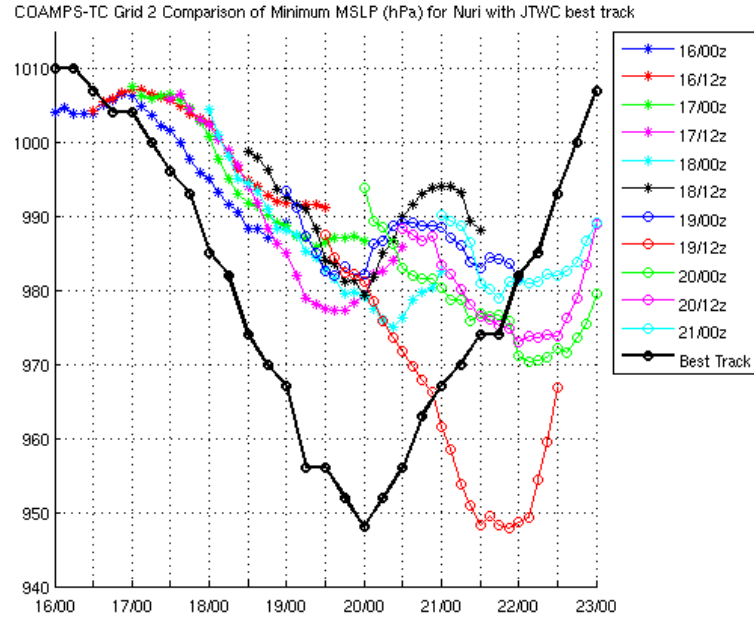


Figure 8. COAMPS-TC grid 2 forecasts of MSLP (hPa) from various initial times (DDHHs, see insert) compared to the JTWC best-track MSLP values for Nuri.

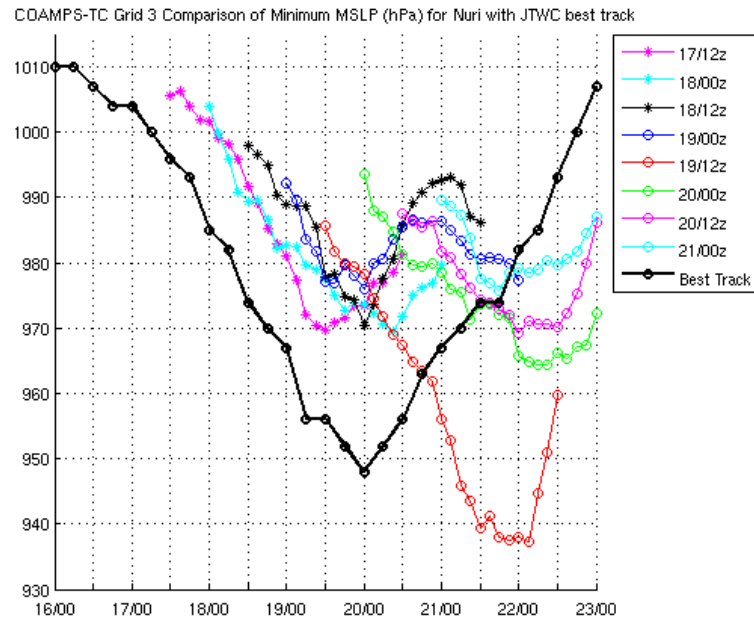


Figure 9. COAMPS-TC grid 3 forecasts of MSLP (hPa) from various initial times (DDHHs, see insert) compared to the JTWC best-track MSLP values for Nuri. Grid 3 forecasts only began with the 1200 UTC 17 August integration when JTWC had declared Nuri was a tropical storm.

Because the surface winds were not available in the archived ECMWF forecasts available for this analysis of Nuri, the 950-hPa winds will be utilized. For the ECMWF forecasts (Figure 10) initiated during the formation stage, the maximum winds at 950 hPa do not reflect the increasing values that are depicted in the JTWC best-track, which is the maximum surface winds. The same deficiency was exhibited by the COAMPS-TC grid 1 950-hPa (Figure 11, comparable to Figure 10) or the 10-meter wind (Figure 12) forecast prior to 1200 UTC 17 August when the COAMPS-TC initial conditions contained Nuri. When the COAMPS-TC included the Nuri bogus vortex, the COAMPS-TC grid 1 forecast wind speeds increased dramatically at both 950 hPa (Figure 11) and 10 meters (Figure 12). For example, the 1200 UTC 17 August model run that began with the correct 35 kt wind speed at 10 m did intensify but was too low by about 40 kt when Nuri reached peak intensity (Figure 12). Since the early COAMPS-TC grid 1 950-hPa maximum wind forecasts (Figure 11) were similar to those from the ECMWF (Figure 10) in that they did not indicate an increase in wind speed with time, it is concluded that an inaccurate definition of the TC structure is likely contributing to the poor predictions during the formation stage of Nuri.

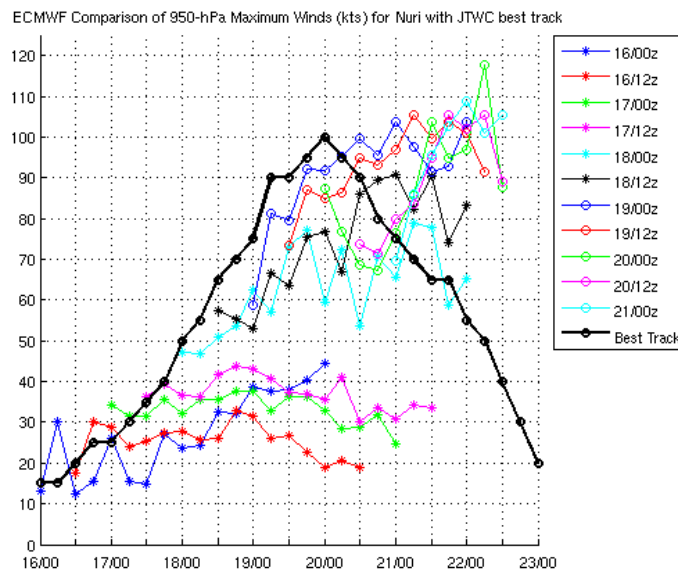


Figure 10. ECMWF forecasts of maximum winds (kt) at 950 hPa from various initial times (DDHHs, see insert) compared with the JTWC best-track maximum wind values for Nuri.

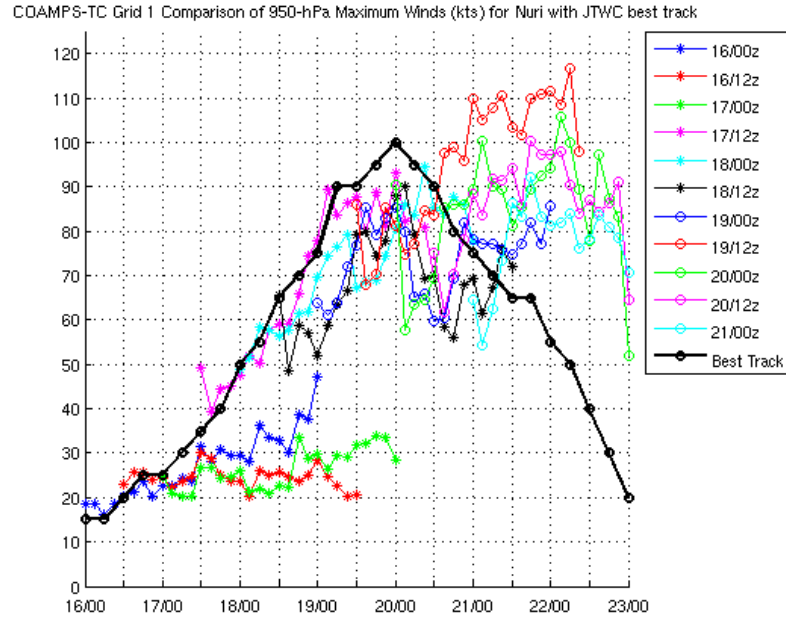


Figure 11. COAMPS-TC grid 1 forecasts of maximum winds (kt) at 950 hPa from various initial times (DDHHs, see insert) compared with the JTWC best-track maximum wind values for Nuri.

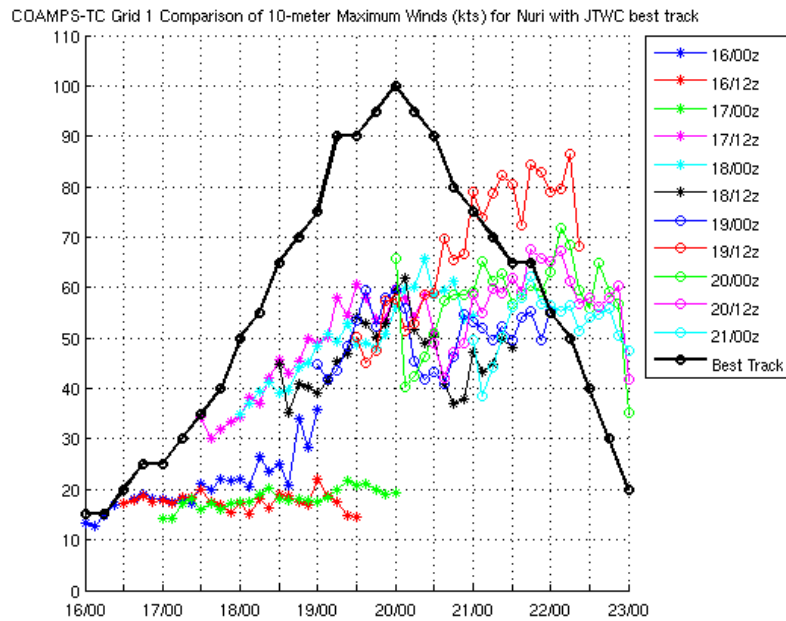


Figure 12. COAMPS-TC grid 1 forecasts of 10-m maximum winds (kt) from various initial times (DDHHs, see insert) that may be more directly compared with the JTWC best-track maximum wind values for Nuri.

The predictions of the formation of Nuri in the COAMPS-TC grid 2 forecasts (Figures 13 and 14) were a significant improvement from that of grid 1 and the ECMWF model. This improvement is attributed to a better definition of the vortex in the initial conditions. The initial 950-hPa wind maximum (Figure 13) of 30 kt and 10-m wind (Figure 14) for the 0000 UTC 16 August COAMPS-TC grid 2 run exceeded the JTWC maximum surface wind estimate of 15 kt. This forecast did result in an intensification and the 950-hPa maximum winds for grid 2 (Figure 13) were similar to the 10-meter maximum winds (Figure 14), except that they were a little higher, which is to be expected. In fact, the maximum 950-hPa winds were forecast on grid 2 to be higher than the best-track intensity.

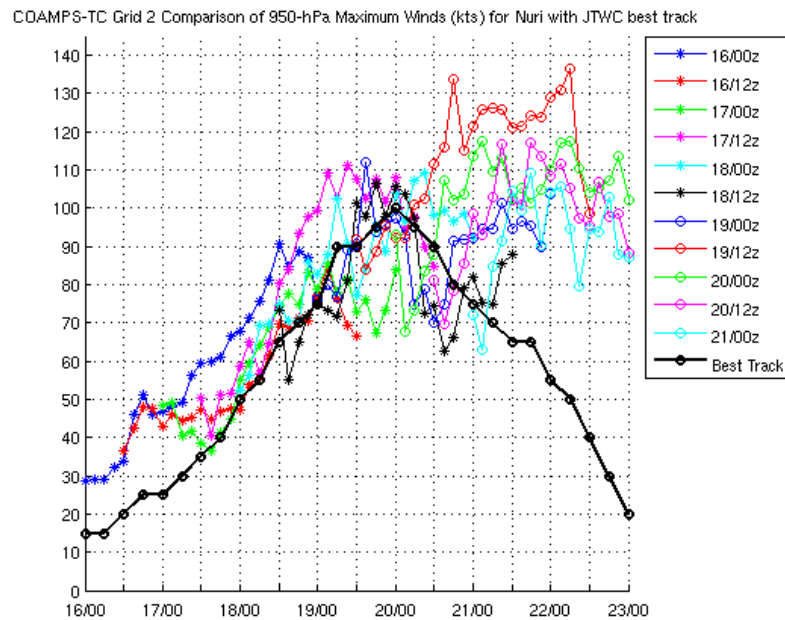


Figure 13. COAMPS-TC grid 2 forecasts of maximum winds (kt) at 950 hPa from various initial times (DDHHs, see insert) compared with the JTWC best track maximum wind values for Nuri.

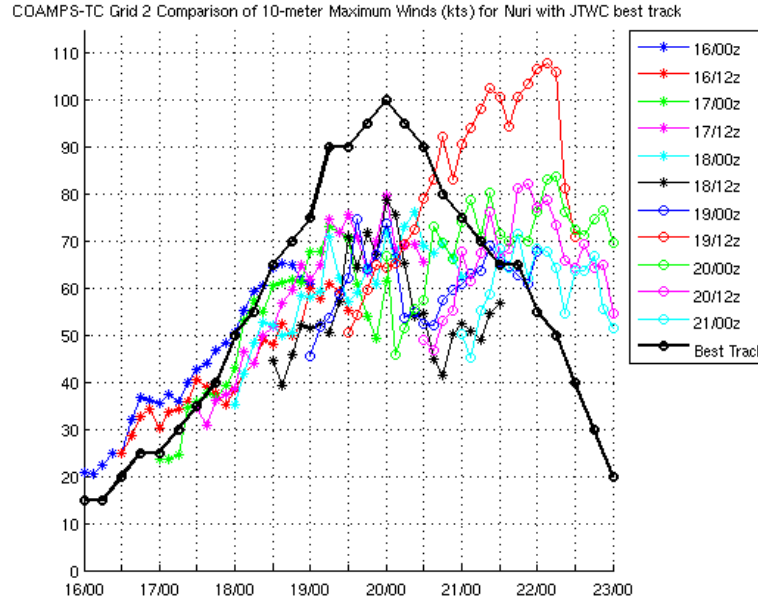


Figure 14. COAMPS-TC grid 2 forecasts of 10-m maximum winds (kt) from various initial times (DDHHs, see insert) that may be more directly compared with the JTWC best-track maximum wind values for Nuri.

As indicated previously, the first COAMPS-TC grid 3 forecast was begun when JTWC declared Nuri was a tropical storm at 1200 UTC 17 August. The grid 3 integration from this time has an accurate prediction of the 950-hPa (Figure 15) and 10-m (Figure 16) winds in terms of the intensification trend. The forecast 10-m wind speed had the peak intensity at the correct time, but was 15 kt lower than the actual wind speed. This COAMPS-TC grid 3 integration again indicates the importance of a representative vortex in the initial conditions during the formation stage.

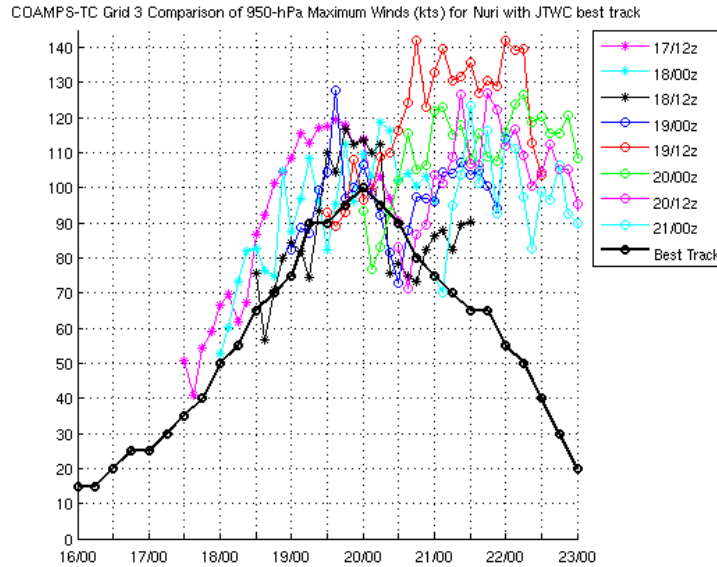


Figure 15. COAMPS-TC grid 3 forecasts of maximum winds (kt) at 950 hPa from various initial times (DDHHs, see insert) compared with the JTWC best-track maximum wind values for Nuri. Grid 3 forecasts only began with the 1200 UTC 17 August integration when JTWC had declared Nuri was a tropical storm.

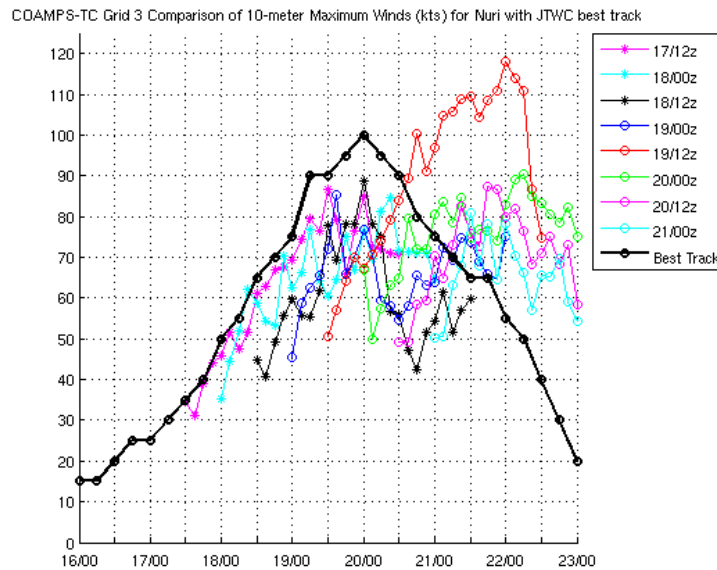


Figure 16. COAMPS-TC grid 3 forecasts of 10-m maximum winds (kt) from various initial times (DDHHs, see insert) that may be more directly compared with the JTWC best-track maximum wind values for Nuri. Grid 3 forecasts only began with the 1200 UTC 17 August integration when JTWC had declared Nuri was a tropical storm.

2. Intensification Stage

Nuri was a tropical storm at the beginning of the intensification stage (as defined in Table 1) and intensified into a category 1 typhoon by the end of the period. The ECMWF and COAMPS-TC forecasts in Figures 6-16 that began during this intensification stage will be described in this subsection. During the intensification stage, the ECMWF forecasts began with initial MSLPs that were 25-30 hPa higher than are specified in the JTWC best-track (Figure 6). In the 0000 UTC 18 August model run, the forecast MSLP had the correct deepening trend and the timing of the minimum MSLP was correct, but the magnitude was approximately 30 hPa higher than the best track. In the subsequent ECMWF integrations beginning from 1200 UTC 18 August and 0000 UTC 19 August, the forecasts had the correct deepening trend but the timing of the minimum MSLP came later than the timing of the observed minimum MSLP (Figure 6). Although the 0000 UTC 19 August ECMWF model run deepened Nuri the most, the minimum MSLP was 20 hPa too high at peak intensity.

The COAMPS-TC grid 1 forecasts (Figure 7) also did not have accurate initial MSLP values during the intensification stage. The minimum MSLP forecasts had the correct deepening trend, but these grid 1 forecasts only had a weak indication of the actual maximum intensity of Nuri. Although the COAMPS-TC grid 2 MSLP forecasts during the intensification stage (Figure 8) also began from MSLPs of Nuri that were too high, these forecasts had a better representation of the deepening trend than the grid 1 forecasts. However, the magnitude of the forecast minimum MSLP was far too weak. The primary differences between MSLP forecasts in grid 2 (Figure 8) and grid 3 (Figure 9) are that the profiles of MSLP in the grid 3 model depict a sharp decrease in pressure that results in a single minimum value rather than a rounded curve of minimum values on grid 2. Although the forecast minimum MSLP in the 1200 UTC 18 August grid 3 forecast is over 20 hPa too high, the shape of the minimum MSLP evolution is similar to that of the best track. As was the case during the formation stage, the COAMPS-TC forecasts of minimum MSLP dramatically improved with higher grid resolution.

For the ECMWF forecasts during the intensification stage, the 950-hPa maximum winds (Figure 10) had initial values that were 10-20 kt lower than the JTWC best-track. All three ECMWF forecasts from 0000 UTC 18 August through 0000 UTC 19 August increased the winds, but then the winds were predicted to keep increasing after Nuri reached peak intensity. The 0000 UTC 19 August model run had maximum winds that were only 10 kt too low compared to the JTWC best-track at the time of peak intensity (0000 UTC 20 August). By comparison, the 1200 UTC 18 August model run was 20 kt too low and the 0000 UTC 18 August run was 40 kt too low at the time of peak intensity.

After a 12-h period of adjustment during which the winds decreased, the COAMPS-TC grid 1 950-hPa forecast maximum winds (Figure 11) increased steadily during the intensification stage. However, the forecast 10-meter maximum winds on grid 1 (Figure 12) were very low compared to the JTWC best-track. This excessive vertical wind shear in the lowest 50 hPa in the COAMPS-TC grid 1 is attributed to excessive boundary layer/frictional effects, although the initial conditions for these grid 1 forecasts during the intensification stage were also too low.

In Figure 14, the COAMPS-TC model grid 2 10-m winds at the initial times were 10-30 kt too low. These model grid 2 forecasts had the correct intensification trend compared to the JTWC best-track and reached peak intensity at about the right time but were 20 kt too low. For example, the 1200 UTC 18 August and 0000 UTC 19 August forecasts under-intensified Nuri after the initial adjustment period of about 12 h. As was the case during the formation stage, the COAMPS-TC grid 2 950-hPa forecast maximum winds (Figure 13) were consistently higher than the best-track winds. However, the intensification trend of the wind maxima was quite accurate, as was the timing of the 950-hPa maximum winds. Given that the 950-hPa winds were too high (Figure 13) and the 10-m (Figure 14) winds on grid 2 were too low, the boundary layer processes are likely contributing to an excessive vertical wind shear in this layer.

The COAMPS-TC grid 3 forecasts had similar error characteristics as the grid 2 forecasts during the intensification stage. The initial 950-hPa maximum winds were too large, a large decrease occurred in the first 12 h, and then the intensification was too

strong so that these maximum winds exceeded the JTWC best-track values (Figure 15). The initial grid 3 10-m maximum winds during the intensification stage were too small by about 15 kt, 30 kt, and 40 kt at 1200 UTC 18 August, 0000 UTC 19 August, and 1200 UTC 10 August (Figure 16). Nevertheless, the maximum winds were 10-20 kts lower than the JTWC best-track at peak intensity, with the 1200 UTC 18 August run resulting in winds that were only 10 kt too low. Consequently, some attention must be given to the specification of the COAMPS-TC grid 3 vortex.

3. Decay Stage

The decay stage includes the 1200 UTC 19 August through 0000 UTC 21 August model runs. The ECMWF and the three grids of the COAMPS-TC all had great difficulty forecasting the decay stage. In each case, the MSLP forecast was that Nuri would continue to deepen and the maximum winds would be increasing when in reality Nuri was starting to fill and weaken. The 1200 UTC 19 August forecasts, which had the largest MSLP and maximum wind errors, will be examined in detail later in this section.

During this decay stage, the ECMWF MSLP forecasts (Figure 6) for Nuri began from initial conditions that were 20-30 hPa too high. These forecasts were consistent in predicting that the MSLP would decrease or at least hold steady when in reality Nuri was filling. The COAMPS-TC grid 1 MSLP forecasts (Figure 7) also began from initial conditions that were too high by 20-40 hPa depending on the forecast. The 1200 UTC 19 August model forecast deepened Nuri to 975 hPa but the time of maximum intensity was 36 hours after the actual time of maximum intensity. The other grid 1 forecasts slowly deepened Nuri by 5-10 hPa and then held the MSLP steady.

The COAMPS-TC grid 2 1200 UTC 19 August forecast was significantly too deep (Figure 8) and late on the timing of lowest MSLP. Although the magnitudes of MSLP errors in subsequent grid 2 forecasts were less than those of 1200 UTC 19 August, all forecasts increased the intensity rather than decreasing as in the JTWC best-track. Similar characteristics existed in the grid 3 forecasts of MSLP (Figure 9). The 1200 UTC 19 August grid 3 forecast began with initial conditions with MSLP that was 30 hPa too

high, but then deepened Nuri to 938 hPa 48 h after the storm actually reached lowest MSLP. All subsequent grid 3 forecasts also deepened the storm when Nuri was filling.

During the decay stage, all ECMWF forecasts (Figure 10) continued to increase the maximum winds at 950 hPa rather than reduce the winds. The initial values of the 950-hPa maximum winds were too low in all of the ECMWF forecasts during the decay stage. The COAMPS-TC grid 1 10-m wind forecasts also began with initial values that were too low by 30-40 kt (Figure 12). All of the COAMPS-TC grid 1 forecasts of 950-hPa and 10-m winds (Figures 11 and 12) increased the wind speed, with the 1200 UTC 19 August forecast having the largest increases. The 950-hPa maximum winds forecast on grid 1 (Figure 11) were closer to the best-track values, but the 10-m winds (Figure 12) were consistently too low. The 1200 UTC 19 August forecast had a maximum wind of 85 kt at 10 m and 118 kt at 950 hPa at 0600 UTC 22 August, which were significantly too high.

The grid 2 forecasts did start to weaken the storm, but not until the last 12-h period of the forecast. All of the grid 2 maximum winds forecasts at 950 hPa and 10 m (Figures 13 and 14) also increased the winds when Nuri was actually weakening. Only the final model forecast predicted a decrease in the maximum winds during the last 12-h of the grid 2 forecast. The 1200 UTC 19 August model forecast intensified Nuri the most with a maximum wind of 109 kt at 10 meter on 0600 UTC 22 August.

The 950 hPa and 10 m wind forecasts on COAMPS-TC grid 3 (Figures 15 and 16) also continued to increase the maximum winds in all forecasts until the last 12-h period of the forecast. At that point, the winds during the decay stage were on average 40 kt too high. The 1200 UTC 19 August model run had a maximum wind of 120 kt at 10 m and 140 kt at 950 hPa. The maximum winds at both levels occurred nearly 48 hours too late.

According to COAMPS-TC experts Rich Hodur and Jim Doyle, the likely explanation for the continued high winds during the decay stage was a “flux boost” at high winds. That is, the surface exchange coefficients had been increased at high wind speeds based on some experiments in which higher exchange coefficients were required

to account for sea spray at high winds. The consistent aspect in all stages of the Nuri development was that COAMPS-TC forecasts were more accurate at higher resolution (grid 3). During the formation stage, forecasts by the ECMWF and on the COAMPS-TC grid 1 were too weak, but the grids 2 and 3 forecasts predicted formation more accurately. During the intensification stage, the ECMWF and grid 1 of the COAMPS-TC forecasts were similar in that they depicted intensification, but were too weak. During the decay stage, the ECMWF and COAMPS-TC grids 1-3 forecasts were consistent in that they continued to intensify rather than decay the storm.

4. Intensity Error

The summary of intensity errors by the COAMPS-TC for the initial times of 1200 UTC 17 August to 0000 UTC 21 August indicate a trend of under-forecasting intensity at short-range intervals to over-forecasting intensity at larger range intervals (Figure 17). The sample size (Table 2) is small since only one storm is analyzed. The under-forecast error in the first 30 h is attributed to unrepresentative initial conditions for the vortex. The over-forecast after 30 h is attributed (at least in part) to the flux boost for the surface heat and moisture exchange at high wind speeds.

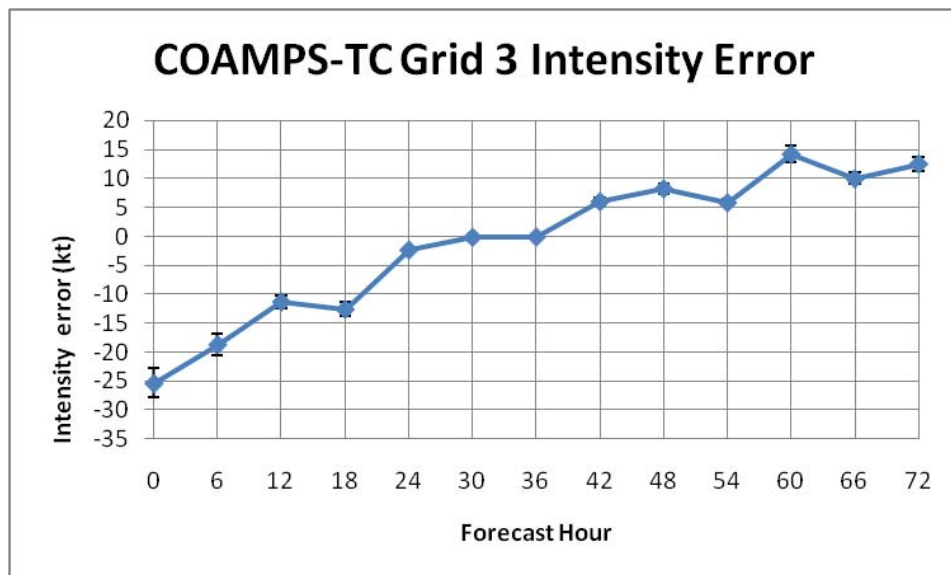


Figure 17. COAMPS-TC grid 3 intensity errors (kt) for forecasts of Nuri each 12 h from initial conditions between 1200 UTC 17 August and 0000 UTC 21 August. Error bars represent a 10% variation in mean values.

Table 2. Sample sizes for intensity forecast errors in Figure 17.

Sample Sizes for Intensity Error	
Forecast Hour	# of Forecasts
0-48	8
54-60	7
66-72	6

B. TRACK

Numerical model forecasts provide more accurate guidance for forecasting the track than for forecasting the intensity of tropical cyclones. This is true in the case of Typhoon Nuri. Most current research is focused on mesoscale models that can accurately predict the intensity of the tropical cyclones. The primary reason for the slower progress was stated in Marks and Shay (1998): track prediction depends more on large-scale processes, and intensity depends on the inner-core dynamics and its relationship to the environment (Davis et al., 2008).

The ECMWF forecast tracks are based on the center location of the 975-hPa wind center while the COAMPS-TC grid 3 forecast tracks are based on the MSLP locations. The ECMWF forecast tracks start at 0000 UTC 16 August and go through 0000 UTC 21 August. The COAMPS-TC grid 3 forecasts start at 1200 UTC 17 August when Nuri became a tropical storm and extend through 0000 UTC 21 August. Whereas the ECMWF tracks were manually established, the COAMPS-TC locations were generated in the model post-processing as one of the output variables during the TCS-08 experiment. The sample size varied for each model since the ECMWF forecast tracks include the times when Nuri was a tropical depression and the COAMPS-TC forecast tracks do not start until Nuri reached tropical storm strength (Table 3).

Table 3. Sample sizes for COAMPS-TC and ECMWF track errors.

Sample Sizes for Track Error		
Forecast Hour	# of Forecasts	
	COAMPS-TC	ECMWF
0-48	8	11
54-60	7	10
66-72	6	9

Overall, the ECMWF model forecast track errors were smaller than the COAMPS-TC grid 3 errors, except for the initial time (Figure 18). These COAMPS-TC track errors for Typhoon Nuri are similar to the track errors of all the typhoons during TCS-08 (Figure 19). The track errors for Nuri are worse at the larger time steps compared to the overall TCS-08 sample track errors. Notice also in Figure 19 that the COAMPS-TC errors are very similar to the errors of the NOGAPS model, which is the parent model for COAMPS-TC. Since the TC motion is primarily determined by the large-scale circulations, the COAMPS-TC errors likely arise from the background flow from the NOGAPS model. The ECMWF had the smallest track errors throughout the TCS-08 experiment (Figure 19), which is the same result as the Typhoon Nuri track error, and may be attributed to a superior forecast of the large-scale circulation by the ECMWF model.

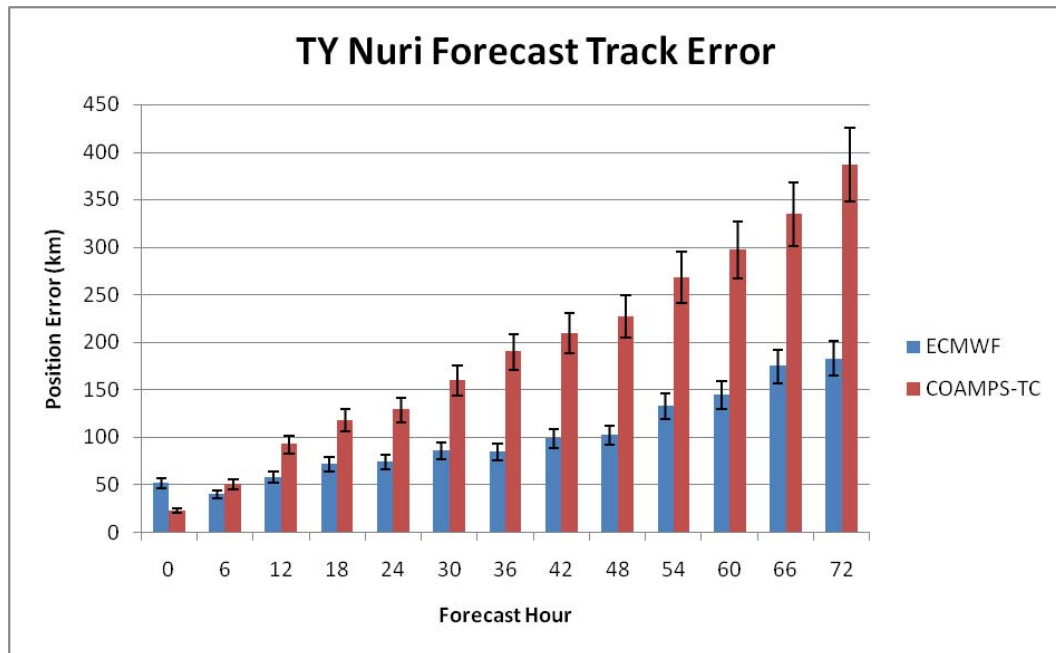


Figure 18. Track errors (km) for the ECMWF and COAMPS-TC models. Error bars represent a 10% variation in mean values.

Track Errors for COAMPS-TC during TCS-08

Homogeneous Sample Compared to all Models for TC 08W-18W

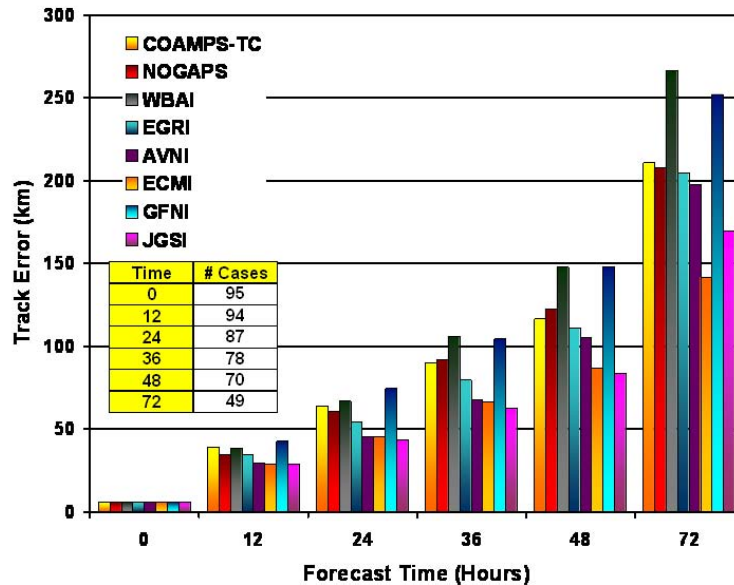


Figure 19. Track errors (km) for TC 08W-18W during TCS-08 for various models (see insert). Image courtesy of Mr. Buck Sampson, NRL-Monterey.

The ECMWF forecasts were especially accurate once Nuri intensified to typhoon strength (Figure 20), which again is probably due to a better prediction of the large-scale features that steered the storm. Since the ECMWF does not insert a bogus vortex for the TC, this may have caused some initialization issues when the storm was weak. For the 0000 UTC 16 August model run, the initial position was 84.5 km to the south/southwest of the best track position, while the 1200 UTC 17 August model run had the largest initial position error of 178 km to the south/southwest. The forecasts initialized between 0000 UTC 16 August – 1200 UTC 17 August tended to turn Nuri to the north and northeast. Starting with the 0000 UTC 18 August run, the ECMWF model initial position is in-line with the best track and only slightly diverges at the end on the position of landfall into China.

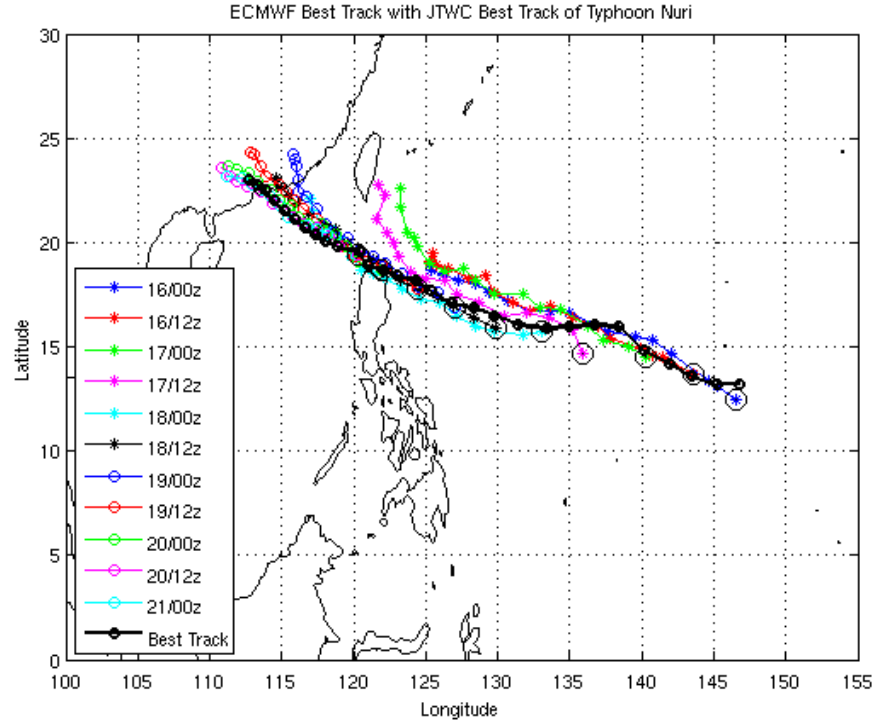


Figure 20. Comparison of ECMWF track forecasts and JTWC best-track as in Figure 1.

Although the initial position errors in the grid 3 COAMPS-TC forecasts were smaller than those of the ECMWF (Figure 18), the forecast errors were larger than for the ECMWF (Figure 21). The smaller initial position errors may be due to the NAVDAS relocation of the center from the model predicted center at analysis time to the JTWC center. The COAMPS-TC grid 3 track forecast errors were largest for the 1200 UTC 17 August model run since the forecast track was first northwestward and then later shifted to a westward motion. Starting with the 1200 UTC 18 August COAMPS-TC forecast, the early motion was along the best track but during the last 24-48 h the model forecast a northward turn while the storm actually moved northwestward (Figure 21).

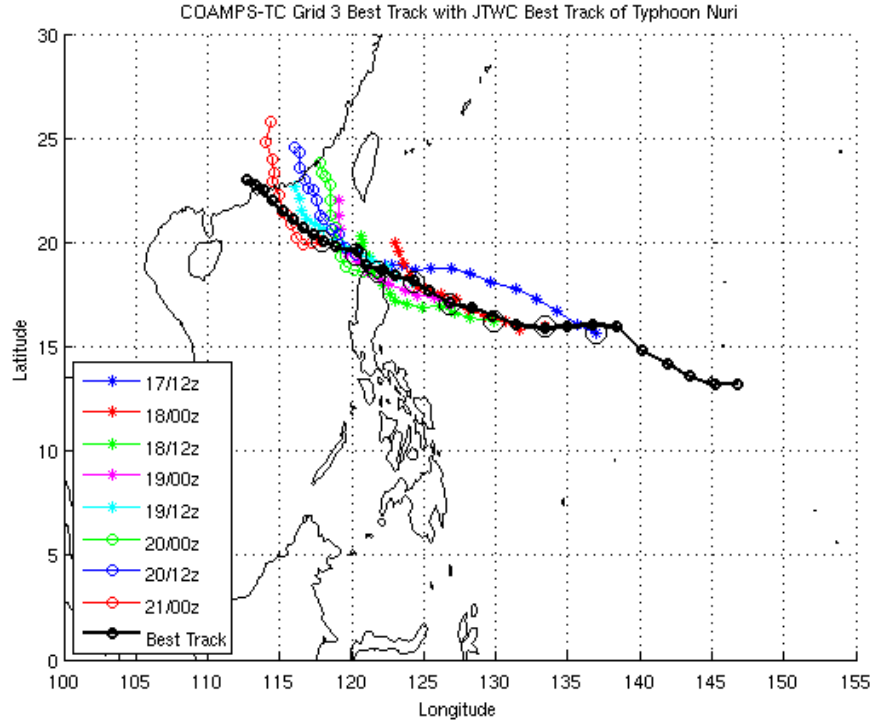


Figure 21. Comparison of COAMPS-TC grid 3 track forecasts with the JTWC best-track as in Figure 1.

C. STRUCTURE FORECAST CHARACTERISTICS

To measure how well the COAMPS-TC model depicted the storm structure, the model-derived radar reflectivity is compared to the 85 Ghz – 91 Ghz microwave satellite imagery for all three stages. Since the radar reflectivity is an accumulated quantity, no image is available at the initial time and the comparison is done for the 12-h through 72-h forecasts. Other comparisons include the forecast vertical wind shear values for the 200-850 hPa layer averaged between 4-6 deg. radii from the storm center, and the azimuthally-averaged tangential winds, cloud water, radial winds, and vertical velocity representative for times during the intensification and decay stages. To obtain a large enough area to get accurate values for the vertical wind shear, grid 2 will be examined. Only the deep layer vertical wind shear (200-850 hPa) will be examined since Nuri was a mature storm and extended past 500 hPa.

1. Formation Stage

For the formation stage, the 1200 UTC 16 August model run is examined. Recall that prior to the formation time, the model was only run with grid 1 and grid 2. For the 12-h COAMPS-TC forecast valid at 0000 UTC 17 August (Figure 22a), Nuri was a tropical depression with no closed eyewall and a symmetric but sporadic convective distribution in the satellite imagery (Figure 22b). A string of deep convective cells existed along the southern portion of the circulation center. The 12-h forecast convection is located along a line oriented northeast-southwest that is approximately 200 km north of the center. This feature may be associated with a wave in the easterlies that had been approaching the area over several days. Whether this forecast convection (Figure 22a) is related to the two outer bands of convection to the east of the center in the infrared portion of Figure 22b is not obvious.

The 24-h forecast (Figure 22c) has an asymmetric distribution of convection with the strongest cell just to the west of the center. The corresponding satellite image also has an asymmetric structure with one primary deep convective cell, but it is located just to the south of the center. The forecast (Figure 22c) continues to have another convective region to the north of the center that again may be related to the easterly wave. By contrast, a region of enhanced convection in the microwave imagery (Figure 22d) is more to the northeast of the center at about four deg. latitude radius.

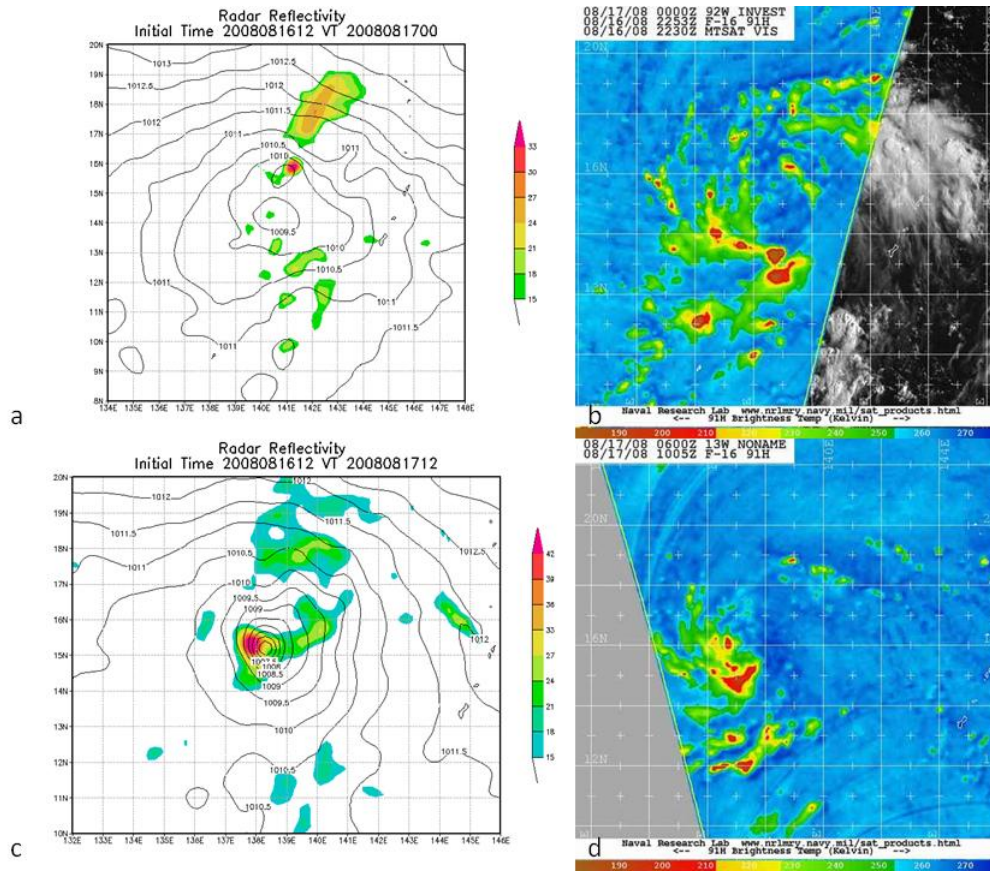


Figure 22. Simulated radar reflectivity from the 1200 UTC 16 August COAMPS-TC model run that verifies at (a) 0000 UTC 17 August, and (c) 1200 UTC 17 August. Microwave imagery at 91 Ghz at (b) 2253 UTC 16 August, and (d) 1005 UTC 17 August. Satellite imagery from http://www.nrlmry.navy.mil/sat_products.html.

In the 0000 UTC 18 August satellite image (Figure 23b), Nuri outer convection has become organized into a long band that covers all sides except the northeast, with concentrated convection just to the south of the center. No closed eye exists at this time. This 36-h forecast (Fig. 23a) has the precipitation on the southwest side of the storm but no banded structure is evident. The heaviest convection is forecast to be just to the west of the center. The forecast also continues to have an area of precipitation to the north-northeast of the center that is not verified in the satellite imagery.

The 48-h forecast radar reflectivity (Figure 23c) has the deep convection along the southern periphery of the center, which corresponds somewhat to the satellite image (Figure 23d) that has the heaviest convection wrapping around the southern semi-circle of

the center. At this forecast interval, the outer regions have extensive convection that wraps around most of the circulation. By contrast, the microwave imagery reveals more of a comma-shaped region of convection wrapping around the western and southern quadrants and minimum deep convection to the northeast.

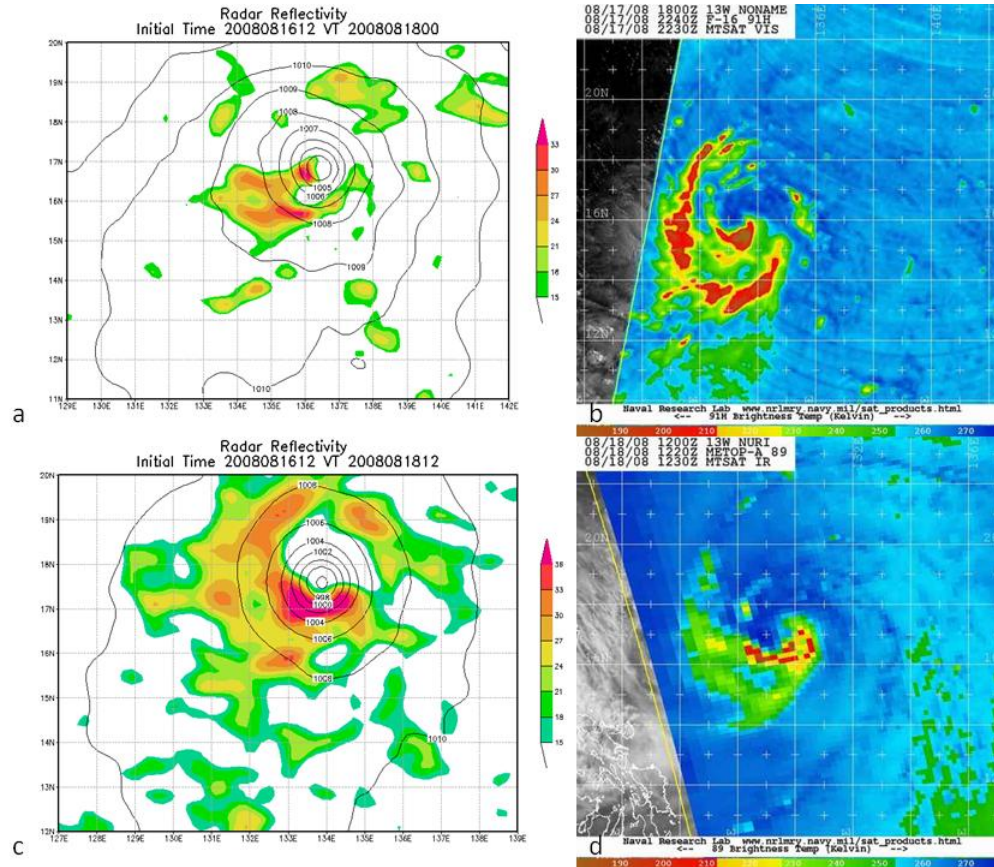


Figure 23. Simulated radar reflectivity from the 1200 UTC 16 August COAMPS-TC model run that verifies at (a) 0000 UTC 18 August, and (c) 1200 UTC 18 August. Microwave imagery at 91 GHz and 89 GHz respectively at (b) 2240 UTC 17 August, and (d) 1220 UTC 18 August. Satellite imagery from http://www.nrlmry.navy.mil/sat_products.html.

Although Nuri had already been a typhoon for 12 h by 0000 UTC 19 August, the eye was not well-defined in the NOAA-17 satellite image (Figure 24b), which has an asymmetric distribution of convection with the heaviest convection to the southwest of the storm. In the verifying 48-h forecast (Figure 24a), the convection is also highly asymmetric with the most significant convection south-southwest of the center. The

COAMPS-TC model continues to predict more organized convection to the northeast of the center than is evident in the satellite image (Figure 24b).

In the 1200 UTC 19 August satellite image (Figure 24d), a closed eye is clearly visible with an asymmetric distribution of outer convection. The corresponding 72-h forecast (Figure 24c) now depicts the highly asymmetric distribution of convection quite well. A closed eye with the heaviest convection in the southern eyewall and the outer convection stretches to the southwest of the center. The precipitation was over-forecast on the western side and extended too far to the southwest of the center. Nevertheless, this 72-h forecast from 1200 UTC 16 August had a surprisingly accurate prediction of the convection of Nuri, especially considering the center is predicted to be displaced to the east of the actual center.

In summary, the forecast distribution of convection as represented by the model-derived radar reflectivity on the 15 km grid 2 became more representative of the satellite-defined distribution as Nuri intensified into a typhoon. In the early stages when convection was less widespread, the forecast convection seemed to be contained in isolated regions rather than reflecting the beginning stages of outer rainbands.

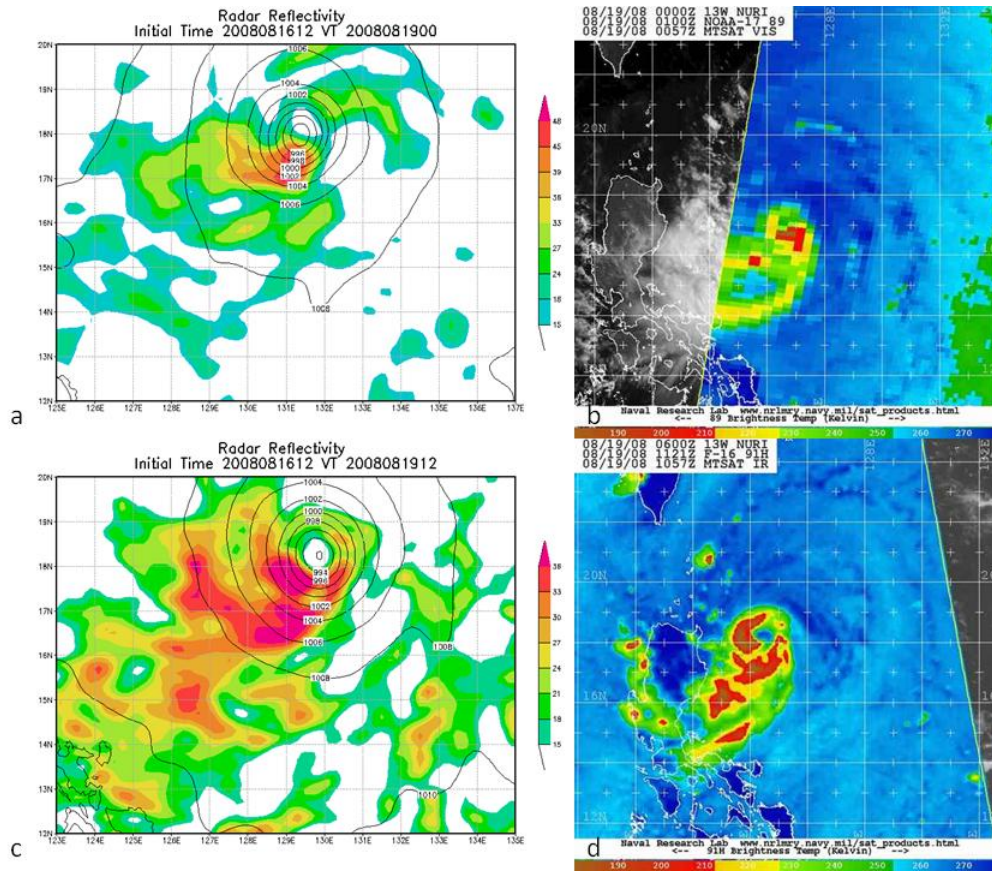


Figure 24. Simulated radar reflectivity from the 1200 UTC 16 August COAMPS-TC model run that verifies at (a) 0000 UTC 19 August, and (c) 1200 UTC 19 August. Microwave imagery at 89 Ghz and 91 Ghz respectively at (b) 0100 UTC 19 August, and (d) 1121 UTC 19 August. Satellite imagery from http://www.nrlmry.navy.mil/sat_products.html.

2. Intensification Stage

a. Simulated Radar Reflectivity

For the intensification stage, the 1200 UTC 18 August model run is examined. Because this time is after Nuri formed, grid 3 forecast fields are available. The microwave satellite image for 0000 UTC 19 August (Figure 25b) does not exhibit a closed eyewall; rather, convection is concentrated to the south of the center with two bands extending to the southwest of the center. In the 12-h forecast (Figure 25a), no closed eyewall is predicted, but most of the convection extends to the west of the storm and the heaviest convection is located to the southwest of the center. The model-derived

radar reflectivity also implies more deep convection to the northeast of the center than is evident in the satellite image (Figure 25b). The 24-h forecast (Figure 25c) is beginning to depict a closed eye with heaviest convection on the west and south side near the center. However, the model continues to predict too much convection northeast of the center where the satellite image (Figure 25d) indicates a minimum of deep convection. In the satellite image, a nearly closed eyewall is evident with the heaviest convection surrounding the eye except on the northeast side. In general, the 24-hour forecast had the correct shape of deep convection to the southwest side of the center, and the primary deficiency is the more extensive convection that is predicted to the northeast, which will be shown below to be a region with considerable vertical wind shear.

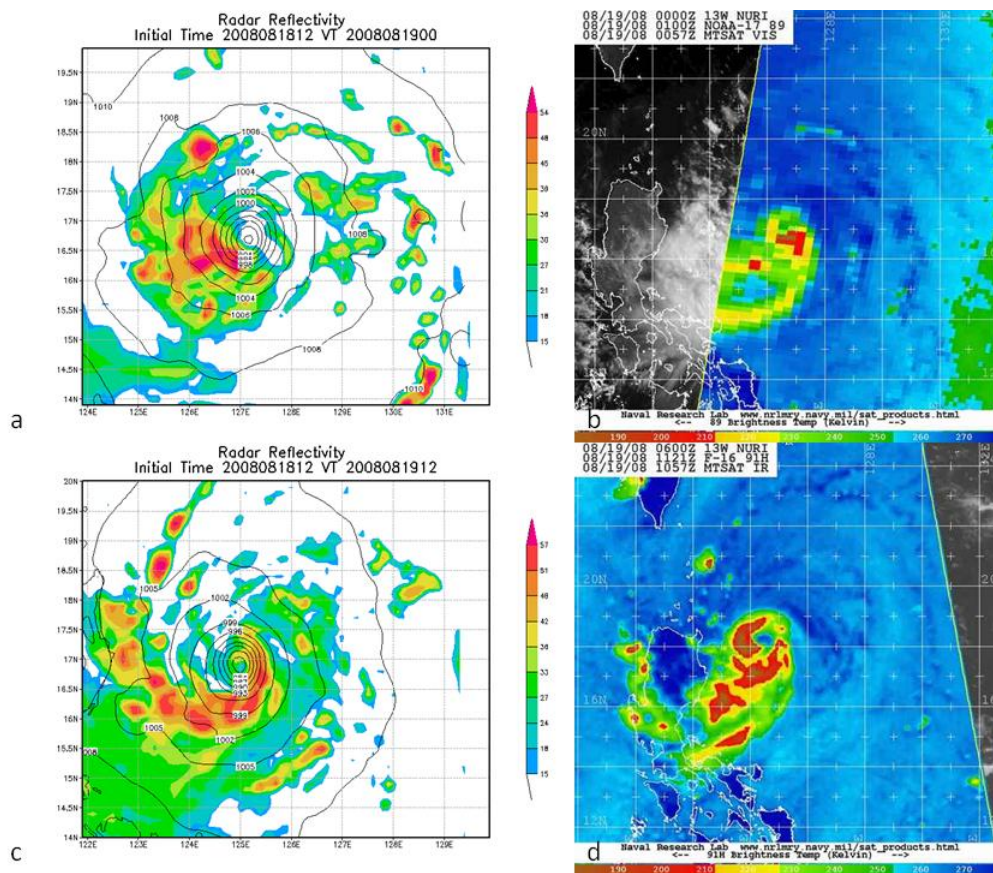


Figure 25. Simulated radar reflectivity from the 1200 UTC 18 August COAMPS-TC model run that verifies at (a) 0000 UTC 19 August, and (c) 1200 UTC 19 August. Microwave imagery at 89 Ghz and 91 Ghz respectively at (b) 0100 UTC 19 August, and (d) 1121 UTC 19 August. Satellite imagery from http://www.nrlmry.navy.mil/sat_products.html.

This 36-h forecast (Figure 26a) during the intensification still did not contain a closed eye, as convection is predicted on all sides except the northwest side. In the satellite image (Figure 26b), the eye is also open to the northwest, and the heaviest convection is located on the south side of the storm. The forecast correctly predicts that the outer convection will be highly asymmetric with maximum convection to the southwest of the center. An over-prediction of the outer convection to the east-northeast, and also far to the northwest, are the primary deficiencies in this 36-h forecast. In the 1200 UTC 20 August satellite image (Figure 26d), the decay stage has clearly begun as the eye has opened up with a partial eyewall on the south side. The bulk of the deep convection is located to the southwest and south of the center. The corresponding model-predicted radar reflectivity (Figure 26c) also has no closed eye with most of the convection to the west and south of the center. Except for the over-forecasting of the areal extent of the precipitation to the southwest, this 48-h forecast does correctly predict the highly asymmetric distribution of convection in Nuri.

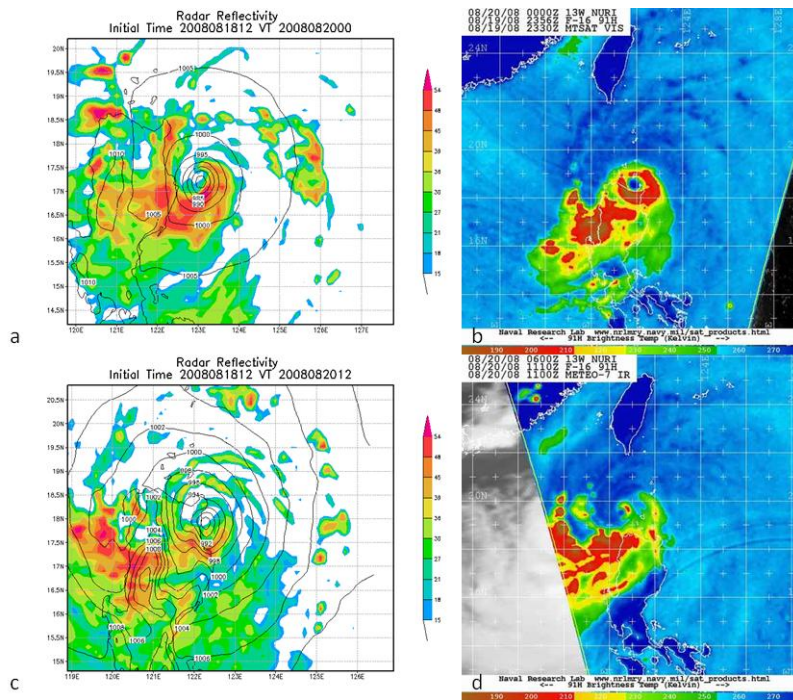


Figure 26. Simulated radar reflectivity from the 1200 UTC 18 August COAMPS-TC model run that verifies at (a) 0000 UTC 20 August, and (c) 1200 UTC 20 August. Microwave imagery at 91 Ghz at (b) 2356 UTC 19 August, and (d) 1110 UTC 20 August. Satellite imagery from http://www.nrlmry.navy.mil/sat_products.html.

In the 60-h forecast (Figure 27a), an open eye is predicted, especially on the western side. The major convection is predicted to be about 150 km to the southwest of the center. The corresponding satellite figure (Figure 27b) clearly depicts the decay of the storm with an open eye and the bulk of the deep convection is to the south of the storm. The model-predicted north-south oriented band to the south-southeast and northeast-southwest oriented outer band to the northwest of the center are not verified in the satellite image (Figure 27b). Further decay of Nuri is quite evident in the satellite image at 1200 UTC 21 August (Figure 27d), since no closed eye is present and the only deep convection is well to the southwest of the center of the storm. In the corresponding 72-h forecast (Figure 27c) a well-organized band of convection wraps around three-quarters of the storm center with the heaviest convection to the southeast of the center. Clearly, the 72-h forecast has a more intense storm with more organized convection than is actually occurring at this time, which was evident in the intensity forecasts (e.g., Figures 11-16).

Overall, the 1200 UTC 18 August forecast predicts the distribution of deep convection in a more consistent manner than did the 1200 UTC 16 August forecast from the formation stage. As the circulation intensified and convection became more organized, the model predicted radar-reflectivity had more features that were similar to the satellite imagery. As the storm matured and moved to the west-northwest, it became under the influence of vertical wind shear from the northeast (to be discussed in the next subsection). This contributed to the asymmetric structure with deep convection predominantly to the south and west of the center. To some extent, the forecast distribution of convection at the later forecast intervals in the 1200 UTC 18 August forecast was similar in location and shape to the observed distribution. Thus, the model-predicted vertical wind shear will be examined next.

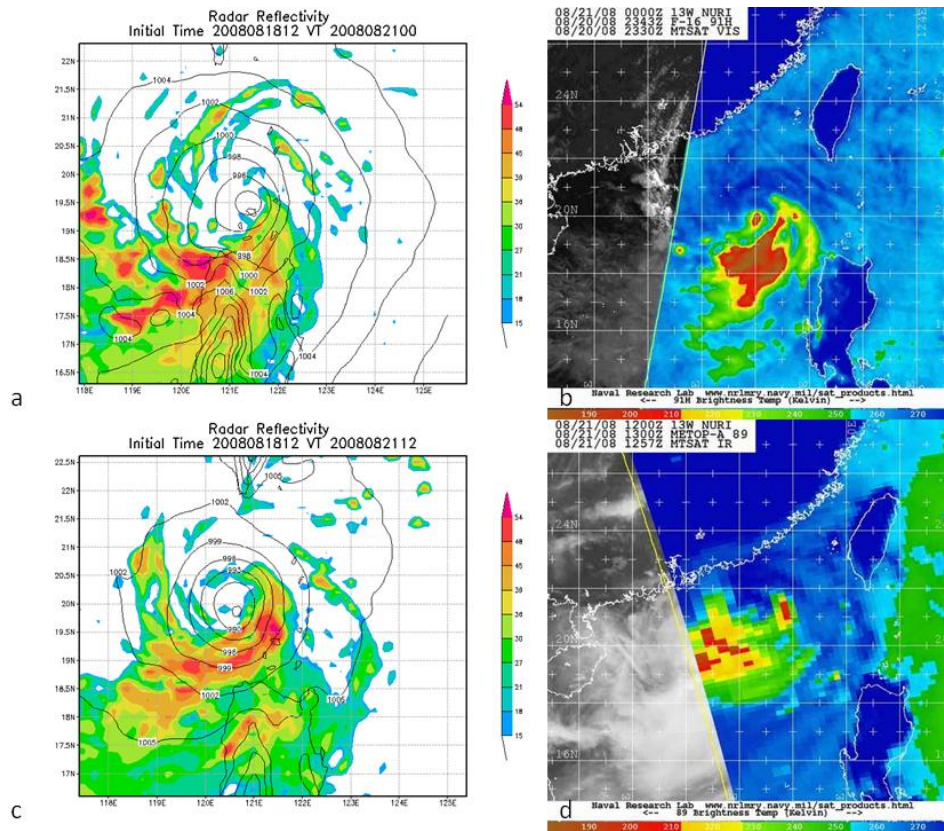


Figure 27. Simulated radar reflectivity from the 1200 UTC 18 August COAMPS-TC model run that verifies at (a) 0000 UTC 21 August, and (c) 1200 UTC 21 August. Microwave imagery at 91 Ghz and 89 Ghz respectively at (b) 2343 UTC 20 August, and (d) 1300 UTC 21 August. Satellite imagery from http://www.nrlmry.navy.mil/sat_products.html.

b. Vertical Wind Shear

An increase in vertical wind shear that may be inferred from the microwave satellite imagery was examined in the 1200 UTC 18 August forecast and subsequent forecasts (Figure 28). The 1200 UTC 18 August forecast has some oscillatory changes superposed on an increasing deep-layer vertical wind shear. Subsequent forecasts also have oscillatory changes superposed on an overall trend that is consistent with the corresponding analysis times. Note that the early vertical wind shear values exceeding 25 kt are generally considered marginal for tropical cyclone formation, and then a large increase in vertical shear begins around 1200 UTC 20 August 2008.

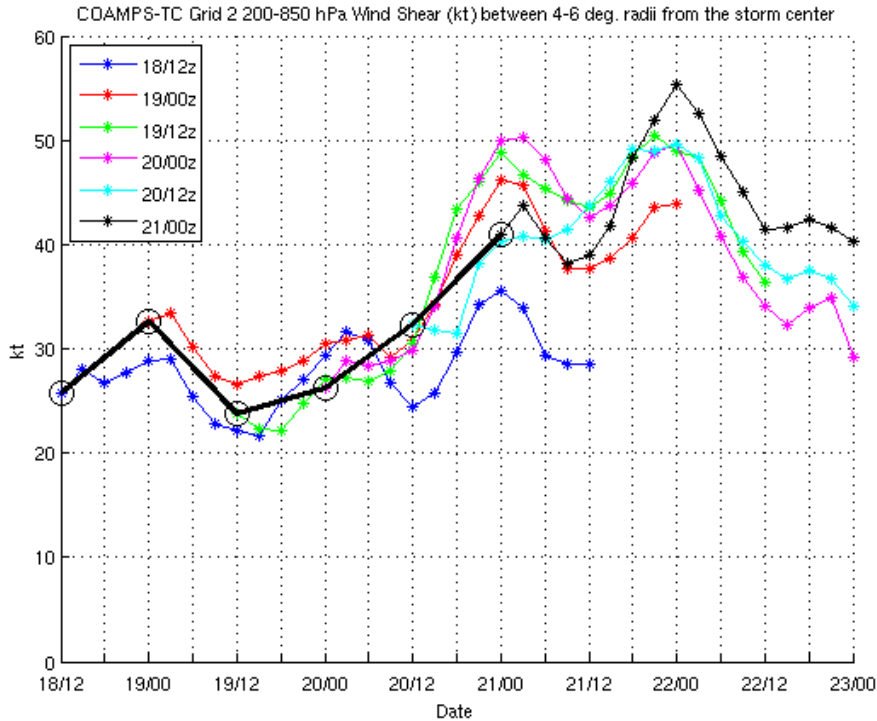


Figure 28. Vertical wind shear (kt) between 200-850 hPa for the COAMPS-TC grid 2 from 1200 UTC 18 August – 0000 UTC 21 August (see insert).

The asymmetric cloud distribution in the microwave satellite imagery suggests the storm was being sheared from the northeast because the deep convection was generally confined to the southwest side of the storm. The forecasts and verifying analyses of vertical wind shear from the 1200 UTC 18 August model run (Figure 29) confirm that the shear is from the east-northeast. Whereas the 12-h, 24-h, and 36-h forecast magnitudes vary only slightly from the verifying analysis magnitudes, the 48-h forecast (Figure 29d) has a shear direction from the east-northeast while the analyzed shear is now from the north-northeast and is about 10 kt greater than the forecast value. Such a shift in the wind shear direction is also not evident in a change in orientation of the radar reflectivity in the 48-h forecast (Figure 26c). The effect of the shift in direction and increase in wind shear magnitude in the analysis (Figure 29d) is evident in the 1200 UTC 20 August microwave satellite image (Figure 26d) by the clearing of deep convection to the north, an open eyewall, and the remaining deep convection is shifted to

the south rather than the southwest. Consequently, the failure of the COAMPS-TC to forecast the beginning of the decay phase (around 1200 UTC 20 August) may be attributed to a failure to forecast the change in direction and large increase in magnitude of the vertical wind shear.

COAMPS-TC Grid 2 200-850 hPa Wind Shear for 1200 UTC 18 August Model Run

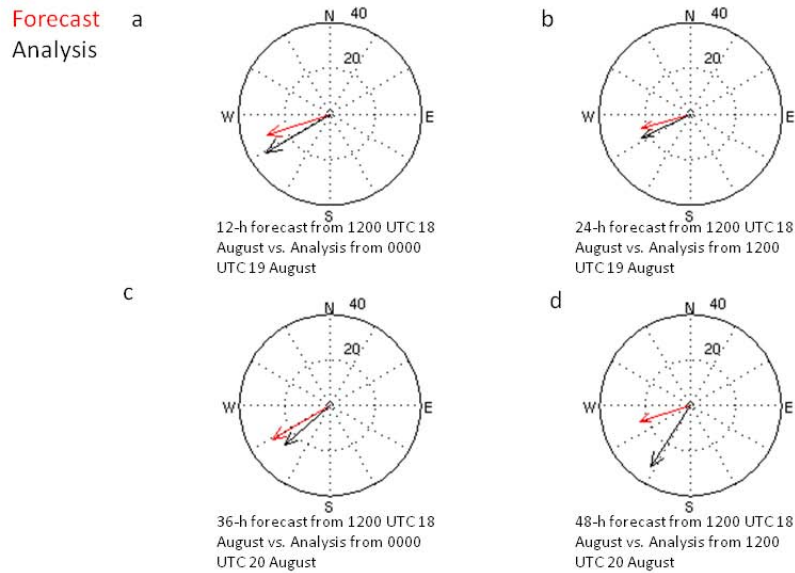


Figure 29. COAMPS-TC grid 2 200-850 hPa wind shear (kt) for the 1200 UTC 18 August model run for (a) 12-h forecast, (b) 24-h forecast, (c) 36-h forecast, and (d) 48-h forecast. The inner dotted (outer solid circle) represents a 20 (40) kt vertical shear. The black (red) arrow is the analysis (forecast) vertical shear.

c. Azimuthally-averaged Structure

To examine the intensification stage more fully, the 15-, 27-, 39-, 51-, and 63-h forecasts from an initial time of 1200 UTC 18 August are compared to the 3-h forecasts at these times. The forecasts cannot be compared with 0000 UTC or 1200 UTC analyses because vertical velocity and cloud water are derived quantities, so there are no analyses for those variables and 3-h forecasts must be used. Whereas the 15-h forecast from the 1200 UTC 18 August initial conditions (Figure 30a) has downward vertical

motion only at low levels in the eye, the verifying field (Figure 30b) has downward motion in the eye throughout the troposphere. In addition, the 15-h forecast has a relative maximum in radial inflow at 360 hPa at about 0.3 deg. radius from the center. Upward motion in the eye above this inflow and downward motion below suggests mid-level convergence in the forecast.

The 27-h forecast from the 1200 UTC 18 August initial conditions (Figure 30c) has mid-tropospheric inflow maxima at 0.6 deg. lat. radius and 250 hPa and at 0.8 deg. lat. and 400 hPa. The verifying field (Figure 30d) has downward motion in the eye above 400 hPa that is not in the forecast (Figure 30c). A broad region of upward vertical motion exists beyond 1.2 deg. radius from the center in the verifying field. Whereas the 27-h forecast also has a vertical motion maximum at around this radius, the forecast has a deep region of upward motion at inner radii.

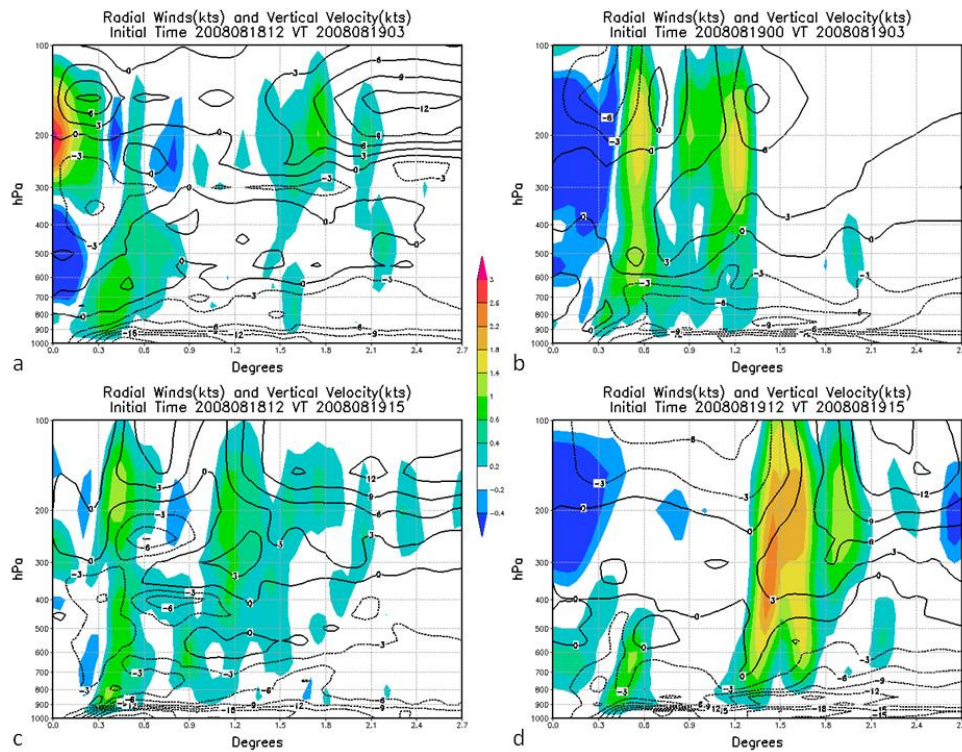


Figure 30. Azimuthally-averaged radial winds (kt) (contoured) and vertical velocity (kt) (shaded, see scale in middle) at (a) 15-h forecast from the 1200 UTC 18 August model run, (b) 3-h forecast from the 0000 UTC 19 August model run, (c) 27-h forecast from the 1200 UTC 18 August model run, and (d) 3-h forecast from the 1200 UTC 19 August model run.

The 39-h forecast from the 1200 UTC 18 August initial conditions (Figure 31a) depicts a much more compact region of ascent, which may be considered an eyewall cloud, than the verifying field (Figure 31b). This is the time of maximum intensity of Typhoon Nuri and the 39-h forecast does have inner-region ascent similar to a strong typhoon. Whereas the 39-h forecast does not have a well-defined region of downward vertical motion in the eye, the width and magnitude of the downward motion in the eye in the verifying field (Figure 31b) appears to be excessive. Similarly, the severe outward tilt of ascending motion to a maximum at about 2.1 deg. lat. radius in the verifying field is not realistic for a mature typhoon. In the 39-h forecast (Figure 31a), the maximum radial inflow in the boundary layer is at 0.3 deg. radius, which is consistent with the upward vertical motion and outflow aloft that depict the secondary circulation of the typhoon. In the verifying field (Figure 31b), the maximum inflow is beyond one deg. radius where the maximum vertical motion is located.

The 51-h forecast structure from the 1200 UTC 18 August initial conditions (Figure 31c) is consistent with a weakening storm. The maximum radial inflow and maximum upward vertical motion are at larger radii and there is no concentrated downward vertical motion in the eye. The verifying field (Figure 31d) has a broad region of ascent at large radii that tilts outward. The maximum radial inflow in the boundary layer, upward vertical motion, and the strong outflow near 150 hPa are consistent with a weak secondary circulation. Because this outer region in Figure 31d is roughly similar to the outer region in Figure 31b when Nuri was near peak intensity, it is likely that this ascent branch is an artifact of deriving the vertical motion from a 3-h integration.

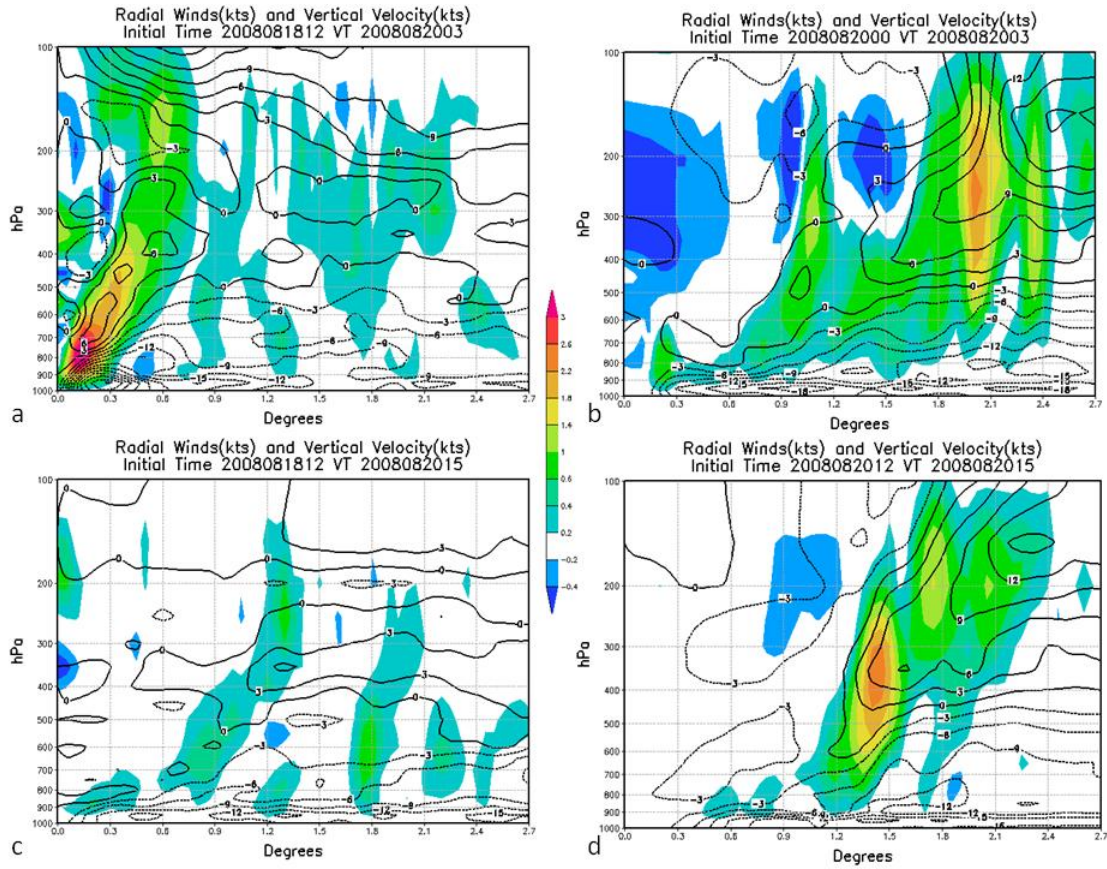


Figure 31. Azimuthally-averaged radial winds (kt) (contoured) and vertical velocity (kt) (shaded, see scale in middle) at (a) 39-h forecast from the 1200 UTC 18 August model run, (b) 3-h forecast from the 0000 UTC 20 August model run, (c) 51-h forecast from the 1200 UTC 18 August model run, and (d) 3-h forecast from the 1200 UTC 20 August model run.

The 63-h forecast from the 1200 UTC 18 August initial conditions (Figure 32a) continues to define a weakening storm with a broad weak ascent branch between 1.1 deg. lat. and 2.2 deg. lat. radius. In the verifying field (Figure 32b), a series of three weak ascent branches at roughly 0.6, 1.2, and 1.8 deg. lat. radius are not consistent with the forecast. The verifying field also has strong downward motion in the eye at the upper levels and maximum radial inflow between 0.9 and 2 deg. lat. radius from the center. Although a maximum upward vertical motion is present in the 63-h forecast (Figure 32a), the secondary circulation is not well-defined, which might be expected with the decaying storm stage.

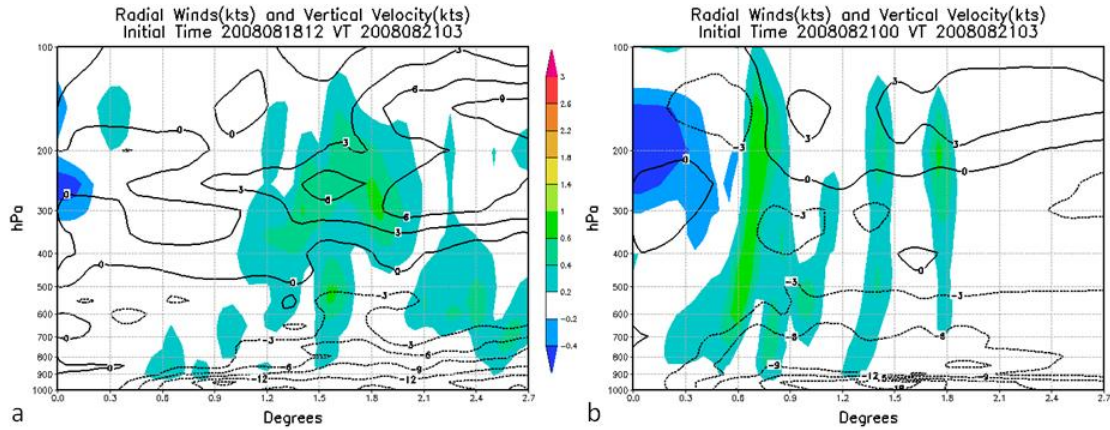


Figure 32. Azimuthally-averaged radial winds (kt) (contoured) and vertical velocity (kt) (shaded, see scale in middle) at (a) 63-h forecast from the 1200 UTC 18 August model run, and (b) 3-h forecast from the 0000 UTC 21 August model run.

The azimuthally-averaged tangential wind in the 15-h forecast from the 1200 UTC 18 August initial conditions (Figure 33a) has a maximum of 55 kt at 0.5 deg. radius from the center of the storm. The location of the maximum winds in the verifying field (Figure 33b) is similar to the 15-h forecast but is 5 kt lower. The 15-h cloud water forecast generally has a similar distribution with radius and height as in the verifying field. That is, the maximum cloud water is between 0.3 and 1 deg. lat. radius and extends up to 500 hPa and the maximum cloud water slants outward from the center of the storm.

The 27-h forecast from the 1200 UTC 18 August initial conditions (Figure 33c) depicts a strengthening storm with maximum winds of 75 kt at 0.3 deg. lat. radius from the center. Although the verifying field (Figure 33d) also depicts an intensifying storm, the maximum winds are only 60 kt at 0.4 deg. lat. radius from the center. Both forecasts show a compact storm with a thin layer of clouds in the eye and a maximum of clouds between 0.3 and 1 deg. lat. radius.

The major difference between the tangential wind fields in Figures 33c and 33d are in the middle to upper troposphere. In the 27-h forecast, the maximum winds extend more vertically near the center, although a region of large vertical wind shear is found between 500 hPa and 400 hPa. By contrast, the maximum tangential winds in the upper troposphere are found at about 1.8 deg. lat. radius in Figure 33d. In addition, the

large vertical wind shear between 600 hPa and 300 hPa is quite unrealistic for a mature TC, and is attributed to an unrealistic bogus vortex in the initial conditions for this time.

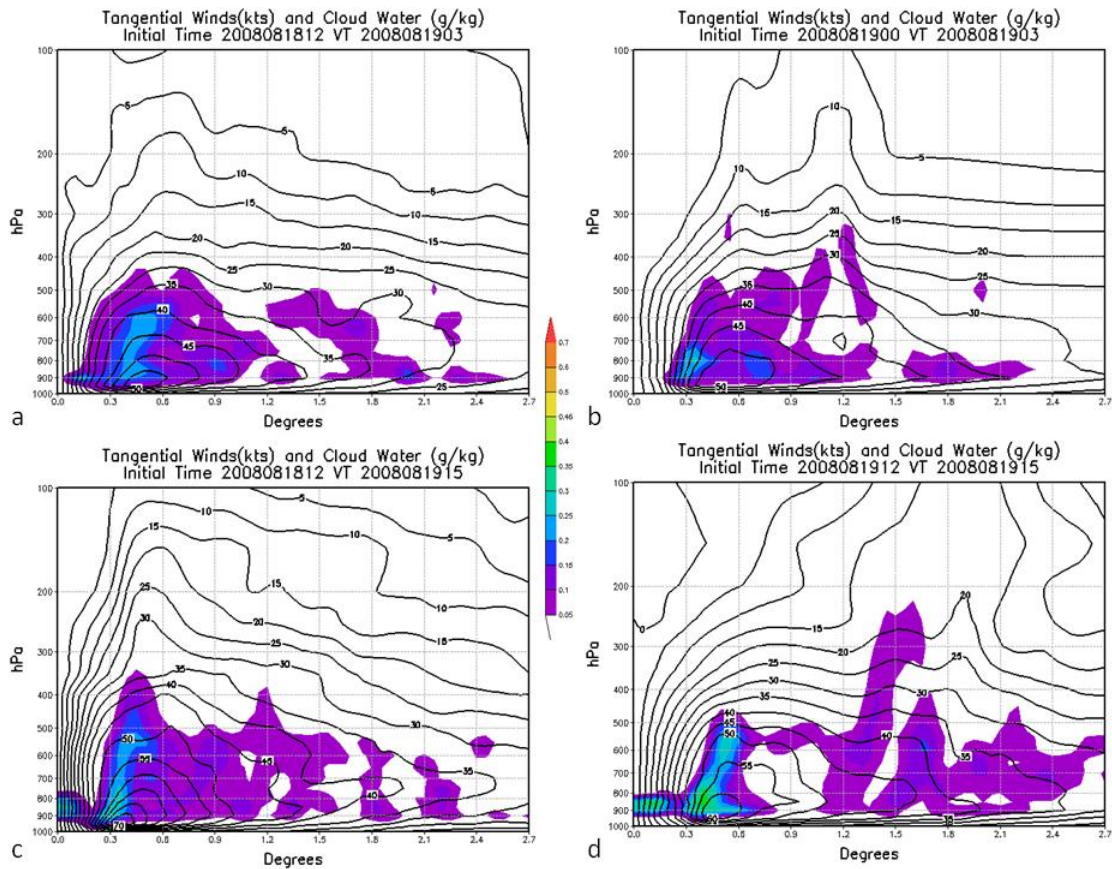


Figure 33. Azimuthally-averaged tangential winds (kt) (contoured) and cloud water (g/kg) (shaded, see scale in middle) at (a) 15-h forecast from the 1200 UTC 18 August model run, (b) 3-h forecast from the 0000 UTC 19 August model run, (c) 27-h forecast from the 1200 UTC 18 August model run, and (d) 3-h forecast from the 1200 UTC 19 August model run.

The 39-h forecast from the 1200 UTC 18 August initial conditions (Figure 34a) indicates the storm has weakened slightly with a maximum wind of 65 kt at 0.3 deg. lat. radius from the center. This forecast also has a very compact eye with cloud water extending inward to very small radius at low levels with an outward slant up to 300 hPa. The verifying field (Figure 34b) has a weaker storm with a large eye and maximum winds of 45 kt from 0.9 to 1.5 deg. lat. radius from the center. As in Figure 32d, the vertical structure of the tangential wind in this verifying field is not realistic—presumably

due to the bogus vortex. The maximum cloud water distribution near the center is also very shallow compared to the forecast and does not extend into the eye.

The 51-h forecast from the 1200 UTC 18 August initial conditions (Figure 34c) has a dramatic weakening and shallowing of the tangential winds, which are primarily below 400 hPa. The vertical structure in the verifying field (Figure 34d) again appears to represent the initial bogus vortex that may not be representative of the decaying stage of Nuri. The 51-h forecast also has a shallow layer of cloud water from very near the center out to 1.9 degrees and only up to 500 hPa.

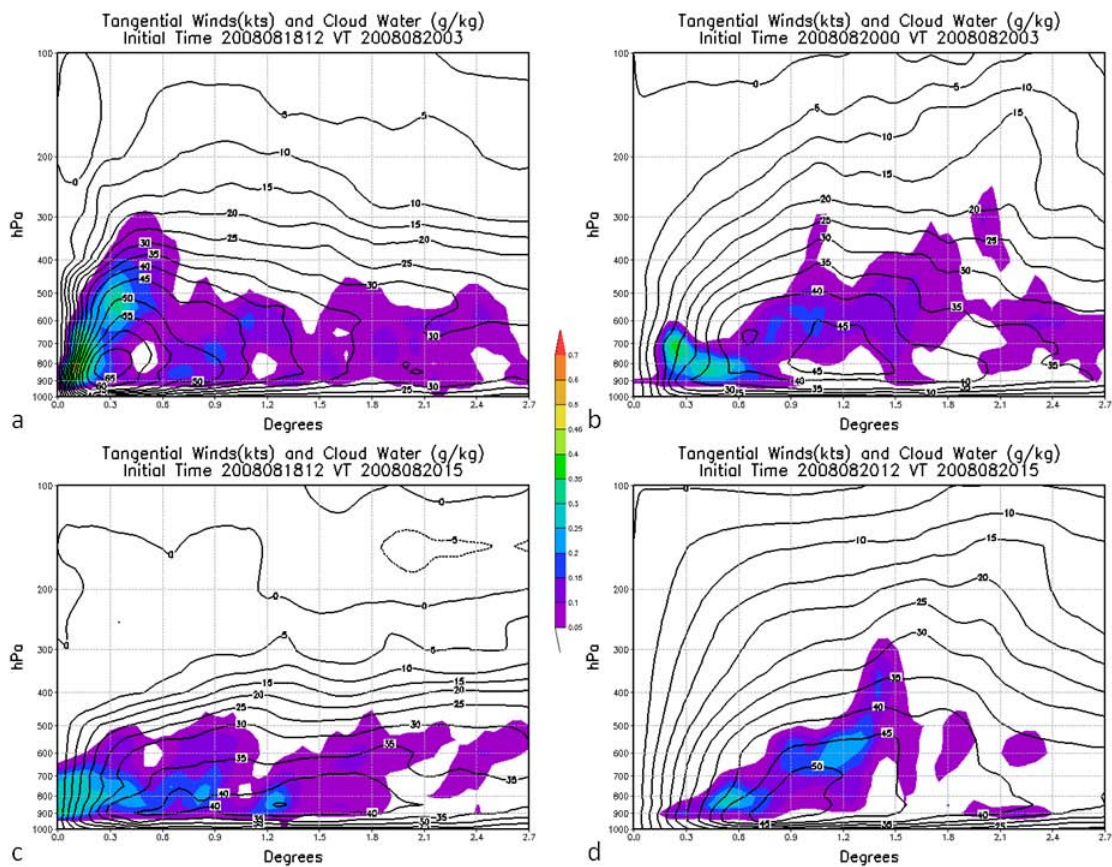


Figure 34. Azimuthally-averaged tangential winds (kt) (contoured) and cloud water (g/kg) (shaded, see scale in middle) at (a) 39-h forecast from the 1200 UTC 18 August model run, (b) 3-h forecast from the 0000 UTC 20 August model run, (c) 51-h forecast from the 1200 UTC 18 August model run, and (d) 3-h forecast from the 1200 UTC 20 August model run.

The 63-h forecast from the 1200 UTC 18 August initial conditions (Figure 35a) has a maximum wind of 45 kt at 1.2 deg. lat. radius from the center and a flat, relatively shallow vortex. Again, the deep vertical structure of the tangential wind in the verifying field (Figure 35b) is likely unrepresentative of the decaying Nuri at this time. Whereas the 63-h forecast may have a somewhat realistic cloud water structure, the cloud water in Figure 35b is more likely determined by the erroneous bogus vortex and should not be the basis for a verification of the forecast.

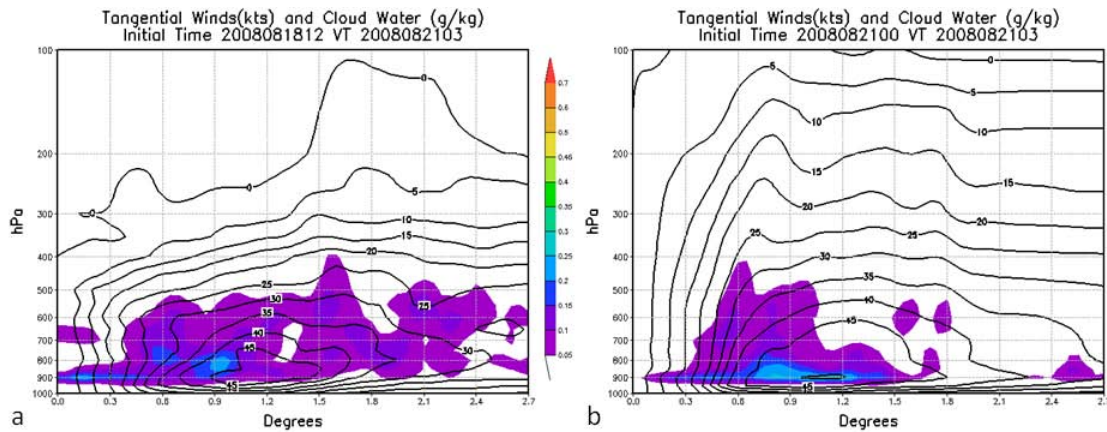


Figure 35. Azimuthally-averaged tangential winds (kt) (contoured) and cloud water (g/kg) (shaded) at (a) 63-h forecast from the 1200 UTC 18 August model run and (b) 3-h forecast from the 0000 UTC 21 August model run.

3. Decay Stage

a. Simulated Radar Reflectivity

For the decay stage, the 1200 UTC 19 August forecast is examined as a representative example, although this forecast over-intensified TY Nuri the greatest of all the model runs. At 0000 UTC 20 August (Figure 36b), TY Nuri is at its peak intensity. Nuri has a closed eye with strong convection defining the eyewall. Most of the outer convection is located to the south of the center, with the maximum deep convection to the southwest of the center. The 12-h forecast radar reflectivity (Figure 36a) matches the satellite image quite well with a closed eye and convection all the way around the eye. One major difference is that the forecast has a significant band to the northeast of the

center that is not present in the satellite image. However, the heaviest convection is correctly predicted to be southwest of the center.

In the 24-h forecast (Figure 36c), the strongest outer convection is located to the south and southwest of the center as is observed (Figure 36d). However, the forecast distribution of inner convection is very different from the corresponding satellite image. In the forecast, the eye is closed with deep convection nearly surrounding the entire eye. By contrast, the satellite image indicates that the eye was open with convection on the southern half of the eyewall. Whereas the satellite image depicts a circulation that is likely undergoing strong vertical wind shear from the north, the model forecast does not indicate the effects of such a shear.

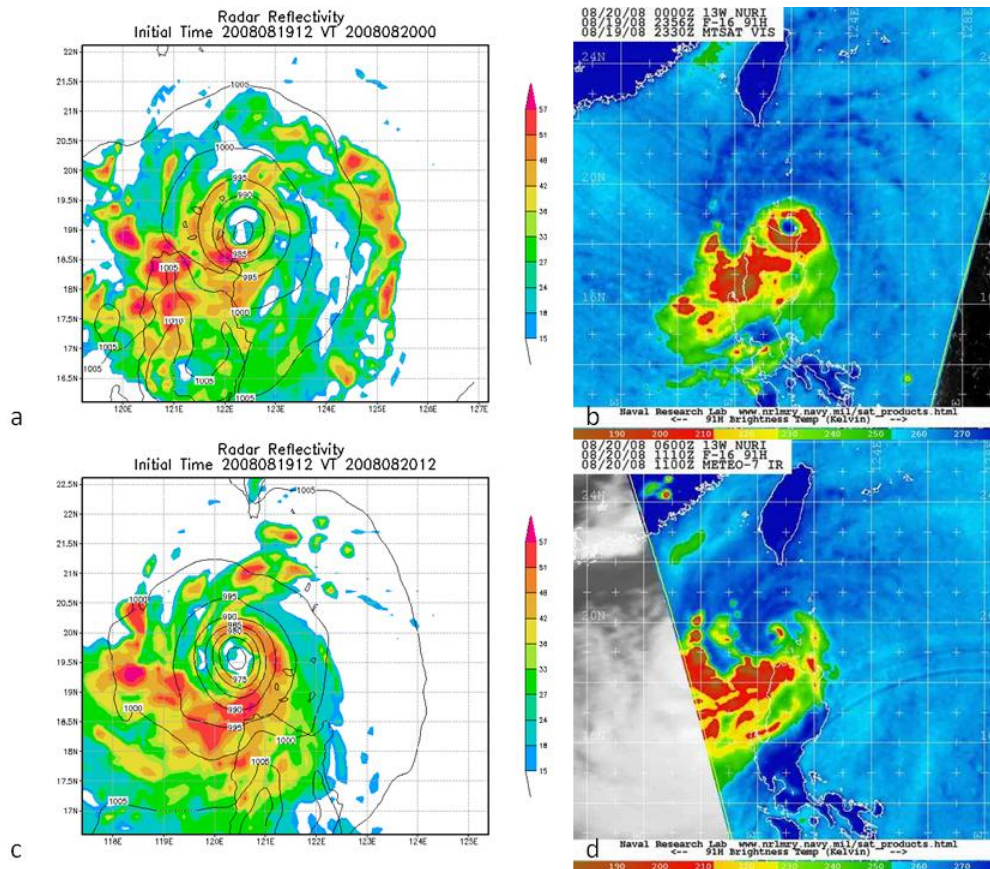


Figure 36. Simulated radar reflectivity from the 1200 UTC 19 August COAMPS-TC model run that verifies at (a) 0000 UTC 20 August, and (c) 1200 UTC 20 August. Microwave imagery at 91 GHz at (b) 2356 UTC 19 August, and (d) 1110 UTC 20 August. Satellite imagery from http://www.nrlmry.navy.mil/sat_products.html.

The 36-h forecast (Figure 37a) continues to depict a closed eyewall with deep convection all the way around the eye and outer convection that is concentrated to the south of the center. The corresponding satellite image (Figure 37b) is quite different as Nuri was weakening at this time. The satellite image indicates an open eyewall with the heaviest convection to the south of the storm. Similarly, the 1200 UTC 21 August satellite image (Figure 37d) indicates further weakening of the typhoon under vertical wind shear with an open eyewall and some convection to the southwest of the storm. By contrast, the 48-h forecast (Figure 37c) has Nuri as a strong typhoon with a closed eyewall and convection all the way around the eyewall.

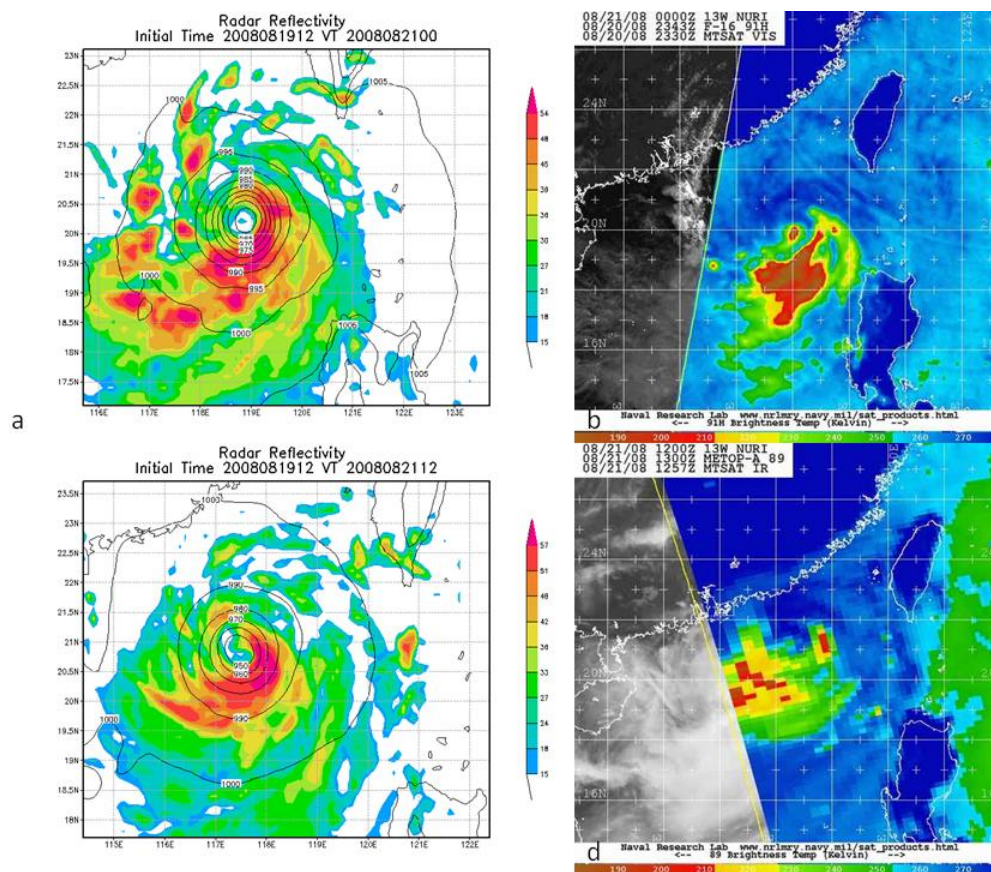


Figure 37. Simulated radar reflectivity from the 1200 UTC 19 August COAMPS-TC model run that verifies at (a) 0000 UTC 21 August, and (c) 1200 UTC 21 August. Microwave imagery at 91 GHz and 89 GHz respectively at (b) 2343 UTC 20 August, and (d) 1300 UTC 21 August. Satellite imagery from http://www.nrlmry.navy.mil/sat_products.html.

The 60-h forecast (Figure 38a) again has a closed eyewall with convection just beginning to weaken on the north side. The heaviest convection is forecast to be to the east through southwest sides of the storm. However, the satellite image at 2153 UTC 21 August (Figure 38b) has an open eyewall with convection extending to the southwest of the center. The 72-h forecast (Figure 38c) depicts a weakening Nuri near landfall. Although the intensity of the inner convection is forecast to have weakened, there is still some indication of a closed eye. By this time, Nuri has actually made landfall near Hong Kong as a tropical storm (Figure 38d), with an open eyewall to the north and some scattered deep convection to the southwest of the center.

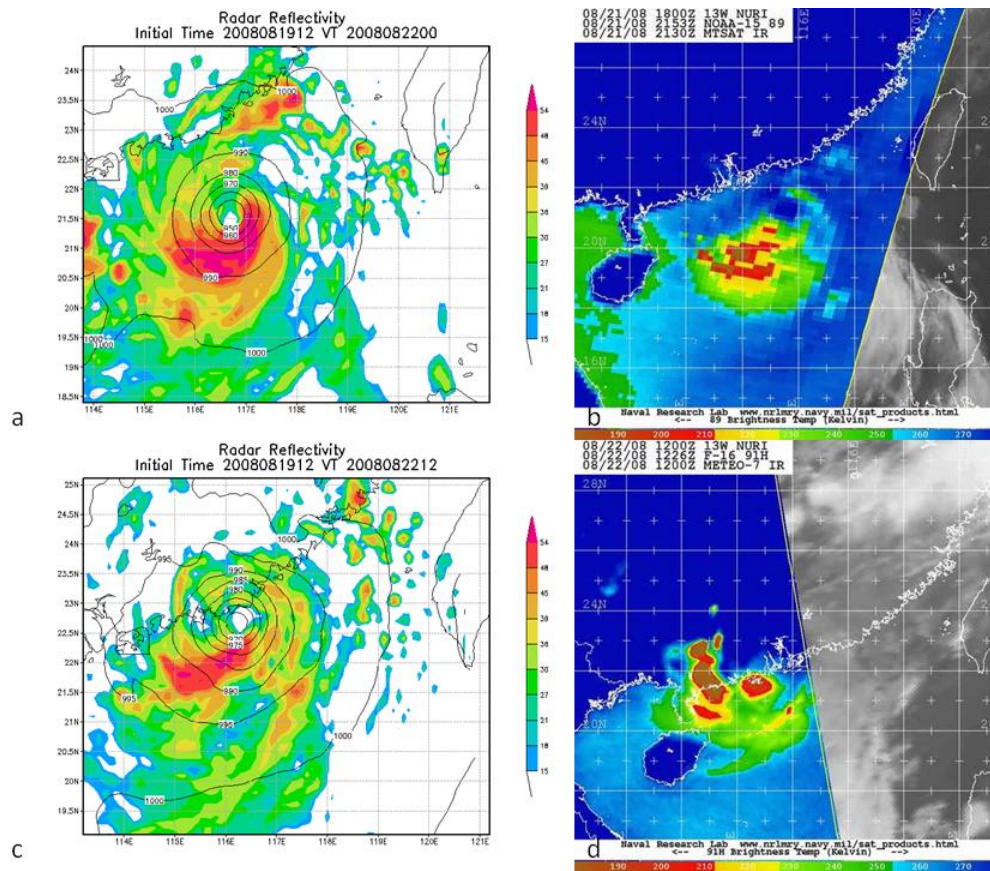


Figure 38. Simulated radar reflectivity from the 1200 UTC 19 August COAMPS-TC model run that verifies at (a) 0000 UTC 22 August, and (c) 1200 UTC 22 August. Microwave imagery at 89 Ghz and 91 Ghz respectively at (b) 2153 UTC 21 August, and (d) 1226 UTC 22 August. Satellite imagery from http://www.nrlmry.navy.mil/sat_products.html.

In summary, the forecast distribution of deep convection as defined by simulated radar reflectivity from the forecasts initiated at 1200 UTC 19 August did not represent the structure of Nuri accurately once peak intensity was reached and Nuri started to weaken. Although the satellite imagery indicated that Nuri came under vertical wind shear from the north to northeast, the forecast maintained a near-symmetric structure rather than one associated with a weakening circulation. The delay in weakening may have been due to the difference between the forecast track and the actual track. It is clear that the forecast position of Nuri is not as near to the coast as observed (i.e., Figure 38), which may have reduced the influence of continental air inflow to the storm in the forecast model.

b. Vertical Wind Shear

As discussed in Chapter III.C.b, TY Nuri was an asymmetric storm later in its life cycle due to the strong northeasterly shear, which is evident in the satellite imagery (Figures 36-38). The vertical wind shear in the 1200 UTC 19 August forecast (Figure 39) increases significantly through 60 h, which is consistent with the verifying analyses values. However, this increasing vertical wind shear is not evident in the radar reflectivity (Figures 36-38) that depict a nearly symmetric storm with a closed eyewall. Furthermore, the 10-m maximum winds were forecast to increase (Figures 12, 14, and 16) instead of decrease as in the JTWC best-track maximum winds.

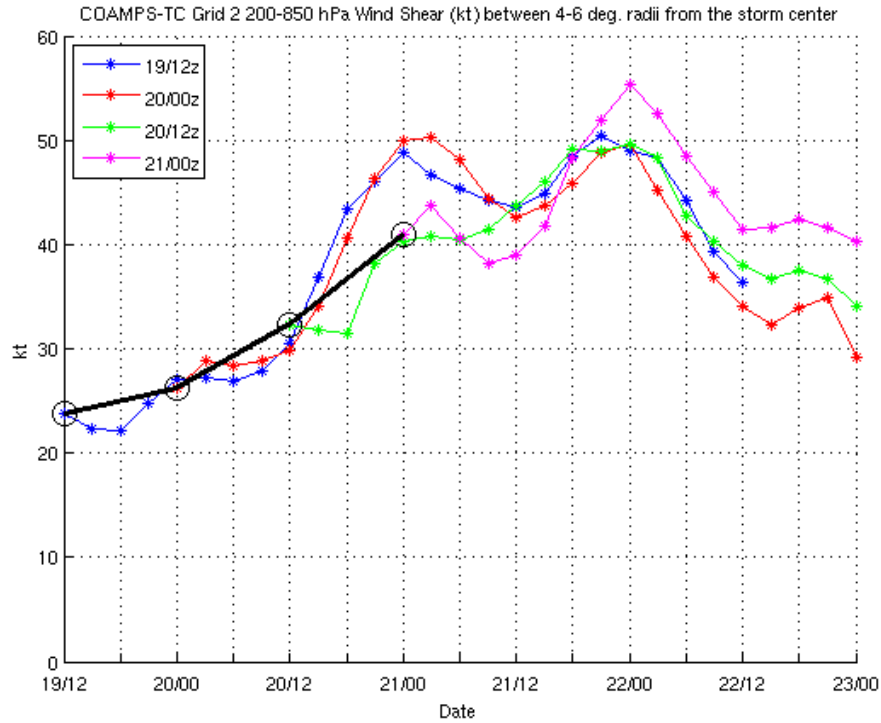


Figure 39. Vertical wind shear (kt) between 200-850 hPa for the COAMPS-TC grid 2 from 1200 UTC 19 August – 0000 UTC 21 August (see insert).

The 12-, 24-, 36-, and 42-h vertical wind shear forecasts (Figure 40) vary from the east-northeast to north-northeast through the forecast period. The 36-h forecast was 10 kt too high compared to the corresponding analysis (Figure 40c). Even though the model forecast the shear relatively accurately, TY Nuri did not have an asymmetric structure in the forecast compared to the satellite images.

COAMPS-TC Grid 2 200-850 hPa Wind Shear for 1200 UTC 19 August Model Run

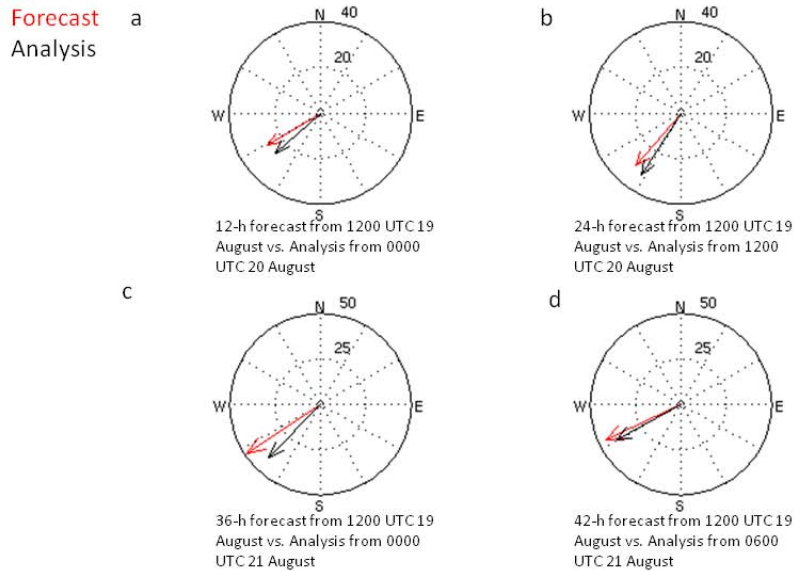


Figure 40. COAMPS-TC grid 2 200-850 hPa wind shear (kt) for the 1200 UTC 19 August model run for (a) 12-h forecast, (b) 24-h forecast, (c) 36-h forecast, and (d) 42-h forecast. The inner dotted (outer solid circle) represents a 20 (40) kt vertical shear in the 12- and 24-h forecast while the inner dotted (outer solid circle) represents a 25 (50) kt vertical shear in the 36- and 42-h forecast. The black (red) arrow is the analysis (forecast) vertical shear.

c. Azimuthally-Averaged Structure

To examine the 1200 UTC 19 August forecast more fully, the azimuthally-averaged structure in the 15-, 27-, and 39-h forecasts are compared to verifying times that are again 3-h forecasts because vertical velocity and cloud water are derived quantities so there are no analyses for those variables. The 15-h forecast from the 1200 UTC 19 August initial conditions (Figure 41a) is at the time of maximum intensity of Nuri. The maximum azimuthally-averaged radial inflow coincides with the maximum upward vertical motion in the 15-h forecast, but the 3-h forecast that verifies at 0300 UTC 20 August (Figure 41b) contains a much broader circulation. As discussed in Chapter III.c.2.c, the verifying field (Figure 41b) appears to represent a blend between the broad

NOGAPS vortex used in the initial conditions and the COAMPS-TC initialization procedure that is beginning to generate an inner-core circulation. Therefore, the 15-h forecast is likely a better representation of Nuri at maximum intensity.

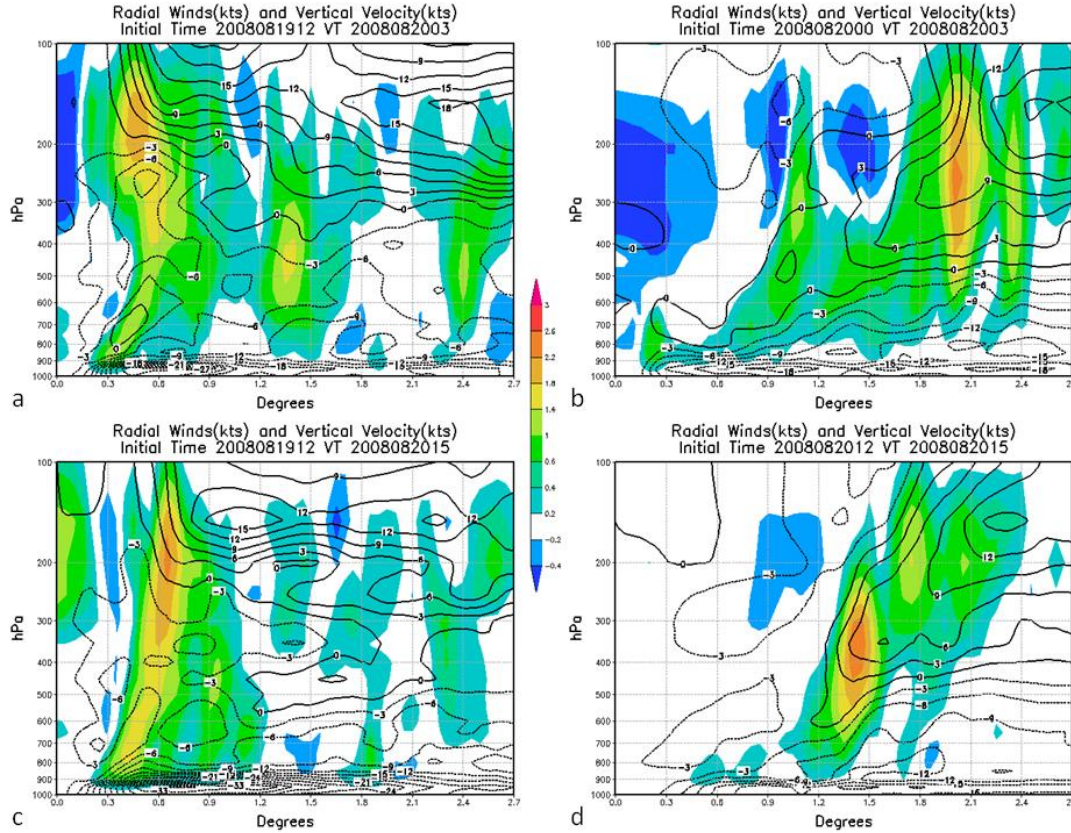


Figure 41. Azimuthally-averaged radial winds (kt) (contoured) and vertical velocity (kt) (shaded) at (a) 15-h forecast from the 1200 UTC 19 August model run, (b) 3-h forecast from the 0000 UTC 20 August model run, (c) 27-h forecast from the 1200 UTC 19 August model run, and (d) 3-h forecast from the 1200 UTC 20 August model run.

The 27-h forecast from the 1200 UTC 19 August initial conditions (Figure 41c) depicts a strengthening storm, whereas the verifying field (Figure 41d) represents a broadening of the vortex as Nuri decays with a large eye. The maximum upward vertical motion is at 1.5 degrees from the center of the storm, which corresponds to the maximum radial inflow and outflow in the secondary circulation. The secondary circulation is also present in the 27-h forecast but is located at 0.5 deg. lat. radius, which is consistent with a much smaller eye.

The 39-h forecast from the 1200 UTC 19 August initial conditions (Figure 42a) continues the strengthening trend of Nuri. The maximum radial inflow is located between 0.3 and 1.5 deg. lat. radius with a maximum vertical upward motion at 0.3 deg. and radial outflow above 300 hPa. The verifying field (Figure 42b) is very different from the 39-h forecast, which is what should be expected since Nuri was actually weakening at this time. The radial inflow maximum is located at 1.5 deg. radius with a maximum vertical upward motion closer to the eye and radial outflow above 300 hPa.

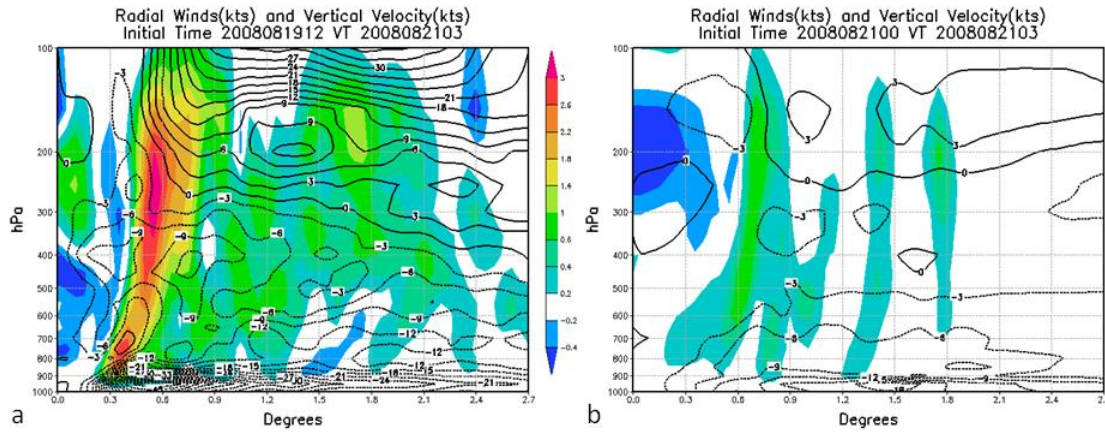


Figure 42. Azimuthally-averaged radial winds (kt) (contoured) and vertical velocity (kt) (shaded) at (a) 39-h forecast from the 1200 UTC 19 August model run and (b) 3-h forecast from the 0000 UTC 21 August model run.

The 15-h forecast of azimuthally-averaged tangential winds and cloud water (Figure 43a) from the 1200 UTC 19 August initial conditions depicts a small eye with a maximum of 70 kt between 0.3 and 0.5 deg. lat. radius from the center of the storm. The cloud water distribution slopes outward from the center and up to 300 hPa. As was found for the distribution of radial winds and vertical motion, the 15-h forecast is more representative of the actual storm than the verifying fields (Figure 43b) that seem to contain a blend of NOGAPS vortex and COAMPS analysis. Thus, the verifying fields depict a weaker storm with a larger eye, maximum winds of 45 kt between 0.9 and 1.5 deg. lat. radius, and the maximum cloud water only extends vertically to 600 hPa.

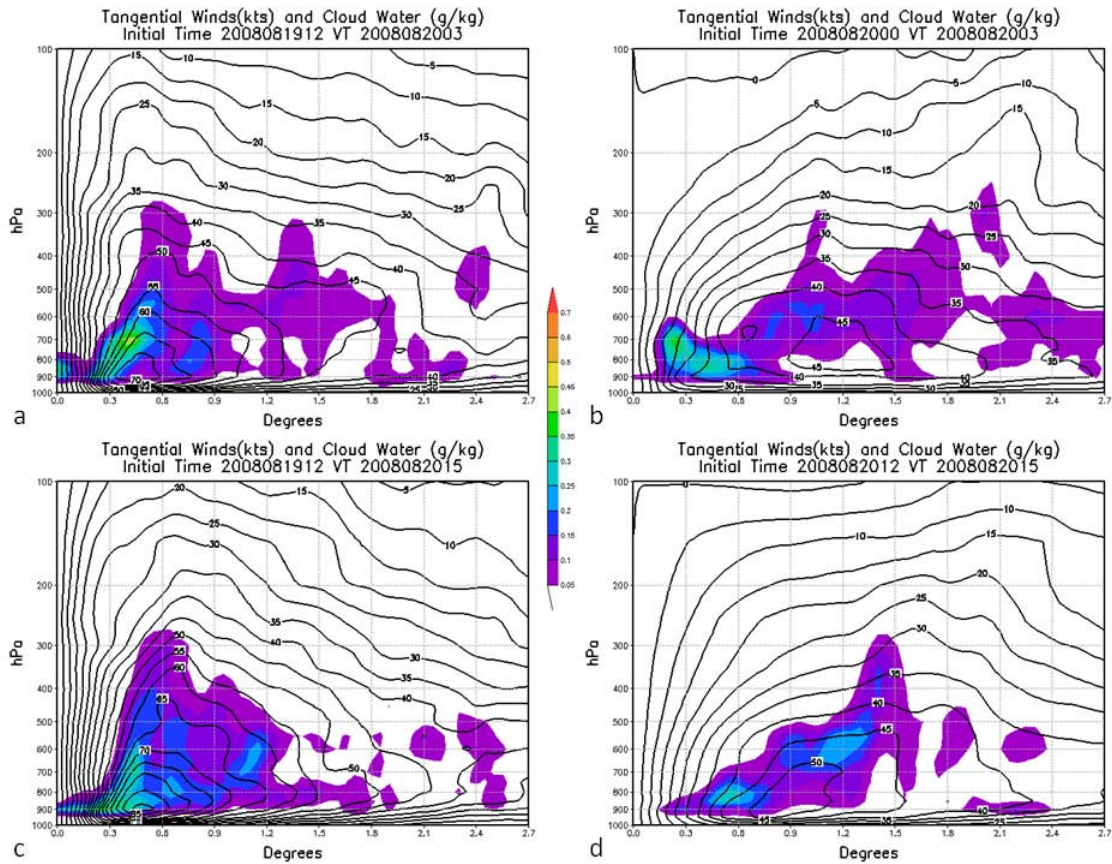


Figure 43. Azimuthally-averaged tangential winds (kt) (contoured) and cloud water (g/kg) (shaded) at (a) 15-h forecast from the 1200 UTC 19 August model run, (b) 3-h forecast from the 0000 UTC 20 August model run, (c) 27-h forecast from the 1200 UTC 19 August model run, and (d) 3-h forecast from the 1200 UTC 20 August model run.

The 27-h forecast from the 1200 UTC 19 August initial conditions (Figure 43c) continues to strengthen Nuri with a maximum wind of 90 kt at 0.4 deg. lat. radius from the center. The cloud water extends up to 300 hPa between 0.3 and 0.9 deg. lat. radius from the center. Whereas, in the forecast Nuri has a very small eye, the verifying field (Figure 43d) depicts a weakening storm with a large eye and a maximum wind of 50 kt at 0.9 deg. The maximum cloud water distribution has a maximum vertical extent located at 1.5 deg. instead of 0.6 deg. as in the 27-h forecast.

The 39-h forecast from the 1200 UTC 19 August initial conditions (Figure 44a) deepens Nuri even further with a maximum wind of 105 kt at 0.4 deg. radius from

the center. By contrast, the verifying field (Figure 44b) only has a maximum wind of 50 kt at 1.2 deg. lat. radius from the center. The cloud water distribution in the forecast (Figure 44a) is also more representative of an intense typhoon with the vertical extent in the eyewall region to 275 hPa and a broad horizontal extent as well. By contrast, the verifying cloud water distribution is concentrated within the radius of maximum winds and has limited vertical extent, which might be expected in a decaying storm.

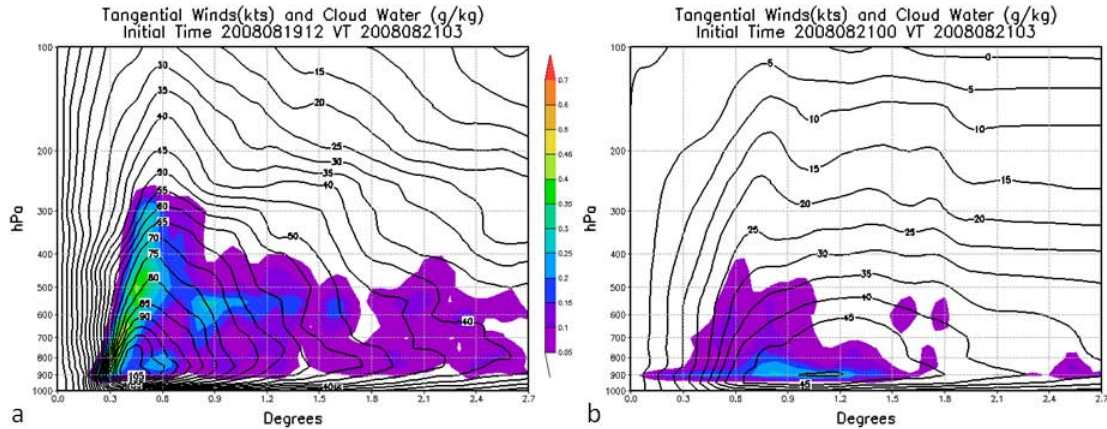


Figure 44. Azimuthally-averaged tangential winds (kt) (contoured) and cloud water (g/kg) (shaded) at (a) 39-h forecast from the 1200 UTC 19 August model run and (b) 3-h forecast from the 0000 UTC 21 August model run.

In summary, these azimuthally-averaged fields during the decay stage depict clearly the differences between forecasts of an intensifying storm when Nuri was actually decaying. The forecasts have a strong secondary circulation with strong radial inflows to small radii where the maximum tangential winds are located and then ascent and outflow at high elevations. By contrast, the verifying fields are more representative of a decaying storm with a broad vortex and a weak secondary circulation at much larger radii.

D. AIRCRAFT OBSERVATIONS

To understand the contributions that the initial conditions for the model may have contributed to forecast error during the intensification and decay stages, the 0000 UTC 18 August and 0000 UTC 19 August initial conditions are compared to the flight-level and surface winds from AOP-3 and AOP-4, respectively. Flight-level (near 700 hPa) winds

of the WC-130J are compared to the analysis 700-hPa winds, and the surface winds from the Stepped Frequency Microwave Radiometer (SFMR) onboard the WC-130J are compared with the analysis 10-m winds. Two passes through the center of the storm were available for each flight.

1. 0000 UTC 18 August Flight

The 0000 UTC 18 August analysis is centered in the middle of the AOP-3 mission. At this time, Nuri was still a tropical storm with a maximum wind of 50 kt and minimum MSLP of 985 hPa. Tropical storm Nuri did not yet have a well-defined structure with lots of clouds in the eye (Figure 45a) and a likely vertical tilt from the surface to 700 hPa. Pass 2 of the flight (Figure 45b) passed closer to the center location of Nuri in the model.

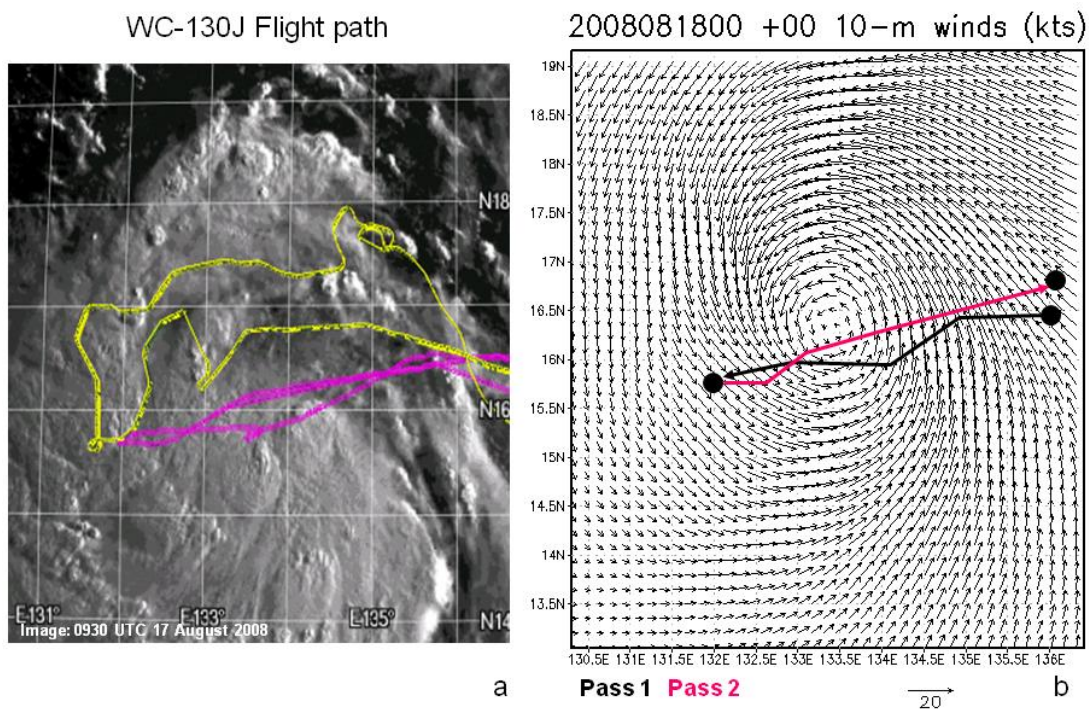


Figure 45. Flight information for 0000 UTC 18 August (a) WC-130J flight path (pink) and (b) 10-m wind (kt) analysis for the 0000 UTC 18 August model run with flight path overlay (Pass 1-black, Pass 2-pink). Satellite image is from 0930 UTC 17 August 2008.

The aircraft flight-level winds during pass 1 (Figure 46), define a broad circulation center. The 700-hPa winds from the 0000 UTC 18 August analysis have a similar shape as the flight-level winds, except for a secondary minimum after the aircraft passed through the center and the winds have started to increase. The 10-m winds from the 0000 UTC 18 August analysis (Figure 47) did not closely match the SFMR winds from pass 1. The 10-m wind analysis has a broader and weaker vortex than is indicated by the SFMR winds that have a distinct maximum of 50 kt.

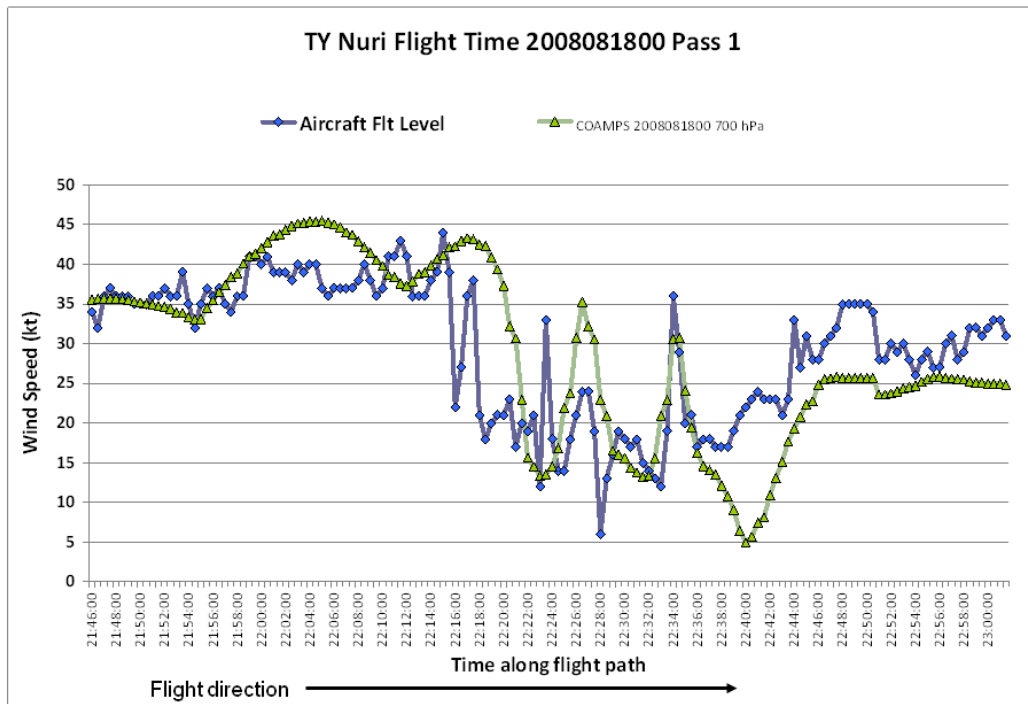


Figure 46. Flight-level winds (kt) at 0000 UTC 18 August from pass 1 (diamonds) and COAMPS-TC 0000 UTC 18 August 700 hPa winds (kt) (triangles).

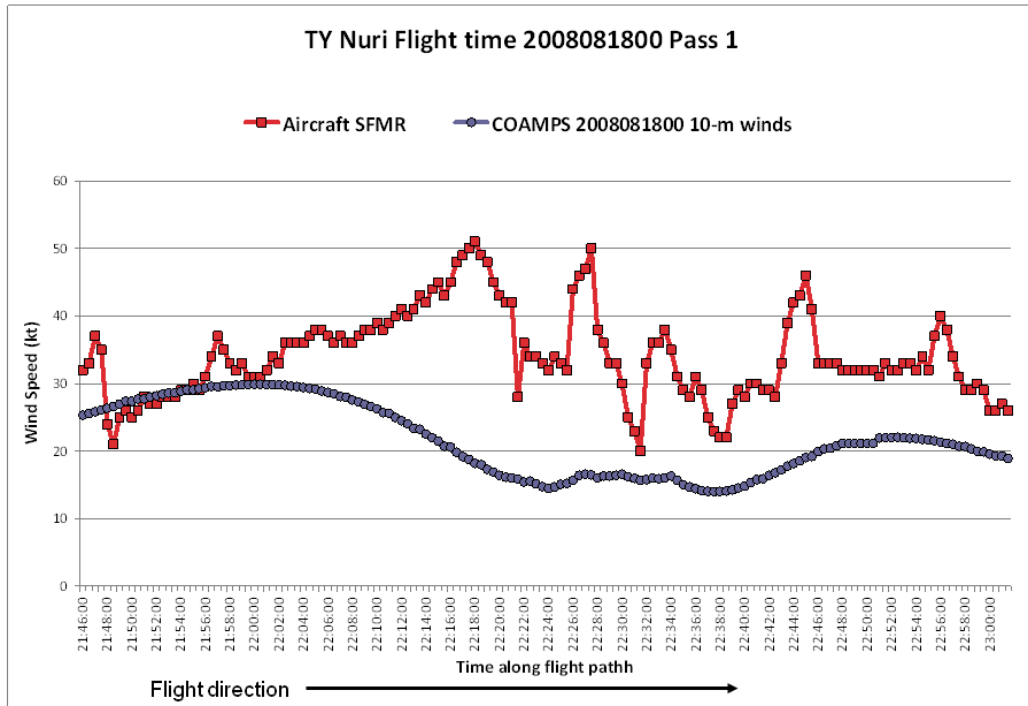


Figure 47. Surface winds (kt) from pass 1 (squares) and COAMPS-TC 0000 UTC 18 August 10-m winds (kt) (circles).

Whereas the 700-hPa winds from the 0000 UTC 18 August analysis (Figure 48) have the same general shape as the flight-level winds from pass 2, the model analysis did not have the 60 kt peak wind that existed on the eastern side of the center. The 10-m winds from the 0000 UTC 18 August analysis (Figure 49) have a very broad center as was depicted during the first pass. Although the 10-m winds matched up well on the location of the minimum wind, the SFMR winds document a dramatic increase in 10-m winds below the 700-hPa peak wind (Figure 48) that is completely missed in the analysis. The overly broad low-level wind field in COAMPS-TC is consistent with the patterns identified in azimuthally-averaged tangential and radial winds. It is likely that the initial circulation structure in COAMPS-TC is too broad due to the incorporation of the vortex from NOGAPS in the background field for the COAMPS-TC initial conditions.

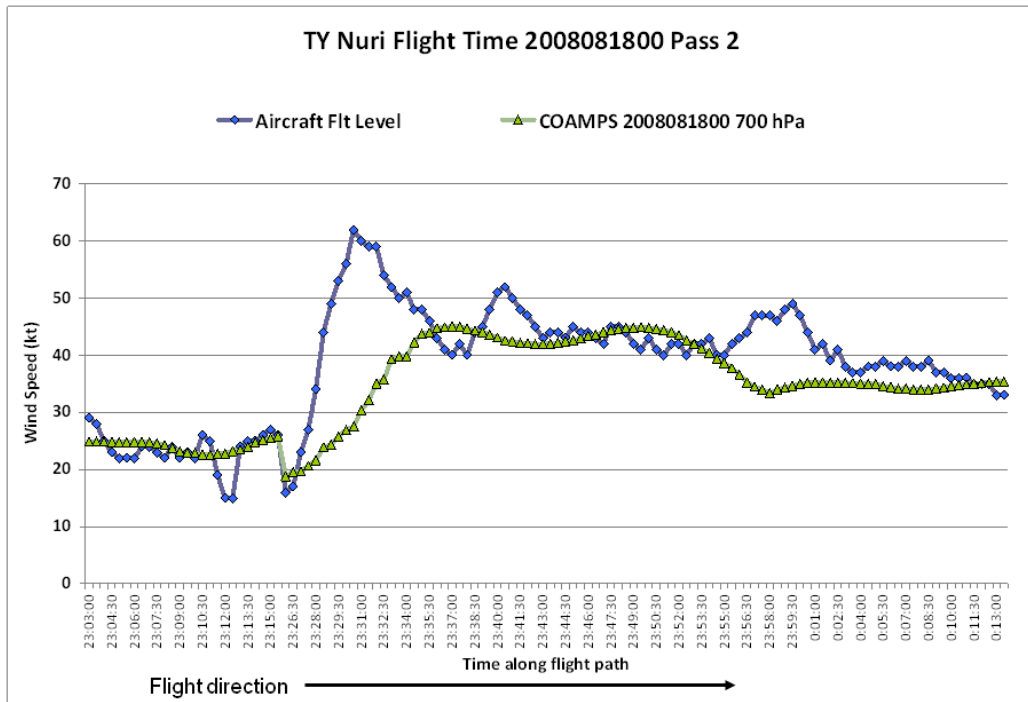


Figure 48. Flight-level winds (kt) at 0000 UTC 18 August from pass 2 (diamonds) and COAMPS-TC 0000 UTC 18 August 700 hPa winds (kt) (triangles).

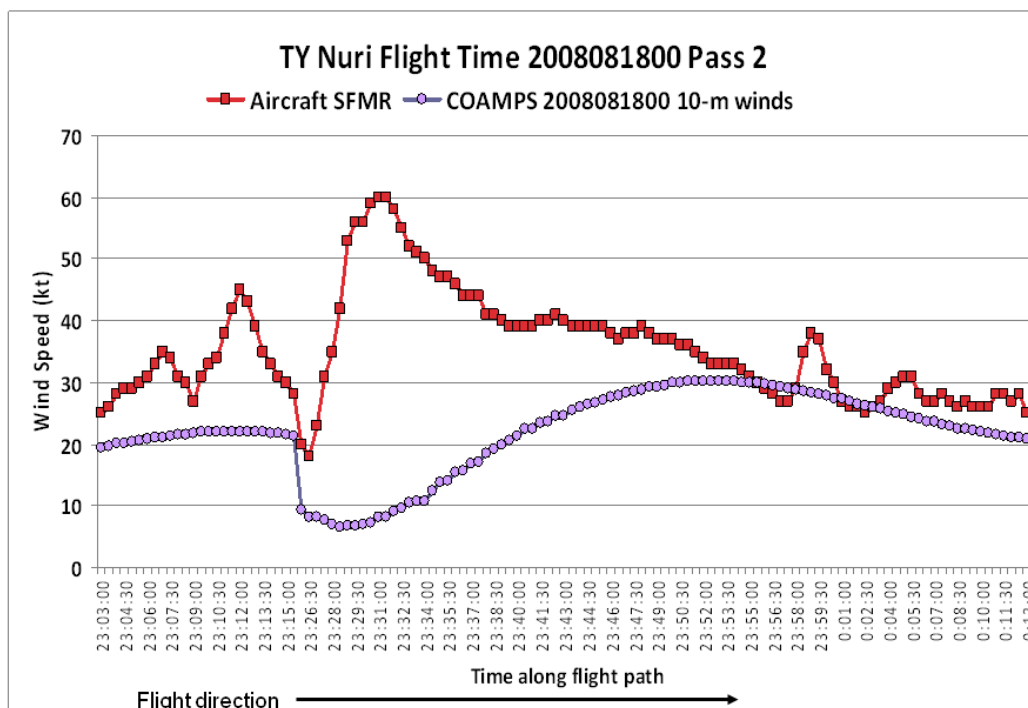


Figure 49. Surface winds (kt) from pass 2 (squares) and COAMPS-TC 0000 UTC 18 August 10-m winds (kt) (circles).

2. 0000 UTC 19 August Flight

The 0000 UTC 19 August analysis is centered in the middle of the AOP-4 mission. At this time, Nuri was a typhoon with a maximum wind of 75 kt and minimum MSLP of 967 hPa. The eye of TY Nuri (Figure 50a) is more discernable for this flight compared to the 0000 UTC 18 August flight. Both passes are near or through the center of circulation in the 0000 UTC 19 August 10-m wind analysis (Figure 50b).

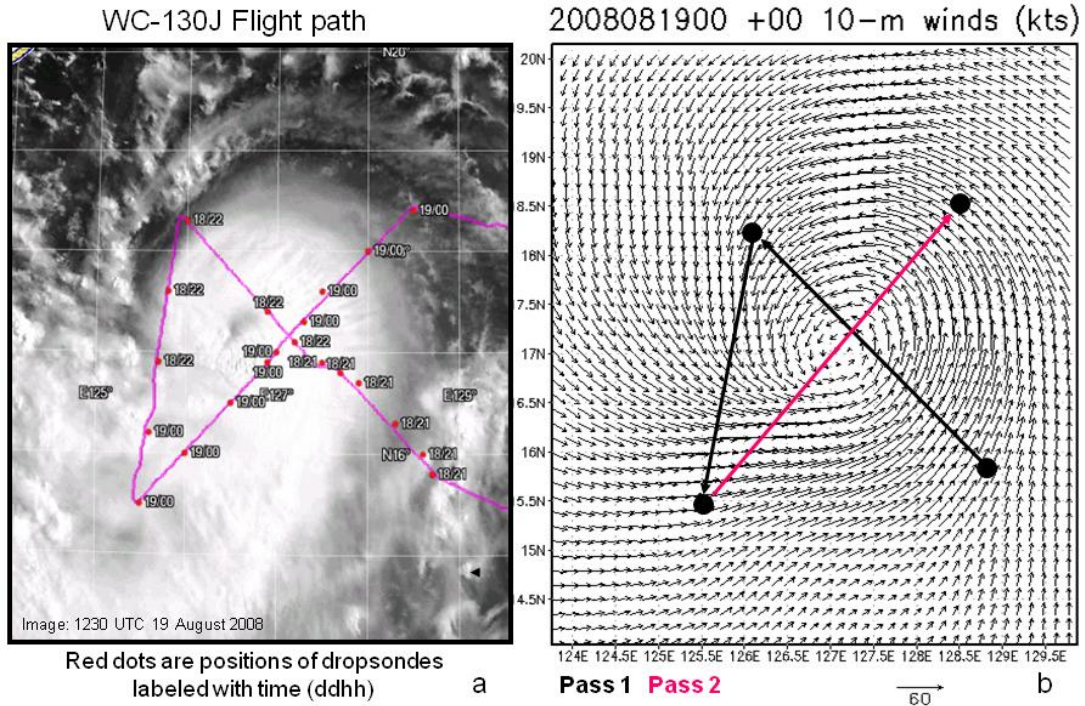


Figure 50. Flight information for 0000 UTC 19 August (a) WC-130J flight path and (b) 10-m winds (kt) analysis from the 0000 UTC 19 August model run with flight path overlay (Pass 1-black, Pass 2-pink). Satellite image is from 1230 UTC 19 August 2008.

The 0000 UTC 19 August analysis 700-hPa winds (Figure 51) from pass 1 indicate what appear to be two centers in TY Nuri. The inner center matches the flight-level data closely except the winds do not decrease to zero. The second center is at a larger radius. The presence of a second broad center is consistent with several of the vertical motion plots (e.g., Figure 30b) in which a major updraft was at a larger radius and a weaker updraft was closer to the center. Again, the presence of the broad circulation is likely due to the inclusion in the initial conditions of the NOGAPS

circulation. Other than the issue with the double eye, the analysis from 0000 UTC 19 August has the same shape as the aircraft flight level.

The 10-m winds from the 0000 UTC 19 August analysis (Figure 52) from pass 1 indicate a broad, weaker vortex in which the location of the eye was well displaced from the well-defined eye in the SFMR winds. The 10-m winds were also weaker than the SFMR winds. Consequently, the COAMPS-TC forecast began from initial conditions that had a poor representation of the initial vortex—both in terms of a weaker vortex with a broad horizontal structure and an incorrect tilt in the vertical.

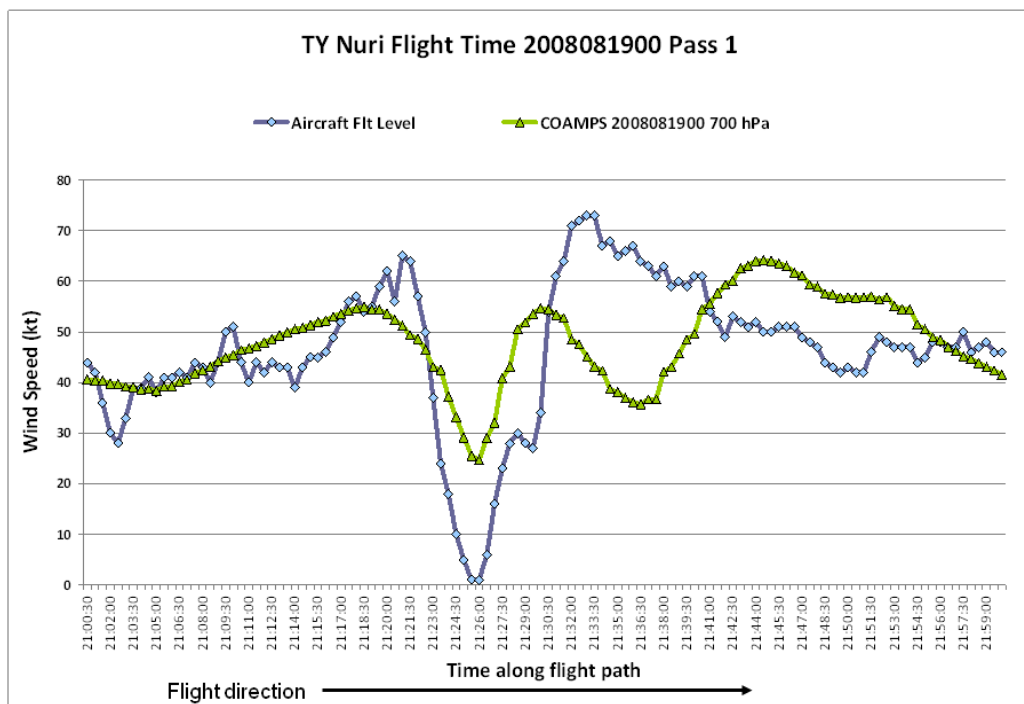


Figure 51. Flight-level winds (kt) at 0000 UTC 19 August from pass 1 (diamonds) and COAMPS-TC 0000 UTC 19 August 700 hPa winds (kt) (triangles).

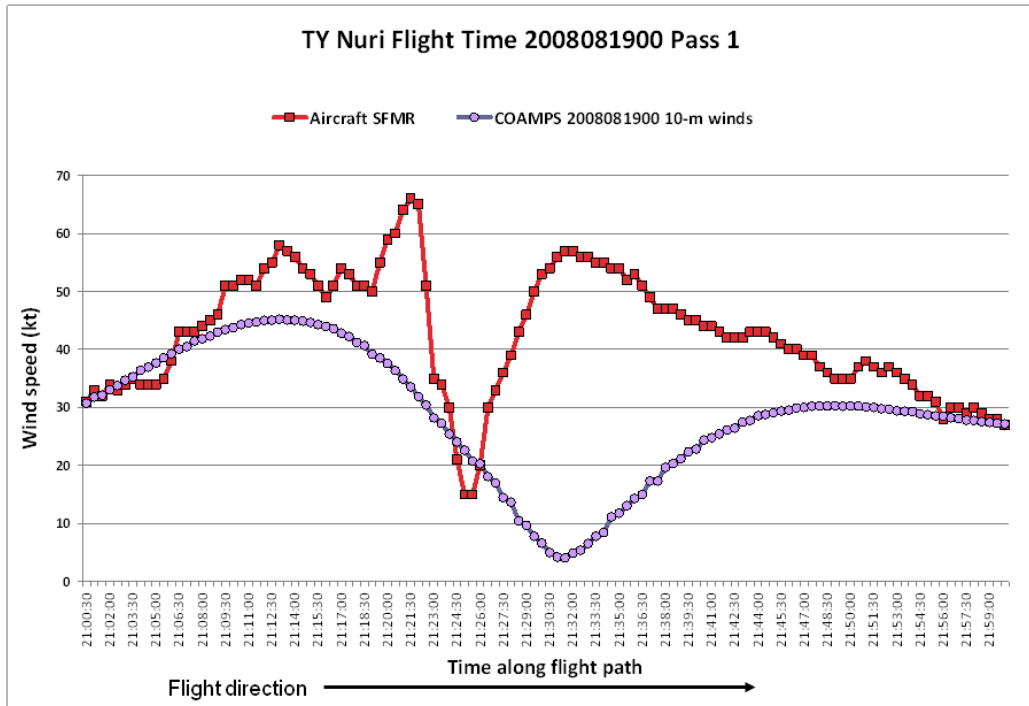


Figure 52. Surface winds (kt) at 0000 UTC 19 August from pass 1 (squares) and COAMPS-TC 0000 UTC 19 August 10-m winds (kt) (circles).

During the second pass from the southwest to the northeast (Figure 50b), a well-defined center was present in the flight-level winds and in the 700 hPa winds from the 0000 UTC 19 August analysis (Figure 53). The 700-hPa winds depict a broader and weaker vortex than the aircraft flight-level winds, but the center position matches the aircraft data. Similarly, the 10-m wind center from the 0000 UTC 19 August analysis (Figure 54) is in the same location as the center from the SFMR winds but the vortex is much wider and weaker (40 kt versus 70 kt) than in the SFMR winds. This issue of weaker 10-m maximum winds than in the SFMR observations is found in all of the analyses for the COAMPS-TC model.

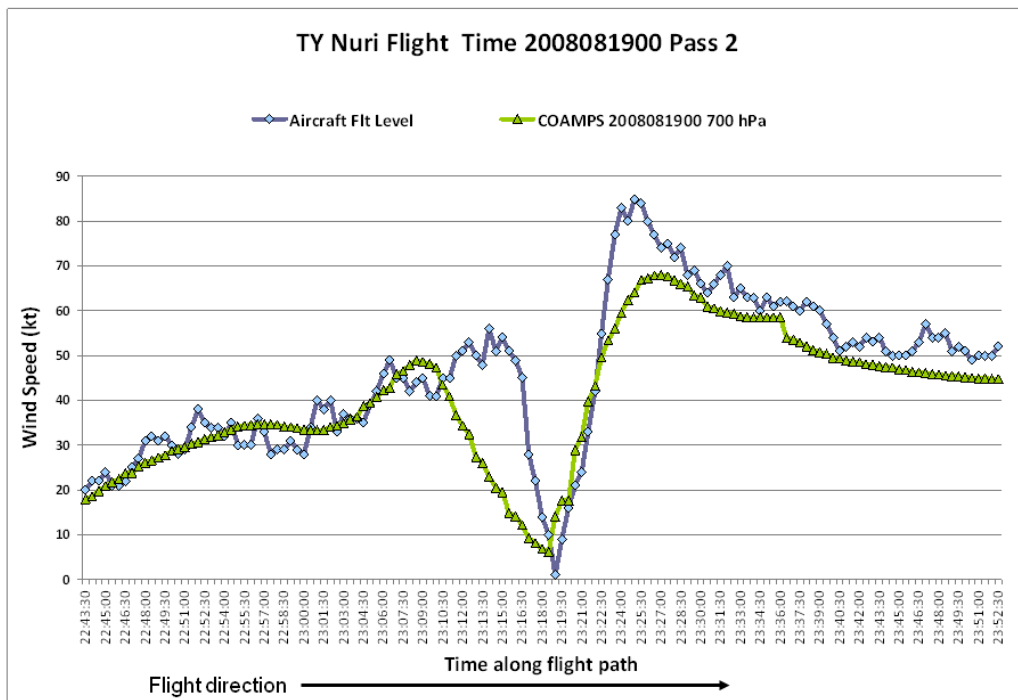


Figure 53. Flight-level winds (kt) at 0000 UTC 19 August from pass 2 (diamonds) and COAMPS-TC 0000 UTC 19 August 700 hPa winds (kt) (triangles).

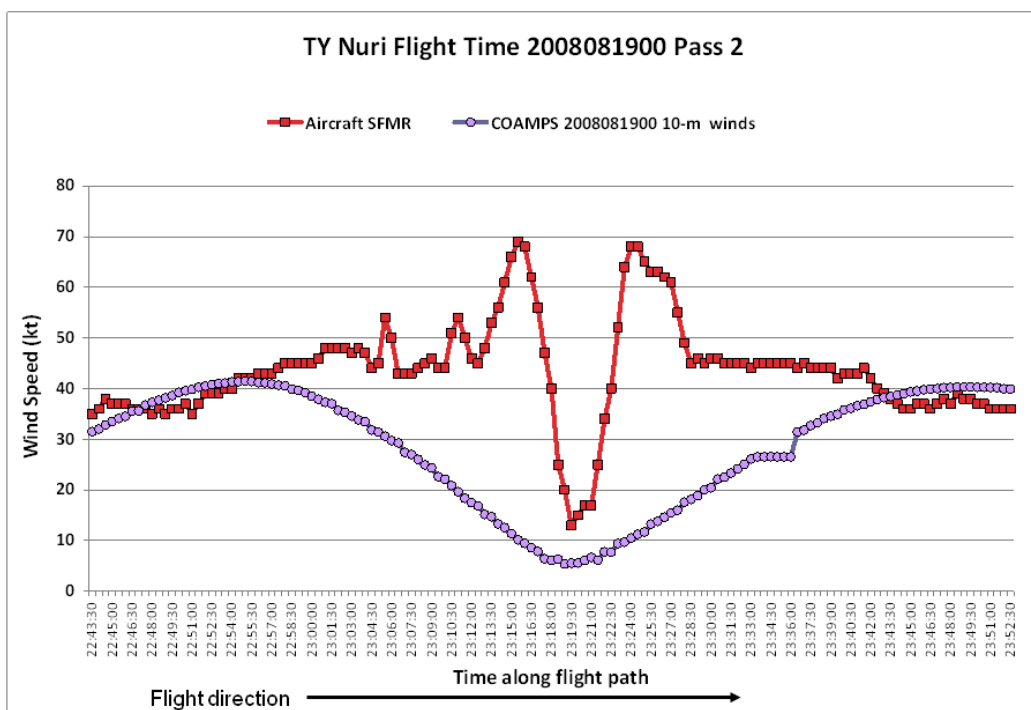


Figure 54. Surface winds (kt) at 0000 UTC 19 August from pass 2 (squares) and COAMPS-TC 0000 UTC 19 August 10-m winds (kt) (circles).

THIS PAGE INTENTIONALLY LEFT BLANK

IV. SUMMARY AND RECOMMENDATIONS

A. SUMMARY

During August–October 2008, the Tropical Cyclone Structure — 2008 (TCS-08) field experiment was conducted in the western North Pacific (WNP) to study TC formation, structure, and intensification. In all, the TCS-08 aircraft flew in four typhoons during the experiment. In this thesis, the COAMPS-TC model forecasts during TY Nuri in August 2008 were evaluated and compared to some in situ observations gathered from aircraft operated during the field programs. Tropical cyclone characteristics that were investigated include the distribution of deep convection, dynamic structure, wind distribution, and track. The COAMPS-TC model was also compared against the track and intensity of the ECMWF model to evaluate how well a mesoscale model does compared to a global model.

Typhoon Nuri originated from an easterly wave in the WNP and was the first typhoon during TCS-08. Once the pre-Nuri tropical disturbance reached tropical storm strength on 1200 UTC 17 August, the COAMPS-TC model was automatically run. The COAMPS-TC model has three grids with resolutions of 45, 15, and 5 km. The 15 and 5 km grids move with the typhoon. To evaluate how well the model forecast the intensity and structure of typhoon Nuri, the forecasts are identified in three separate stages of the TC life cycle (Table 1): formation, intensification, and decay. One model run from each stage was chosen to examine in detail.

The intensity of TY Nuri was examined at first by evaluating the minimum MSLP and maximum wind of the COAMPS-TC and ECMWF models. The intensity errors were calculated for the 1200 UTC 17 August through 0000 UTC 21 August COAMPS-TC model runs. Overall, the COAMPS-TC under-forecast the intensity in the shorter times and over-forecast in the longer periods. The formation stage includes forecasts from grid 1 and grid 2 and all three grids for the 1200 UTC 17 August model run. Forecasts of formation in the ECMWF and COAMPS-TC grid 1 model fields were very

weak. However, COAMPS-TC forecasts on grid 2 and grid 3 represented the formation quite well, and this suggests that the better the model resolution, the better the forecast.

The intensification stage was forecast by COAMPS-TC on all three grids. Again, the grid 3 forecasts were most accurate in defining the minimum MSLP and maximum winds. The forecast intensities were too low compared to the JTWC best-track values for Nuri, but the trend was correct. During the decay stage, all three grids from the COAMPS-TC model and the ECMWF model continued to strengthen the storm after Nuri had reached peak intensity on 0000 UTC 20 August. Thus, the forecasts from the intensification stage had the best overall representation of Nuri. In all of the stages, both models had initialization errors that could have contributed to their over- or under-forecasting of TY Nuri.

The ECMWF forecasts include tracks from when Nuri was a cloud cluster to a typhoon, while the COAMPS-TC tracks start when Nuri reached tropical storm strength. Overall, the ECMWF provided much superior forecasts of the track of TY Nuri except at the early times when the ECMWF model often had large initial position errors. The better early COAMPS-TC track forecast are likely due to the synthetic observations of the tropical cyclone that are included in the COAMPS-TC model.

For the formation stage, the structure forecasts by COAMPS-TC from the 1200 UTC 16 August initial conditions were examined. Since only grid 1 and 2 were only available for this forecast, only the simulated radar reflectivity from grid 2 was examined and compared with the corresponding microwave satellite imagery. By the 72-h forecast, the simulated radar reflectivity had the same structure as defined in the microwave satellite imagery except for the location of Nuri. For the intensification stage, the 1200 UTC 18 August forecast was examined. The simulated radar reflectivity, vertical wind shear, and azimuthally-averaged tangential winds, radial winds, vertical velocity, and cloud water were evaluated for grid 3 of the COAMPS-TC model. Except for the location of the storm, the overall radar reflectivity pattern from the COAMPS-TC compared favorably with the microwave satellite imagery during the intensification stage. However, an increase in vertical wind shear from the northeast that led to the asymmetric

convection in Nuri at the beginning of the decay stage was not evident in the model-simulated radar reflectivity. The structure in terms of tangential winds, radial winds, vertical velocity, and cloud water was generally correct in the COAMPS-TC forecasts during the intensification stage.

The 1200 UTC 19 August forecast was examined for the decay stage. All of the model forecasts in the decay stage continued to intensify Nuri when in fact Nuri was weakening. Whereas the simulated radar reflectivity from the 1200 UTC 19 August forecast represented well the convection of Nuri in the first 12 hours, when Nuri started to weaken due to increased vertical wind shear, the simulated radar reflectivity remained similar to a symmetric storm. Even though the model forecast an increasing vertical shear out of the northeast, that shear effect is not evident in the radar reflectivity images or the azimuthally-averaged plots. Rather, the tangential winds, radial winds, vertical velocity, and cloud water forecasts were more similar to a strong typhoon with a compact eye until the last 12 hours of the 1200 UTC 19 August forecast.

To document the contribution of initial condition errors in the COAMPS-TC forecasts, in situ observations from two aircraft flights were compared to the initial analyses of the corresponding model runs. The flight-level winds and 700 hPa winds were compared for the 0000 UTC 18 August aircraft flight and the 0000 UTC 19 August aircraft flight. This thesis also looked at the SFMR winds from the aircraft compared to the 10-m winds from the model. Overall, the 700 hPa winds in the model analyses matched aircraft flight-level data. However, the analysis 10-m winds depicted a broad, weak vortex in comparison with the SFMR winds, and the analysis had a tilted vortex between 10 m and 700 hPa instead of a vertical orientation.

The COAMPS-TC model contained two major deficiencies. The initial fields seem to be overly impacted by the NOGAPS circulation used as background for the COAMPS-TC initialization. For the forecast sequences examined, the vortex structure did not recover from the initialization until 12-21 hours into the forecast sequence.

A second issue was the generation of strong radial inflow at small radii and upper levels. Often these inflow regions were related to convergence and vertical motion

couplets of up motion above and down motion below the inflow. At these times, maximum updrafts were located at upper levels not in the lower levels. Although not explored in this thesis, these characteristics are hypothesized to be related to microphysical properties and the transition between liquid water and ice that occurs at middle levels in deep convective clouds.

B. RECOMMENDATIONS FOR FUTURE WORK

Further research is recommended on the COAMPS-TC model to better understand why Nuri was forecast to continue to intensify when in reality the storm was weakening considerably. Examination of the initialization procedure and also the model physics is strongly recommended. Another area of study may be to understand why the COAMPS-TC model continued to strengthen the storm when the vertical wind shear increased to unfavorable values. Since the ECMWF model also continued to intensify Nuri when it was weakening, the case study should include the ECMWF model fields as well.

Further studies may include case studies on all of the storms from the TCS-08 time period and compare the model forecasts to the in situ observations from the aircraft data. Such studies would establish whether the COAMPS-TC model performance characteristics in this study of Nuri generally apply.

LIST OF REFERENCES

- Bell, M. M., and M. T. Montgomery, 2008: Observed structure, evolution, and potential intensity of category 5 Hurricane Isabel (2003) from 12 to 14 September. *Monthly Weather Review*, **136**, 2023-2046.
- COAMPS, cited: COAMPS website [Available online at <http://www.nrlmry.navy.mil/coamps-web/web/research?spg=3&no=1>], 1 March 2009.
- Davis, C., W. Wang, S. S. Chen, Y. Chen, K. Corbosiero, M. DeMaria, J. Dudhia, G. Holland, J. Klemp, J. Michalakes, H. Reeves, R. Rotunno, C. Snyder, and Q. Xiao, 2008: Prediction of landfalling hurricanes with the Advanced Hurricane WRF model. *Monthly Weather Review*, **136**, 1990-2005.
- ECMWF, cited 2006: ECMWF website [Available online at http://www.ecmwf.int/products/data/operational_system/description/description_2006.html], 1 March 2009.
- Elsberry, R. L., and P. A. Harr, 2008: Tropical Cyclone Structure (TCS08) field experiment science basis, observational platforms, and strategy. *Asia Pacific J. Atmos. Sci.*, **44**, 209-231.
- Gray, W. M., 1968: Global view of the origin of tropical disturbance and storms. *Monthly Weather Review*, **96**, 669-700.
- Gray, W. M., 1979: Hurricanes: Their formation, structure and likely role in the tropical circulation. *Meteorology over the Tropical Oceans*, 155-218.
- Hock, T. F., and J. L. Franklin, 1999: The NCAR GPS dropwindsonde. *Bulletin of the American Meteorological Society*, **80**, 407-420.
- Kain, J. S., and J. M. Fritsch, 1990: A one-dimensional entraining/detraining plume model and its application in convective parameterization. *J. Atmos. Sci.*, **47**, 2784-2802.
- Kain, J. S., and J. M. Fritsch, 1993: Convective parameterization for mesoscale models: The Kain-Fritsch scheme. *The Representation of Cumulus Convection in Numerical Models, Meteor. Monogr.*, No. 46. Amer. Meteor. Soc., 165-170.
- Louis, J. F., 1979: A parametric model of vertical eddy fluxes in the atmosphere. *Bound. Layer. Meteor.*, **17**, 187-202.

JTWC, cited 2009: Collaboration Site [Password protected
<https://pzal.nmci.navy.mil/cgi-bin/collab.cgi>], 1 March 2009.

Marks, F. D., and L. K. Shay, 1998: Landfalling tropical cyclones: forecast problems and associated research opportunities. *Bulletin of the American Meteorological Society*, **79**, 305-323.

Navy Research Laboratory (NRL), 2003: *COAMPS Version 3 Model Description: General Theory and Equations*. NRL Publication, USA.

NRL, cited 2009: NRL Monterey Tropical Cyclone Homepage [Available online at
http://www.nrlmry.navy.mil/tc-bin/tc_home2.cgi], 1 March 2009.

INITIAL DISTRIBUTION LIST

1. Defense Technical Information Center
Ft. Belvoir, Virginia
2. Dudley Knox Library
Naval Postgraduate School
Monterey, California
3. Dr. Rich Hodur
Naval Research Laboratory
Monterey, California
4. Dr. Jim Doyle
Naval Research Laboratory
Monterey, California
5. Professor Patrick Harr
Naval Postgraduate School
Monterey, California
6. Professor Russell Elsberry
Naval Postgraduate School
Monterey, California
7. Professor Michael Montgomery
Naval Postgraduate School
Monterey, California
8. Air Force Weather Technical Library
Asheville, North Carolina
9. Captain Jennifer Hensley
17 Operational Weather Squadron
Hickam Air Force Base, Hawaii
10. CDR Daniel Eleuterio
Office of Naval Research
Washington, D.C.
11. Dr. Ronald Ferek
Office of Naval Research
Washington, D.C.

12. Director, Joint Typhoon Warning Center
Pearl Harbor, Hawaii